



**University of Kerbala**

**College of Science**

**Department of Chemistry**

**Synthesis and Characterization of Novel Compounds: Kinetic Study  
of Enzymatically Catalyzed Diels-Alder Reactions**

**A Thesis**

Submitted to the Council of the College of Science - University of Kerbala

in Partial Fulfillment of the Requirements for the Master Degree in

Chemistry Science

**Written By**

Zainab Adil Jasim

B.Sc. Chemistry (٢٠١٩) / University of Kerbala

**Supervised By**

Asst. Prof. Dr. - Thaer Mahdi Madloul

Prof. Dr. - Zeid Hassan Abood

July / ٢٠٢٤ A.D

Muharram / ١٤٤٦ A.H

بِسْمِ اللَّهِ الرَّحْمَنِ الرَّحِيمِ

وَأَنْ لَّيْسَ لِلْإِنْسَانِ إِلَّا مَا سَعَىٰ (٣٩) وَأَنْ سَعْيُهُ سَوْفَ يُرَىٰ (٤٠) ثُمَّ يُجْزَاهُ  
الْجَزَاءَ الْآوْفَىٰ (٤١)

صَدَقَ اللَّهُ الْعَلِيِّ الْعَظِيمِ

سورة النجم

## Report of the Head of the Chemistry Department

According to the recommendation presented by the Chairman of the Postgraduate Studies Committee, I forward this thesis "Synthesis and Characterization of Novel Compounds: Kinetic Study of Enzymatically Catalyzed Diels-Alder Reactions" for examination.

Signature:



Assist. Prof. **Dr. Thaer Mahdi Madlool**

Head of Chemistry Department

Address: University of Kerbala, College of Science, Department of Chemistry

Date: 12/8/2024




Kerbala University  
Science College

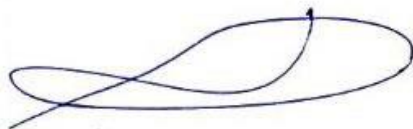


Asst. Prof. Dr. Thaer M. M. Al-Rammahi  
Head of Chemistry Department


### Examination Committee Certification


We certify that we have read this entitled "Synthesis and Characterization of Novel Compounds: Kinetic Study of Enzymatically Catalyzed Diels-Alder Reactions. " at the examining committee, examined the student " Zainab Adil Jasim" on its contents, and that in our opinion, its adequate for the partial fulfillment of the requirements for the Degree of Master in science of chemistry


Signature:   
Name: Dr. Narjis Hadi AL-Saadi  
Title: Professor  
Address: University of Kerbala, College of Science,  
Department of Chemistry.  
Date: 2 / 10 / 2024  
(Chairman)

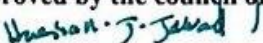


Signature:  
Name: Dr. Rahman Tama AL-Tamimi  
Title: Professor  
Address: University of Kerbala, College of  
Science, Department of Chemistry.  
Date: 2 / 10 / 2024  
(Member)

Signature:   
Name: Dr. Wisam Kadhun H. Al-Hashemi  
Title: Assistant Prof  
Address: University of Al-Nahrian, College of  
Science, Department of Chemistry.  
Date: 2 / 10 / 2024  
(Member)

Signature:   
Name: Dr. Thaer Mahdi Madlool  
Title: Assistant Prof  
Address: University of Kerbala, College of  
Science, Department of Chemistry.  
Date: 2 / 10 / 2024  
(Member & supervisor )

Signature:   
Name: Dr. Zeid Hassan Abood  
Title: Prof  
Address: University of Kerbala, College of  
Science, Department of Chemistry.  
Date: 2 / 10 / 2024  
(Member & supervisor )

Approved by the council of the College of Science  
Signature:   
Name: Dr. Hassan Jameel Al-Fatlawy  
Title: Professor  
Address: Dean of College of Science, University of Kerbala.  
Date: / / 2024

## Dedication

This work is sincerely dedicated to my supportive parents who encouraged me and inspired me in conducting this study. They have never left my side throughout the process and gave me strength and hope. They provided me with a great sense of enthusiasm and perseverance in continuing this. Without their love and assistance, this research would not have been made possible.

I would also like to dedicate this work to Asst.lec. Nabaah Hassan Naif and to Asst. prof. Husam Hameed Tizgam.

**Zainab Adil Jassim**

## **Acknowledgments**

In the name of Allah, the most gracious and the most merciful. First and foremost, I am thankful to Almighty ALLAH for giving me the strength, knowledge, ability and opportunity to undertake this study and complete it satisfactorily.

I would like to acknowledge and give my warmest thanks to my supervisors Asst. Prof. Dr. Thaer Mahdi Madlool, and Prof. Dr. Zeid Hassan Abood, who made this work possible. Their guidance and advice carried me through all the stages of writing my project.

To my dear family, my respected friends, today i pleased to share with you all my joy on this occasion. Thanks to everyone who supported me during the study period. Thanks to everyone who provided me real or moral assistance. And thanks to everyone who lit the way for me to achieve the dream i seek.

To my friend Nabaa, who has always been supportive with my work, thank you so much for your time and effort that you were able to share with me for the entire duration of constructing this research. For helping me to pass this hard time.

As well as, I thank the management of the chemistry department and its staff, for their support in doing this work and complete this thesis successfully.

**Zainab Adil Jassi**

## Summary

Diels-Alder (D-A) reaction is one of the important chemical transformations between diene and dienophile in a coordinated thermal pericyclic reaction to create the C–C bonds with predicted regio- and stereo-selectivity, which lead to the forming of bulk organic molecules. Despite of the significant efforts in this filed, the control of the stereoselectivity of Diels-Alder reactions remain so difficult. Despite the significant efforts in this field, controlling of stereoselectivity of Diels-Alder reactions remains so difficult.

Biosynthetic enzymes, Diels-Alderase are functionally distinct enzymes that catalyze  $[\pi + \pi]$  cycloaddition processes. The design of the enzymatic Diels-Alder reactions provides scientists with a huge advantage in increasing the selectivity of Diels-Alder reaction products.

Morus alba Diels-Alderase has ability to catalyze non-redox D-A reactions of different dienophiles and different types of natural and artificial polyphenolic dienes. Morus alba Diels-Alderase only have endo-selectivity. Moreover, it was shown that the Morus alba Diels-Alderase had great enantioselectivity when it came to catalyzing the Diels–Alder reaction, producing only enantiopure products with high stereoselectivity.

This work focused on applying the friendly environmental method includes the application of the current approach in enzymatic D-A reactions by formation the new organic compounds through the enzymatic D-A reactions between anthracene derivatives as dienes and pyrrole derivatives as dienophiles. in addition to control the stereoselectivity of the final products.

Furthermore, monitoring the enzymatic reaction of *Morus alba* Diels-Alderase.

All D-A reactions were carried out in the inert environment using the nitrogen gas. The prepared compounds were characterized using various techniques including mass spectroscopy, nuclear magnetic resonance, and Fourier transform infrared.

The final products of Diels-Alder reaction were Meso 9-(hydroxymethyl)-13-methyl-9,10-dihydro-12H,12H-9,10-(epiethane[1,1,2]triazolanoethane[1,2,2]triazyl)anthracene-12,12-dione (P<sub>1</sub>), Meso 9-(hydroxymethyl)-13-propyl-9,10-dihydro-12H,12H-9,10-(epiethane[1,1,2]triazolanoethane[1,2,2]triazyl)anthracene-12,12-dione (P<sub>2</sub>), Meso(9-(hydroxymethyl)-12,12-dioxo-9,10-dihydro-13H-9,10-(epiethane[1,1,2]triazolanoethane[1,2,2]triazyl)anthracen-13-yl)acetic acid (P<sub>3</sub>), Meso(13-methyl-12,12-dioxo-9,10-(epiethane[1,1,2]triazolanoethane[1,2,2]triazyl)anthracen-9(10H)-yl)boronic acid(P<sub>4</sub>), Meso(12,12-dioxo-13-propyl-9,10-(epiethane[1,1,2]triazolanoethane[1,2,2]triazyl)anthracen-9(10H)-yl)boronic acid (P<sub>5</sub>), Meso (9-(dihydroxyboranyl)-12,12-dioxo-9,10-dihydro-13H-9,10-(epiethane[1,1,2]triazolanoethane[1,2,2]triazyl)anthracen-13-yl)acetic acid (P<sub>6</sub>).

Depending on the results, the mechanisms of enzymatic Diels-Alder reaction was suggested.

The kinetics of preparation of these products in presence of *Morus alba* Diels-Alderase were studied by applying the Michaelis-Menten equation. The maximum velocity ( $V_{max}$ ) and the Michaelis-Menten constant ( $K_m$ ) for



all the enzymatic Diels Alder reaction. The least affinity between diene and enzyme found in Meso(13-methyl-12,14-dioxo-9,10-(epiethane[1,1,2]triazolanoethane[1,2,2]triazyl)anthracen-9(10H)-yl)boronic acid ( $P_4$ ) because it had the highest  $K_m$  value 0.3027. while, 2 Meso (9-(dihydroxyboranyl)-12,14-dioxo-9,10-dihydro-13H-9,10-(epiethane[1,1,2]triazolanoethane[1,2,2]triazyl)anthracen-13-yl)acetic acid ( $P_7$ ) achieved the highest affinity by having the lowest  $K_m$  value 0.2292.

In addition, the optimization of the enzymatic Diels Alder reactions which were included the concentration of the substrate, the enzymatic activity, and the temperature were performed to determine the best concentration of each substrate in addition to best enzyme activity at the optimum temperature. which found in  $P_7$  by using anthracen-9-ylmethanol as diene and in  $P_7$  by using anthracen-9-ylboronic acid as diene at 20°C

The thermodynamic parameters, which include enthalpy change ( $\Delta H$ ), Gibbs free energy change ( $\Delta G$ ) and entropy change ( $\Delta S$ ) were determined. All of the products are spontaneous and thermodynamically favorable, While the most favorable is  $P_7$ . in addition, all the products are endothermic except  $P_7$  is exothermic

However, there are other three compounds have been prepared by using 9,10-diphenylanthracene as diene but didn't give the expected result based on FTIR, NMR, and Mass spectroscopy analysis.

## List of contents

Division	Subject	Page number
	Summary	III-I
	List of contents	IV- XIV
	List of Tables	XV - XVI
	List of Figures	XVII - XXII
	List of Appendixes	XXII - XXV
	List of Abbreviations and Symbol	XXVI - XXVIII
	<b>Chapter one: Introduction and Literatures Review</b>	
۱.۱	Introduction	۱-۶
۱.۲	Literature Review	۶-۹
۱.۲.۱	Types of Diels Alder reactions:	۹
۱.۲.۱.۱	Normal Diels-Alder Reaction	۹-۱۰
۱.۲.۱.۲	Inverse-Electron-Demand Diels-Alder(IEDDA) Reaction	۱۰-۱۱
۱.۲.۱.۳	Intramolecular Diels-Alder Reaction	۱۲
۱.۲.۱.۴	Hetero-Diels-Alder Reaction	۱۳
۱.۲.۱.۵	Tandem or Cascade Diels-Alder Reaction	۱۴
۱.۲.۱.۶	The Retro Diels-Alder reaction	۱۵
۱.۲.۲	Catalyzing of Diels-Alder Reaction	۱۶

1.2.2.1	Chemical catalysis	16
1.2.2.1.1	Lewis Acid Catalysis	16
1.2.2.1.2	Brønsted Acid Catalysis	16-17
1.2.2.1.3	Metal Catalysis	17
1.2.2.1.4	Organocatalysts	18
1.2.2.2	Biological catalysis	18
1.2.2.2.1	D-A Reactions Catalyzed by Antibodies	18-19
1.2.2.2.2	de novo computational enzyme design	19-20
1.2.2.2.3	Reactions Catalyzed by Artificial Metalloenzymes	20-23
1.2.2.2.4	Natural Diels-Alderase	23-24
1.2.2.2.4.1	Moraceae family	24-25
1.2.3	Aim and objectives of Study	26
<b>Chapter Two: Materials and Methods</b>		
2	Materials and Methods	28
2.1	Chemical and Materials	28-29
2.1.1	Instrument and equipment	30
2.2	Subjects and Methods	31
2.2.1	Preparation of Morus alba Diels-Alderase (MaDA)	31
2.3	Preparation and Monitoring the Kinetic Parameters of Meso <sup>9</sup> -(hydroxymethyl)-1 <sup>3</sup> -methyl- <sup>9,10</sup> -dihydro- 1 <sup>2</sup> H,1 <sup>4</sup> H- <sup>9,10</sup> - (epiethane[1,1,2]triazanoethane[1,2,2]triazyl)anthracene- 1 <sup>2,14</sup> -dione (P <sub>1</sub> )	31
2.3.1	Preparation of Meso <sup>9</sup> -(hydroxymethyl)-1 <sup>3</sup> -methyl- <sup>9,10</sup> -dihydro-1 <sup>2</sup> H,1 <sup>4</sup> H- <sup>9,10</sup> - (epiethane[1,1,2]triazanoethane[1,2,2]triazyl)anthracene-	31-34

	12,14-dione (P <sub>1</sub> )	
2.3.2	Preparation of P <sub>1</sub> Solutions	34
2.3.3	Determination the Appropriate Concentration for anthracen-9-ylmethanol and 1-methyl-1 <i>H</i> -pyrrole-2,5-dione(P <sub>1</sub> )	35
2.3.4	Determination of Optimal MaDA Enzyme Activity for P <sub>1</sub> .	35-36
2.3.5	Thermodynamic Study for P <sub>1</sub>	36
2.4	Preparation and Monitoring the Kinetic Parameters of Meso 9-(hydroxymethyl)-13-propyl-9,10-dihydro-12H,14H-9,10-(epiethane[1,1,2]triazolanoethane[1,2,2]triazyl)anthracene-12,14-dione (P <sub>2</sub> )	36
2.4.1	Preparation of Meso 9-(hydroxymethyl)-13-propyl-9,10-dihydro-12H,14H-9,10-(epiethane[1,1,2]triazolanoethane[1,2,2]triazyl)anthracene-12,14-dione (P <sub>2</sub> )	36-38
2.4.2	Preparation of P <sub>2</sub> Solutions	38
2.4.3	Determination the Appropriate Concentration for anthracen-9-ylmethanol(D <sub>1</sub> ) and 1-propyl-1 <i>H</i> -pyrrole-2,5-dione (Dp <sub>2</sub> ).	38
2.4.4	Determination of Optimal MaDA Enzyme Activity for P <sub>2</sub>	39
2.4.5	Thermodynamic Study for P <sub>2</sub>	39
2.5	Preparation and Monitoring the Kinetic Parameters of	40

	Meso (9-(hydroxymethyl)-12,14-dioxo-9,10-dihydro-13H-9,10-(epiethane[1,1,2]triazolanoethane[1,2,2]triazyl)anthracen-13-yl)acetic acid (P <sub>r</sub> )	
2.5.1	Preparation of Meso (9-(hydroxymethyl)-12,14-dioxo-9,10-dihydro-13H-9,10-(epiethane[1,1,2]triazolanoethane[1,2,2]triazyl)anthracen-13-yl)acetic acid (P <sub>r</sub> )	40-41
2.5.2	Preparation of P <sub>r</sub> Solutions	41
2.5.3	Determination the Appropriate Concentration for anthracen-9-ylmethanol(D <sub>v</sub> ) and 2-(2,6-dioxo-2,6-dihydro-1H-pyrrol-1-yl) acetic acid (Dp <sub>r</sub> ) (Michaelis Menten Equation)	42
2.5.4	Determination of Optimal MaDA Enzyme Activity for P <sub>r</sub>	42-43
2.5.5	Thermodynamic Study for P <sub>r</sub>	43
2.6	Preparation and Monitoring the Kinetic Parameters of Meso (13-methyl-12,14-dioxo-9,10-(epiethane[1,1,2]triazolanoethane[1,2,2]triazyl)anthracen-9(10H)-yl)boronic acid (P <sub>ε</sub> )	43

۲.۶.۱	Preparation of Meso (۱۳-methyl-۱۲, ۱۴-dioxo-۹, ۱۰- (epiethane[۱, ۱, ۲]triazanoethane[۱, ۲, ۲]triazyl)anthracen- ۹(۱۰H)-yl)boronic acid (P <sub>ε</sub> )	۴۳-۴۴
۲.۶.۲	Preparation of P <sub>ε</sub> Solutions	۴۵
۲.۶.۳	Determination the Appropriate Concentration for Anthracen-۹-ylboronic acid (D <sub>۲</sub> ) and ۱-Methyl-۱H- pyrrole-۲, ۵-dione (Dp <sub>۱</sub> ) (Michaelis Menten Equation)	۴۵
۲.۶.۴	Determination of Optimal MaDA Enzyme Activity for P <sub>ε</sub>	۴۶
۲.۶.۵	Thermodynamic Study for P <sub>ε</sub>	۴۶
۲.۷	Preparation and Monitoring the Kinetic Parameters of Meso (۱۲, ۱۴-dioxo-۱۳-propyl-۹, ۱۰- (epiethane[۱, ۱, ۲]triazanoethane[۱, ۲, ۲]triazyl)anthracen- ۹(۱۰H)-yl)boronic acid (P <sub>σ</sub> )	۴۷
۲.۷.۱	Preparation of Meso (۱۲, ۱۴-dioxo-۱۳-propyl-۹, ۱۰- (epiethane[۱, ۱, ۲]triazanoethane[۱, ۲, ۲]triazyl)anthracen- ۹(۱۰H)-yl)boronic acid (P <sub>σ</sub> )	۴۷-۴۸
۲.۷.۲	Preparation of P <sub>σ</sub> Solutions	۴۸

۲.۷.۳	Determination the Appropriate Concentration for Anthracen-۹-ylboronic acid (D <sub>۱</sub> ) and ۱-propyl-۱H-pyrrole-۲,۵-dione(Dp <sub>۱</sub> ) (Michaelis Menten Equation)	۴۸-۴۹
۲.۷.۴	Determination of Optimal MaDA Enzyme Activity for P <sub>۵</sub>	۴۹
۲.۷.۵	Thermodynamic Study for P <sub>۵</sub>	۵۰
۲.۸	Preparation and Monitoring the Kinetic Parameters of Meso (۹-(dihydroxyboranyl)-۱۲,۱۴-dioxo-۹,۱۰-dihydro-۱۳H-۹,۱۰-(epiethane[۱,۱,۲]triazanoethane[۱,۲,۲]triazyl)anthracen-۱۳-yl)acetic acid (P <sub>۱</sub> )	۵۰
۲.۸.۱	Preparation of Meso (۹-(dihydroxyboranyl)-۱۲,۱۴-dioxo-۹,۱۰-dihydro-۱۳H-۹,۱۰-(epiethane[۱,۱,۲]triazanoethane[۱,۲,۲]triazyl)anthracen-۱۳-yl)acetic acid (P <sub>۱</sub> )	۵۰-۵۱
۲.۸.۲	Preparation of P <sub>۱</sub> Solutions	۵۲
۲.۸.۳	Determination the Appropriate Concentration for Anthracen-۹-ylboronic acid (D <sub>۱</sub> ) and ۲-(۲,۵-dioxo-۲,۵-dihydro-۱H-pyrrol-۱-yl) acetic acid (Dp <sub>۱</sub> ) (Michaelis Menten Equation)	۵۲

٢.٨.٤	Determination of Optimal MaDA Enzyme Activity for $P_1$	٥٣
٢.٨.٥	Thermodynamic Study for $P_1$	٥٣
٢.٩	preparation of Diels-Alder reaction by using ٩,١٠-diphenylanthracene as diene	٥٤-٥٥
٢.١٠	Monitoring of Kinetic Parameters	٥٥
٢.١٠.١	Michaelis-Menten Equation	٥٥
٢.١٠.٢	Determine the product's concentration	٥٥-٥٦
٢.١٠.٣	Find the values of the reaction rate constant and enzymatic reaction rate	٥٦
٢.١٠.٤	Calculating the values of $K_m$ and $V_{-Max}$ for each reaction	٥٦-٥٧
٢.١٠.٥	Achieving the optimal activity for enzyme reaction	٥٧
٢.١٠.٦	Determine the optimal temperature for enzymatic action	٥٧
٢.١٠.٧	Calculate the Thermodynamic Parameters $\Delta H$ , $\Delta S$ and $\Delta G$	٥٨
Chapter Three: Results and Discussion		



۳.۱	Characteristics of Meso ۹-(hydroxymethyl)-۱۳-methyl- ۹,۱۰-dihydro-۱۲H,۱۴H-۹,۱۰- (epiethane[۱,۱,۲]triazolazanoethane[۱,۲,۲]triazol)anthracene- ۱۲,۱۴-dione (P۱)	۶۰-۶۴
۳.۲	Kinetic Study of Meso ۹-(hydroxymethyl)-۱۳-methyl- ۹,۱۰-dihydro-۱۲H,۱۴H-۹,۱۰- (epiethane[۱,۱,۲]triazolazanoethane[۱,۲,۲]triazol)anthracene- ۱۲,۱۴-dione (P۱)	۶۴
۳.۲.۱	Determine the values of the reaction rate constant (Michaelis-Menten constant) and the maximum velocity of the enzymatic reaction for P۱	۶۵-۶۶
۳.۲.۲	Finding of Enzymatic Activity of P۱	۶۶-۶۷
۳.۲.۳	Finding Optimum Temperature for P۱	۶۷
۳.۲.۴	Finding the Thermodynamic Parameters for P۱	۶۷-۶۸
۳.۳.	Characteristics of Meso ۹-(hydroxymethyl)-۱۳-propyl- ۹,۱۰-dihydro-۱۲H,۱۴H-۹,۱۰- (epiethane[۱,۱,۲]triazolazanoethane[۱,۲,۲]triazol)anthracene- ۱۲,۱۴-dione (P۲).	۶۹-۷۴
۳.۴	Kinetic Study of Meso ۹-(hydroxymethyl)-۱۳-propyl- ۹,۱۰-dihydro-۱۲H,۱۴H-۹,۱۰- (epiethane[۱,۱,۲]triazolazanoethane[۱,۲,۲]triazol)anthracene- ۱۲,۱۴-dione (P۲).	۷۴
۳.۴.۱	Determine the values of the reaction rate constant (Michaelis-Menten constant) and the maximum velocity of the enzymatic reaction for P۲	۷۴-۷۶

۳.۴.۲	Finding of Enzymatic Activity of P <sub>r</sub>	۷۶
۳.۴.۳	Finding Optimum Temperature for P <sub>r</sub>	۷۷
۳.۴.۴	Finding the Thermodynamic Parameters for P <sub>r</sub>	۷۷-۷۸
۳.۵	Characteristics of Meso (۹-(hydroxymethyl)-۱۲,۱۴-dioxo-۹,۱۰-dihydro-۱۳H-۹,۱۰-(epiethane[۱,۱,۲]triazanoethane[۱,۲,۲]triazyl)anthracen-۱۳-yl)acetic acid (P <sub>r</sub> )	۷۹-۸۳
۳.۶	Kinetic Study of Meso (۹-(hydroxymethyl)-۱۲,۱۴-dioxo-۹,۱۰-dihydro-۱۳H-۹,۱۰-(epiethane[۱,۱,۲]triazanoethane[۱,۲,۲]triazyl)anthracen-۱۳-yl)acetic acid (P <sub>r</sub> )	۸۳
۳.۶.۱	Determine the values of the reaction rate constant (Michaelis-Menten constant) and the maximum velocity of the enzymatic reaction for P <sub>r</sub>	۸۴
۳.۶.۲	Finding of Enzymatic Activity of P <sub>r</sub>	۸۵
۳.۶.۳	Finding Optimum Temperature for P <sub>r</sub>	۸۶
۳.۶.۴	Finding the Thermodynamic Parameters for P <sub>r</sub>	۸۶-۸۷
۳.۷	Characteristics of Meso (۱۳-methyl-۱۲,۱۴-dioxo-۹,۱۰-(epiethane[۱,۱,۲]triazanoethane[۱,۲,۲]triazyl)anthracen-۹(۱۰H)-yl)boronic acid (P <sub>s</sub> )	۸۸-۹۲
۳.۸	Kinetic Study of Meso (۱۳-methyl-۱۲,۱۴-dioxo-۹,۱۰-(epiethane[۱,۱,۲]triazanoethane[۱,۲,۲]triazyl)anthracen-۹(۱۰H)-yl)boronic acid (P <sub>s</sub> )	۹۲
۳.۸.۱	Determine the values of the reaction rate constant	۹۲-۹۴

	(Michaelis Menten constant) and the maximum velocity of the enzymatic reaction for P <sub>ξ</sub>	
۳.۸.۲	Finding of Enzymatic Activity of P <sub>ξ</sub>	۹۴
۳.۸.۳	Finding Optimum Temperature for P <sub>ξ</sub>	۹۵
۳.۸.۴	Finding the Thermodynamic Parameters for P <sub>ξ</sub>	۹۵-۹۶
۳.۹	Characteristics of Meso (۱۲, ۱۴-dioxo-۱۳-propyl-۹, ۱۰- (epiethane[۱, ۱, ۲]triazanoethane[۱, ۲, ۲]triazyl)anthracen- ۹(۱-H)-yl)boronic acid (P <sub>ο</sub> )	۹۷-۱۰۱
۳.۱۰	Kinetic Study of Meso (۱۲, ۱۴-dioxo-۱۳-propyl-۹, ۱۰- (epiethane[۱, ۱, ۲]triazanoethane[۱, ۲, ۲]triazyl)anthracen- ۹(۱-H)-yl)boronic acid (P <sub>ο</sub> )	۱۰۱
۳.۱۰.۱	Determine the values of the reaction rate constant (Michaelis Menten constant) and the maximum velocity of the enzymatic reaction for (P <sub>ο</sub> )	۱۰۱- ۱۰۲
۳.۱۰.۲	Finding of Enzymatic Activity of P <sub>ο</sub>	۱۰۳
۳.۱۰.۳	Finding Optimum Temperature for P <sub>ο</sub>	۱۰۴
۳.۱۰.۴	Finding the Thermodynamic Parameters for P <sub>ο</sub>	۱۰۴- ۱۰۵
۳.۱۱	Characteristics of Meso (۹-(dihydroxyboranyl)-۱۲, ۱۴- dioxo-۹, ۱۰-dihydro-۱۳H-۹, ۱۰- (epiethane[۱, ۱, ۲]triazanoethane[۱, ۲, ۲]triazyl)anthracen- ۱۳-yl)acetic acid (P <sub>τ</sub> )	۱۰۶- ۱۱۰
۳.۱۲	Kinetic Study of Meso (۹-(dihydroxyboranyl)-۱۲, ۱۴- dioxo-۹, ۱۰-dihydro-۱۳H-۹, ۱۰-	۱۱۱

	(epiethane[1,1,2]triazanoethane[1,2,2]triazyl)anthracen- 13-yl)acetic acid (P <sub>1</sub> )	
3.12.1	Determine the values of the reaction rate constant (Michaelis Menten constant) and the maximum velocity of the enzymatic reaction for P <sub>1</sub>	111- 112
3.12.2	Finding of Enzymatic Activity of P <sub>1</sub>	112- 113
3.12.3	Finding Optimum Temperature for P <sub>1</sub>	113- 114
3.12.4	Finding the Thermodynamic Parameters for P <sub>1</sub>	114- 115
	Conclusions	122
	Recommendations	123
	References	124- 141
	Appendixes	142- 156

## List of Tables

No.	Title	Page No.
Table (۲-۱)	Chemicals and their origin	۲۸-۲۹
Table (۲-۲)	The devices and their suppliers	۳۰
Table (۲-۳)	The solubility of P <sub>۱</sub>	۳۴
Table (۲-۴)	The solubility of P <sub>۲</sub>	۳۷-۳۸
Table (۲-۵)	The solubility of P <sub>۳</sub>	۴۱
Table (۲-۶)	The solubility of P <sub>۴</sub>	۴۴
Table (۲-۷)	The solubility of P <sub>۵</sub>	۴۸
Table (۲-۸)	The solubility of P <sub>۶</sub>	۵۱
Table (۲-۹)	Physical properties and the yield of D-A products	۵۴
Table (۳-۱)	The Values of K <sub>m</sub> and V <sub>max</sub> for the D-A reaction of P <sub>۱</sub>	۶۶
Table (۳-۲)	The values of (ΔH), (ΔS) and (ΔG) for P <sub>۱</sub>	۶۸
Table (۳-۳)	The Values of K <sub>m</sub> and V <sub>max</sub> for the D-A reaction of P <sub>۲</sub>	۷۶
Table (۳-۴)	The values of (ΔH), (ΔS) and (ΔG) for P <sub>۲</sub>	۷۸
Table (۳-۵)	The Values of K <sub>m</sub> and V <sub>max</sub> for the D-A reaction of P <sub>۳</sub>	۸۴
Table (۳-۶)	The values of (ΔH), (ΔS) and (ΔG) for P <sub>۳</sub>	۸۷

Table (۳-۶)	The Values of $K_m$ and $V_{max}$ for the D-A reaction of $P_\xi$	۹۳
Table (۳-۷)	The values of ( $\Delta H$ ), ( $\Delta S$ ) and ( $\Delta G$ ) for $P_\xi$	۹۶
Table (۳-۸)	The Values of $K_m$ and $V_{max}$ for the D-A reaction of $P_\circ$	۱۰۲
Table (۳-۹)	The values of ( $\Delta H$ ), ( $\Delta S$ ) and ( $\Delta G$ ) for $P_\circ$	۱۰۵
Table (۳-۱۰)	The Values of $K_m$ and $V_{max}$ for the D-A reaction of $P_\gamma$	۱۱۲
Table (۳-۱۱)	The values of ( $\Delta H$ ), ( $\Delta S$ ) and ( $\Delta G$ ) for $P_\gamma$	۱۱۵
Table (۳-۱۲)	Show the FTIR peaks for the products( $P_\gamma$ - $P_\gamma$ )	۱۱۶-۱۷
Table (۳-۱۳)	Show the $^1H$ NMR peaks for the products( $P_\gamma$ - $P_\gamma$ )	۱۱۸-۱۱۹
Table (۳-۱۴)	Show the $^{13}C$ NMR peaks for the products( $P_\gamma$ - $P_\gamma$ )	۱۲۰-۱۲۱

## List of Figures

No.	Title	Page No.
Figure (1-1)	The most basic Diels-Alder cyclo addition	2
Figure (1-2)	Representation of HOMO and LUMO orbital role	2
Figure (1-3)	(a)Diagram illustrating the Diels-Alder reaction's preicyclic transition state using an s-cis diene arrangement, (b)showing the way in which the s-trans conformation blocks this	4
Figure (1-4)	The process of catalysis	6
Figure (1-5)	Show the <i>ortho-para</i> rule	10
Figure (1-6)	The difference between Normal and Invers D-A	11
Figure (1-7)	Types of Intramolecular Diels-Alder Reaction	12
Figure (1-8)	The cycloaddition of 1,3-butadiene and hetero-dienophile	13

	D-A reactions	
Figure (1-9)	The Retro Diels–Alder reaction	10
Figure (1-10)	Strategy used for the generation of catalytic monoclonal antibodies	19
Figure (1-11)	protein scaffold, an abiotic cofactor can be stably localized using four different anchoring techniques. (a) covalent, (b) supra molecular, (c) dative, (d) metal substitution	22
Figure (2-1)	An image showing the change in the color of the reaction mixture from light brown to pale yellow	32
Figure (2-2)	(a)The filtration technique which was used to separate the reaction products from the solvent, where the pale yellow ppt. on the filter surface is the product, While the solvent in the reactor, (b) The TLC technique.	33
Figure (2-3)	The main product P <sub>1</sub> of D-A reaction	33
Figure (2-4)	The main product P <sub>2</sub> of D-A reaction	37



Figure (γ-ϖ)	The main product P <sub>γ</sub> of D-A reaction	εϖ
Figure (γ-ϗ)	The main product P <sub>ε</sub> of D-A reaction	εε
Figure (γ-Ϙ)	The main product P <sub>ο</sub> of D-A reaction	εϘ
Figure (γ-ϙ)	The main product P <sub>γ</sub> of D-A reaction	ογ
Figure (γ-Ϡ)	The FTIR spectra for P <sub>γ</sub>	ϗγ
Figure (γ-ϡ)	The <sup>1</sup> H NMR spectra for P <sub>γ</sub>	ϗϘ
Figure (γ-Ϣ)	The <sup>13</sup> C NMR spectrum of P <sub>γ</sub>	ϗϙ
Figure (γ-ϣ)	The mass spectra for P <sub>γ</sub>	ϗε
Figure (γ-Ϥ)	Michaelis-Menten diagram and line weaver - Burk diagram of the D-A reaction of P <sub>γ</sub>	ϗο
Figure (γ-ϥ)	The appropriate enzyme activity of MaDA for P <sub>γ</sub>	ϗϗ
Figure (γ-Ϧ)	Showing the ideal temperature for P <sub>γ</sub>	ϗϘ
Figure (γ-ϧ)	Van't Hoff equation for P <sub>γ</sub>	ϗϙ
Figure (γ-Ϩ)	The FTIR spectra for P <sub>γ</sub>	Ϙο
Figure (γ-ϩ)	The <sup>1</sup> H NMR spectra for P <sub>γ</sub>	Ϙγ
Figure (γ-Ϫ)	The <sup>13</sup> C NMR spectrum of P <sub>γ</sub>	Ϙε
Figure (γ-ϫ)	The mass spectra for P <sub>γ</sub>	Ϙε
Figure (γ-Ϭ)	Michaelis-Menten diagram and line weaver - Burk diagram of the	Ϙο

	D-A reaction of P <sub>r</sub>	
Figure (3-14)	The appropriate enzyme activity of MaDA for P <sub>r</sub>	76
Figure (3-15)	Showing the ideal temperature for P <sub>r</sub>	77
Figure (3-16)	Van't Hoff equation for P <sub>r</sub>	78
Figure (3-17)	The FTIR spectra for P <sub>r</sub>	80
Figure (3-18)	The <sup>1</sup> H NMR spectra for P <sub>r</sub>	81
Figure (3-19)	The <sup>13</sup> C NMR spectrum of P <sub>r</sub>	82
Figure (3-20)	The mass spectra for P <sub>r</sub>	83
Figure (3-21)	Michaelis-Menten diagram and line weaver - Burk diagram of the D-A reaction of P <sub>r</sub>	84
Figure (3-22)	The appropriate enzyme activity of MaDA for P <sub>r</sub>	85
Figure (3-23)	Image showing the ideal temperature for P <sub>r</sub>	86
Figure (3-24)	Van't Hoff equation for P <sub>r</sub>	87
Figure (3-25)	The FTIR spectra for P <sub>i</sub>	89
Figure (3-26)	The <sup>1</sup> H NMR spectra for P <sub>i</sub>	90
Figure (3-27)	The <sup>13</sup> C NMR spectrum of P <sub>i</sub>	91
Figure (3-28)	The mass spectra for P <sub>i</sub>	92
Figure (3-29)	Michaelis-Menten diagram and line weaver - Burk diagram of the D-A reaction of P <sub>i</sub>	94
Figure (3-30)	The appropriate enzyme activity	95

	of MaDA for P <sub>ξ</sub>	
Figure (۳-۳۱)	Showing the ideal temperature for P <sub>ξ</sub>	۹۵
Figure (۳-۳۲)	Van't Hoff equation for P <sub>ξ</sub>	۹۶
Figure (۳-۳۳)	The FTIR spectra for P <sub>۰</sub>	۹۸
Figure (۳-۳۴)	The <sup>1</sup> H NMR spectra for P <sub>۰</sub>	۹۹
Figure (۳-۳۵)	The <sup>13</sup> C NMR spectrum of P <sub>۰</sub>	۱۰۰
Figure (۳-۳۶)	The mass spectra for P <sub>۰</sub>	۱۰۱
Figure (۳-۳۷)	Michaelis-Menten diagram and line weaver - Burk diagram of the D-A reaction of P <sub>۰</sub>	۱۰۰
Figure (۳-۳۸)	The appropriate enzyme activity of MaDA for P <sub>۰</sub>	۱۰۲
Figure (۳-۳۹)	Showing the ideal temperature for P <sub>۰</sub>	۱۰۳
Figure (۳-۴۰)	Van't Hoff equation for P <sub>۰</sub>	۱۰۵
Figure (۳-۴۱)	The FTIR spectra for P <sub>۱</sub>	۱۰۷
Figure (۳-۴۲)	The <sup>1</sup> H NMR spectra for P <sub>۱</sub>	۱۰۸
Figure (۳-۴۳)	The <sup>13</sup> C NMR spectrum of P <sub>۱</sub>	۱۰۹
Figure (۳-۴۴)	The mass spectra for P <sub>۱</sub>	۱۱۰
Figure (۳-۴۵)	Michaelis-Menten diagram and line weaver - Burk diagram of the D-A reaction of P <sub>۱</sub>	۱۱۱
Figure (۳-۴۶)	The appropriate enzyme activity	۱۱۳

	of MaDA for $P_1$	
Figure (३-११)	Showing the ideal temperature for $P_1$	१११
Figure (३-१२)	Van't Hoff equation for $P_1$	११०

### Appendixes

No.	Title	Page No.
Appendix (१)	calibration curve of $P_1$	१११
Appendix (२)	represents the values used to draw the Michaelis-Menten and Line Weaver-Burk equations for $P_1$	१११
Appendix (३)	Values for $P_1$ velocity plot against enzymatic activity	११२
Appendix (४)	Values of the velocity versus temperature plot and the Arrhenius equation, respectively for $P_1$	११२

Appendix (°)	calibration curve of P <sub>r</sub>	١٤٩
Appendix (٦)	represents the values used to draw the Michaelis-Menten and Line Weaver-Burk equations for P <sub>r</sub>	١٤٩
Appendix (٧)	Values for P <sub>r</sub> velocity plot against enzymatic activity	١٥٠
Appendix (٨)	Values of the velocity versus temperature plot and the Arrhenius equation, respectively for P <sub>r</sub>	١٥٠
Appendix (٩)	calibration curve of P <sub>r</sub>	١٥١
Appendix (١٠)	represents the values used to draw the Michaelis-Menten and Line Weaver-Burk equations for P <sub>r</sub>	١٥١
Appendix (١١)	Values for P <sub>r</sub> velocity plot against enzymatic activity	١٥٢
Appendix (١٢)	Values of the velocity versus temperature plot and the Arrhenius	١٥٢

	equation, respectively for $P_r$	
Appendix (13)	calibration curve of $P_\xi$	103
Appendix (14)	represents the values used to draw the Michaelis-Menten and Line Weaver-Burk equations for $P_\xi$	103
Appendix (15)	Values for $P_\xi$ velocity plot against enzymatic activity	104
Appendix (16)	Values of the velocity versus temperature plot and the Arrhenius equation, respectively for $P_\xi$	104
Appendix (17)	calibration curve of $P_o$	100
Appendix (18)	represents the values used to draw the Michaelis-Menten and Line Weaver-Burk equations for $P_o$	100
Appendix (19)	Values for $P_o$ velocity plot against enzymatic activity.	106
Appendix (20)	Values of the velocity	106

	versus temperature plot and the Arrhenius equation, respectively for P <sub>o</sub> .	
Appendix (۲۱)	calibration curve of P <sub>۱</sub>	۱۵۷
Appendix (۲۲)	represents the values used to draw the Michaelis-Menten and Line Weaver-Burk equations for P <sub>۱</sub>	۱۵۷
Appendix (۲۳)	Values for P <sub>۱</sub> velocity plot against enzymatic activity	۱۵۸
Appendix (۲۴)	Values of the velocity versus temperature plot and the Arrhenius equation, respectively for P <sub>۱</sub>	۱۵۸
Appendix (۲۵)	The FTIR spectra for P <sub>v</sub>	۱۵۹
Appendix (۲۶)	The FTIR spectra for P <sub>λ</sub>	۱۵۹
Appendix (۲۷)	The FTIR spectra for P <sub>۱</sub>	۱۶

### List of Abbreviations and symbols

Abbreviation	Terms
$[S]_0$	concentration of the substrate at zero time
$[S]_T$	concentration of the substrate at a certain time
$1/T$	Reciprocal of temperature
A	Absorbance
b	Broad
C	Concentration
$C^\circ$	Celsius
cm	Centimeter
$^{13}\text{C}$ NMR	Carbone- $^{13}$ nuclear magnetic resonance
d	doublet
D-A	Diels-Alder
DAs	Diels-Alderases
dd	Doublet of doublet
DMSO- $d_6$	dimethyl sulfoxide- $d_6$
$E_a$	Activation energy
EDG	electron-donating group
$\text{Et}_2\text{O}$	Diethyl ether
EWG	Electron with drawing group



$\epsilon$	Molar absorption coefficient
FAD	Flavin adenine dinucleotide
FMO	Frontier molecular orbital theory
FT-IR	Fourier- Transform Infrared Radiation
g	Gram
h	Hour
$^1\text{H}$ NMR	Hydrogen nuclear magnetic resonance
HOMO	Highest Occupied Molecular Orbital
IEDDA	Inverse-Electron-Demand Diels-Alder
IMDA	Intramolecular Diels-Alder
$J$	Coupling constant
J	Joule
K	kelvin
K	Reaction rate constant
Kcal	Kilocalories
$K_m$	Michaels constant
LA	Lewis Acid
Ln K	Natural logarithm of the reaction rate constant
LUMO	Lowest Unoccupied Molecular Orbital
m	Multiplet
m	Medium
MaDA	Morus alba Diels-Alderase
MaMO	Morus alba moracin C oxidase

mg	Milligram
min	Minute
ml	Milliliter
mM	Mill molar
nm	Nanometer
NMR	Nuclear magnetic resonance
OC	oxidocyclase
pH	Acidic function
R	Gas constant
rD-A	Retro-Diels-Alder
s	Singlet
s	Strong
t	Triplet
T.S	Transition state
THF	TetrahydroFuran
U	Unit
UV-Vis	ultra violate – visible spectroscopy
$V_{\max}$	Equals half the maximum speed
w	Weak
$\lambda_{\max}$	Maximum wavelength
V	Rate of the enzymatic reaction



## *Chapter one*

### *Introduction and Literature Review*

## 1.1. Introduction

Diels-Alder (D-A) reaction is one of the most significant chemical reactions that produces C-C bonds with multiple stereo-centers in a single reaction step with recognized regio and stereo- selectivities, which is widely utilized organic chemical transformation in the organic chemistry field (1-3). As well as, due to its efficiency, predictability, and ability to construct complex cyclic structures, The product of Diels-Alder reaction plays significant role in the synthesis of many organic compounds, including natural products, pharmaceuticals and materials. Along with synthetic chemistry, D-A reaction is considered as a symbol for biology that has a variety of biological properties, such as anti-inflammatory, anti-HIV, antibacterial, and anticancer properties (4,5), because it is a key tool for site-specific protein chemical modification, which is used to investigate and regulate protein functions in *vitro* and in biological systems (6).

Generally, D-A reaction involves the two-electrons of the dienophile and the four-electrons of the diene in a coordinated thermal pericyclic reaction to form two new sigma ( $\sigma$ ) bonds and a new  $\pi$  bond are formed when these  $\pi$  bonds break in the [ $\pi + \pi$ ] pericyclic transition state (7-9). The simplest example of a Diels-Alder reaction between ethene and 1,3-butadiene, however, it is also one of the least useful because of the relatively large activation energy required to form the cycloadduct Figure(1-1) (10).

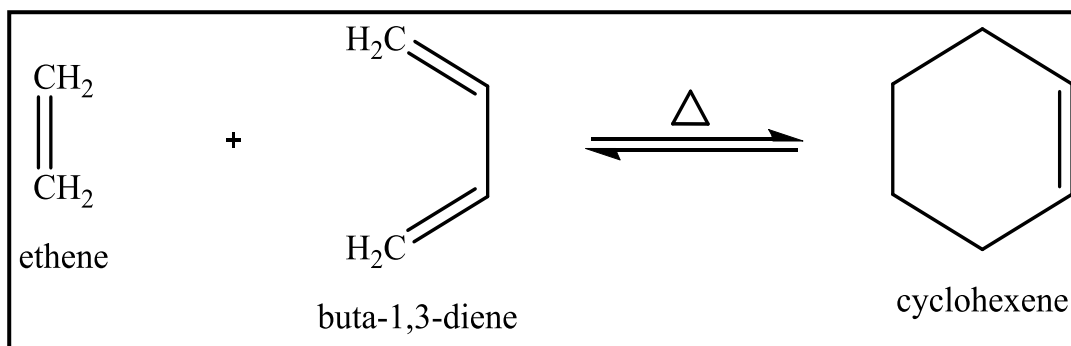


**Figure (1-1): The most basic Diels-Alder cycloaddition**

In this instance the stereo- and regional chemistry of the D-A reaction is governed by the Woodward-Hoffmann rules (11). Furthermore, When the dienophile is substituted by an electron-withdrawing group (EWG, Z) and the diene is carrying an electron-donating group (EDG, X), the Highest Occupied Molecular Orbital (HOMO) of the diene overlaps with the Lowest Unoccupied Molecular Orbital (LUMO) of the dienophile in a suprafacial contact in typical electron-demand D-A reactions, Figure(1-2) (12).

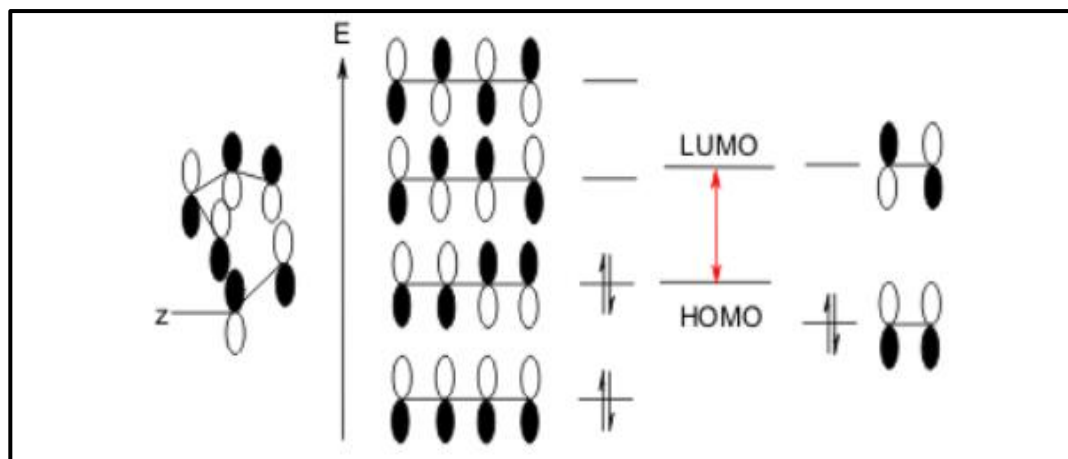


**Figure (1-2): Representation of HOMO and LUMO orbital role (12)**

In addition to this, a molecule can not function as a diene or participate in the D-A process unless it is an *s-cis* conformer, Figure (1-3a). Consequently, the system undergoes steric repulsive strain due to the reduced distance between the substituents in *s-cis* conformers, which lowers their thermodynamic stability. Even though *s-trans* conformers are more stable, the distance between substituent bonds prevents them from participating in a coordinated reaction with a dienophile, Figure (1-3b). Consequently, it has been proposed that compounds with *s-cis* in their structure, such as anthracenes, are highly reactive as dienes and suitable to participate in the D-A process. However, in addition to their regioselectivity, dienophiles can have two possible chemical orientations. The cyclic electron-poor system in maleimide, on the other hand, is particularly favorable as a dienophile according to (D-A) cycloaddition reactions (13, 14) and by attaching a partial positive charge to the  $sp^2$  carbon can enhance its reactivity towards the diene (15, 16), this is possible unless the dienophile possesses at least one EWG such as carbonyl group ( $C=O$ ) or cyano group ( $C\equiv N$ ) that can remove electrons from  $C=C$  exist in the Dienophile (17). In contrast to the *exo* T.S., which displays the opposite orientation, the dienophile substituent in the *endo* T.S. is orientated toward the diene system (18, 19).

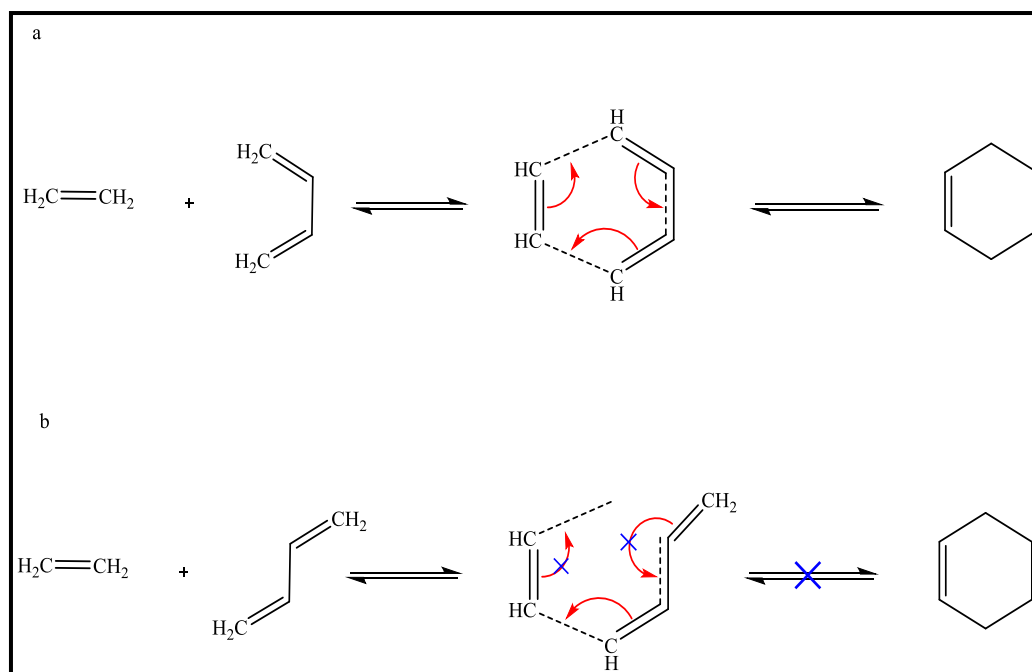


**Figure (1-3):(a) Diagram illustrating the Diels-Alder reaction's preicyclic transition state using an *s-cis* diene arrangement, (b) Showing the way in which the *s-trans* conformation blocks this**

However, controlling the stereoselectivity of Diels-Alder reaction is the most significant challenge in organic synthesis. There are various methods to catalyze the Diels-Alder reaction to increase the rate of reaction, control stereochemistry, or enable the reaction under milder circumstances. Chemists are being more interested in developing catalysts which are more environmentally friendly and utilize renewable resources as a result of our growing concerns about the depletion of petroleum resources and environmental issues (15, 16). One of the main objectives of bio-catalysis is the development of protein catalysts for these processes, which could open up novel, effective, and environmentally friendly synthetic pathways to a wide range of beneficial bioactive molecules (17). Enzymes are extraordinarily selective catalysts.



Where the catalyst is defined as a material that accelerate a chemical reaction without being consumed. Because each catalytic cycle leads to regeneration the catalyst, Figure (1-4), a single catalyst molecule can transform many substrate molecules into product. Similar to all of the catalysts, all known enzymatic reactions reduce activation energy (20,21) to accelerate rate via conserving the structure, charge, and geometry of the evolving transition state, which sometimes differs from the product structure (22). There is very little requirement for the catalyst. While thermodynamic characteristics are associated with energy balance and equilibrium, kinetic characteristics are associated with a reaction's velocity (23,24). The first descriptions of biological catalysts date back to the late 1700s. Initially, studies focused on how stomach secretions break down meat. Later, around the 1800s, similar study was conducted on how saliva and other plant extracts degrade starch into simple sugar. Since the late 1990s, there has been a constant focus on the discovery or design of enzymes that can catalyze the chemical transformation with high efficiency and stereoselectivity.

Additionally, enzymes also play important roles in a variety of industrial productions, such as food, leather, textiles, dyes, water purification, pharmaceuticals, cosmetics, as well as additional biofuels (25,26). In contrast to most industrial chemical methods, enzymes are environmentally friendly (Because enzymes are biodegradable and typically use water as a solvent) (27) and extremely selective, Its products are extremely pure, which minimizes manufacturing costs and increases income (28), they are safer to use, consume little energy because they operate under mild conditions, and significantly limit the creation of toxic by-products (29,30). On the other

hand, enzymes are extremely costly for commercial applications. However, enzymes have a low degree of stability in harsh environments. Stability, enhancing enzymatic efficiency, enzyme activity, and reuse capacity are of highly desirable in order to address these problems (30).

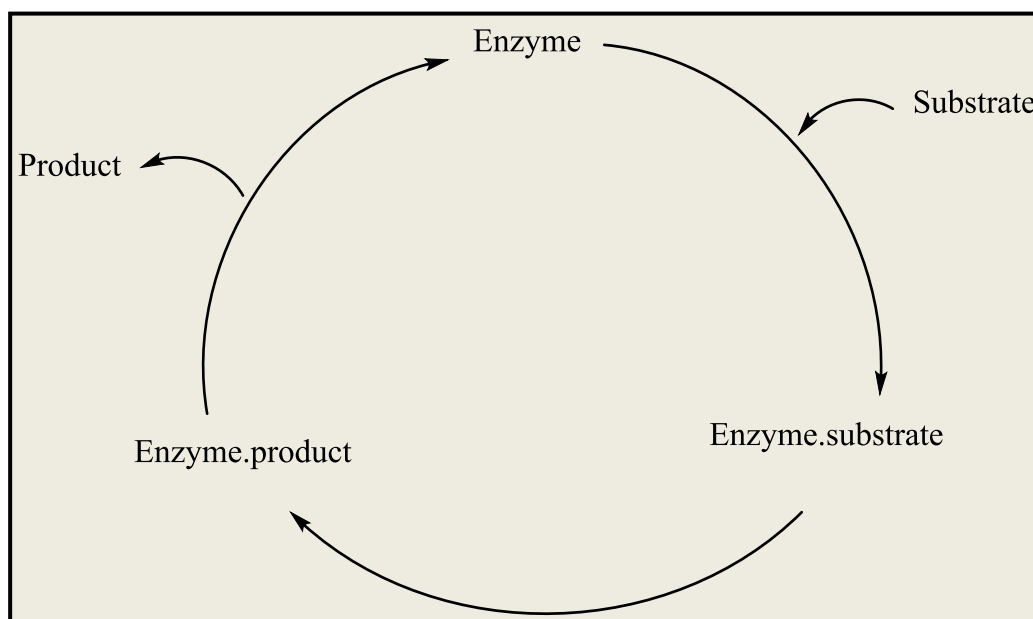


**Figure (1-4): The process of Catalysis**

### 1.1. Literature Review

After multiple near-discoveries of the [4+2] cycloaddition reaction by number of luminaries in the field of organic chemistry around the first decade of the 20<sup>th</sup> century (31).

The Diels-Alder reaction was first described by Professor Otto Diels and his student Kurt Alder in a 1928 publication, They discovered that a highly stereospecific new six-membered ring is created when a conjugated diene

combines with a substituted alkene (32). Diels and Alder noted in their significant 1928 paper that "it appears to us, that the possibility of synthesis of complex compounds similar to or identical with natural products such as terpenes, sesquiterpenes, and potentially even alkaloids" (33).

In 1950, Diels and Alder were jointly awarded Chemistry Nobel Prize for their roles in its development and discovery, Their discovery provided synthetic chemists a useful tool and made an important contribution to the understanding of organic chemistry (10).

After that in 1902, Gates and Tschudi's started synthesis of morphine, which was documented a few months later and used the pericyclic technique (34). Furthermore, even though the reaction's researchers made significant advances in the field of terpene synthesis. their attention was eventually drawn to other areas of research that were more important to them, specifically understanding the reaction's mechanistic foundations (35,36). Notably, these efforts eventually produced such revolutionary findings as the Alder *endo* rule, which controls the stereo-chemical result of the normal Diels - Alder reaction(37).

During 1952-1960, theoretical explanation for the stereochemistry shown in the Diels-Alder reaction was provided by Robert Woodward and Roald Hoffmann (38). Their study, known as the Woodward-Hoffmann rules, contributed to the prediction of the products stereochemistry by using the reacting molecules' orbital symmetry. It was determined that despite all variables that affect the decrease of the energy gap obviously raise the rate of reaction, the reactivity of the D-A reaction depends on the energy separation gap between the HOMO-LUMO of reacting pairs (39). By using

a Lewis acid-catalyzed system, Yates and Eaton published the first report on a high rate accelerated cycloaddition reaction in 1960 (20). Since then, a variety of techniques have been created to speed up cycloaddition pathways. These techniques mostly include the development of transition metal-promoted cycloadditions and improved Lewis acid-catalysis systems (21–23).

Then in the 20th Century many natural products, medications, and other organic molecules were synthesized using the Diels-Alder process (24). The control of regioselectivity, stereoselectivity, and reaction conditions was achieved by chemists using a variety of modifications and techniques (25), furthermore the results was successfully explained by frontier molecular orbital theory (26).

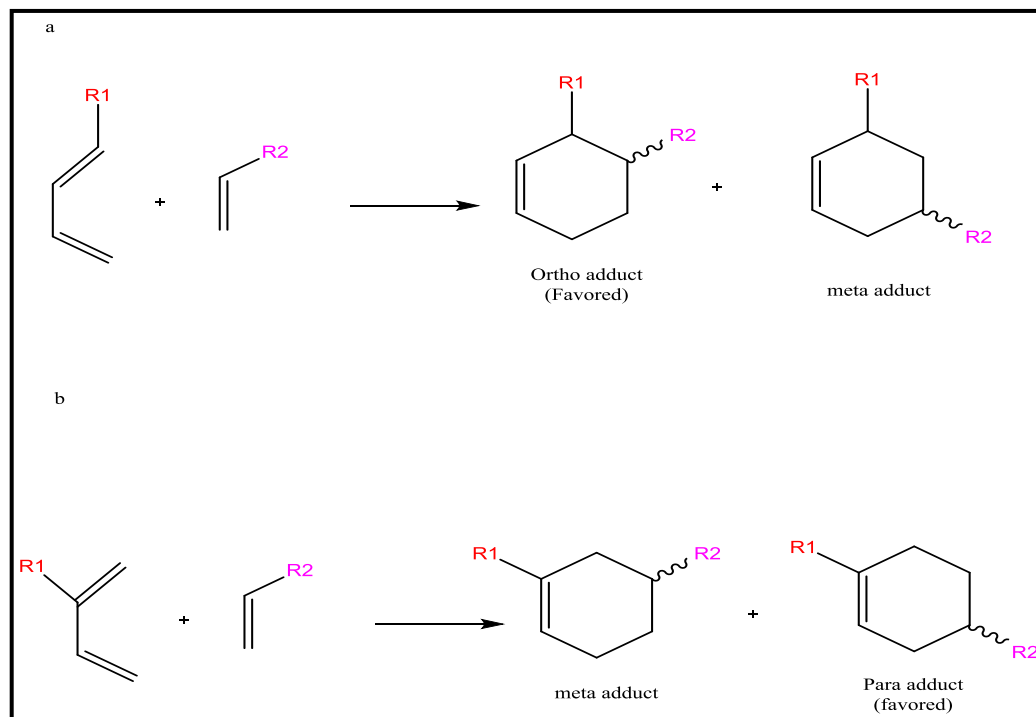
At the end, in the 21st century, researchers have been studied and improved the Diels-Alder reaction in several ways. One of the significant advancement in Diels-alder reaction was the development of the Diels-Alder catalysis, including asymmetric catalysis, natural enzymes, allows for the selective creation of one enantiomer over the other, resulting in chiral products (27). This has been particularly important in the production of pharmaceuticals and other bioactive substances. Additionally, Click chemistry has been widely applied in materials research, radiochemistry, bioconjugation, and drug development (28). Over the past few years, there has been a growing interest in developing bioorthogonal Diels-Alder operations, which are biologically compatible and can be utilized for *in vivo* imaging and selective labeling of biomolecules (29). As well as Researchers explored novel diene and dienophile substances in order to improve the Diels-Alder reaction's utilization. This involves the design of unusual

reactants to achieve specific regioselectivity and avoid steric hindrances (๑๐).

## 1.2.1. Types of Diels-Alder Reactions

### 1.2.1.1. Normal Diels-Alder Reaction

Organic chemistry has been using the Diels-Alder reaction for a wide range of purposes, from the synthesis of complicated natural products to the creation of biomaterials (๑๑). The traditional Diels-Alder reaction forms a six-membered ring when a conjugated diene is carrying an electron-donating group (EDG, X), combines with a substituted alkene (dienophile) carrying an electron-withdrawing group (EWG, Z) with good stereochemical and regio-control (๑๒). Dienes most likely react with dienophiles via the relatively low energy barrier (๑๓), HOMO-diene regulated traditional Diels-Alder reaction. It is possible to predict the process's regioselectivity using the well-known "*ortho-para*" rules (๑๔). When 1,3-dienes with a substituent at position 1 mostly generate monosubstituted dienophile "*ortho*" cyclohexene products Figure (1-๑a), whereas dienes with a substituent at position 2 mostly produce "*para*" products, Figure (1-๑b) (๑๕). Heating the diene and dienophile together or activating the dienophile with a Lewis acid catalyst are two methods for carrying out the coordinated pericyclic transition (๑๖).



Figure(1-5):The *ortho-para* rule

### 1.2.1.2. Inverse-Electron-Demand Diels-Alder (IEDDA)

#### Reaction

As opposed to a normal electron demand Diels-Alder reaction, the Inverse-Electron-Demand Diels-Alder (IEDDA) Reaction is an irreversible reaction between an electron-rich dienophile reacts with an electron-poor diene.

According to the frontier molecular orbital theory (FMO), the IEDDA reaction kinetics is controlled by the energy gap between the respective HOMO and LUMO of the reactants. In instance, any diene or dienophile combinations with a lower HOMO dienophile-LUMO diene energy differential will react faster in IEDDA reactions<sup>(10,11)</sup>, Figure (1-6).

The first reports of using the IEDDA reaction as a tool for modifying biomolecules were published by two groups in 2008 (27,28). Since then, a number of techniques have proved the broad use of biochemistry, including radiolabelling, cancer imaging, materials research and polymerization as well as in *vitro* and in *vivo* investigations for the modification of proteins, oligonucleotides, and sugars (29,30). In contrast to the traditional Diels-Alder reaction, the IEDDA reaction has more characteristics of a typical click reaction since it is more irreversible, has a greater reaction rate (31). Furthermore, it is one of the most common methods to obtain natural products, particularly because it makes it simple to construct the unique heterocyclic structures which these natural chemicals include. In fact, IEDDA reactions can be used to synthesize strychnine, absinthin, or xyloketal D from their respective, well-functionalized precursors (32).

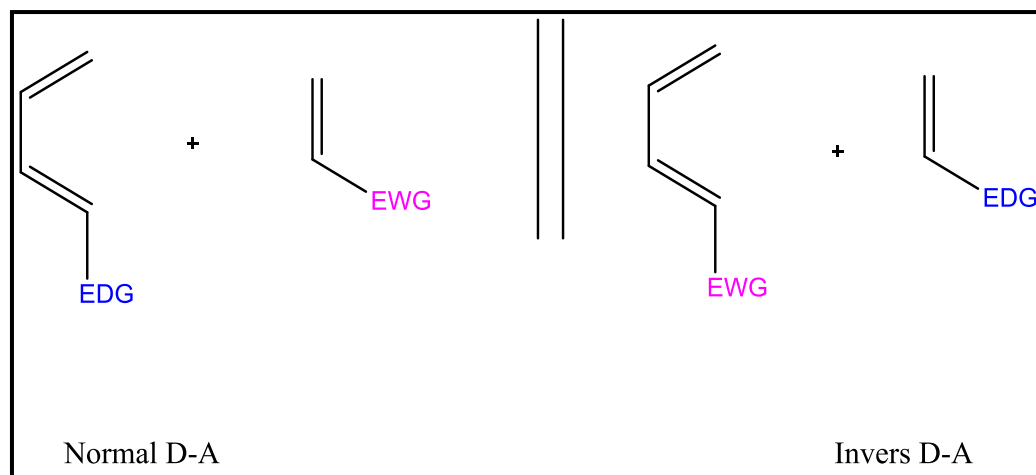


**Figure (1-6): The difference between Normal and Invers D-A**

### 1.2.1.3. Intramolecular Diels-Alder Reaction

When the diene and dienophile are components of the same molecule, a cyclic compound is formed in a single step (12). The intramolecular version of the Diels-Alder process has access to two different kinds of connectivity. When diene and dienophile bond together at position 1 of the diene (type 1), cycloaddition normally gives rise to a fused bicyclic adduct Figure (1-1a). In a second variation, diene and dienophile bind at diene position 2 (type 2), Figure (1-1b). In this case, cycloaddition leads to the creation of a bicyclic ring system which is bridged. Given a lack of techniques that can produce a bridging bicyclic structure from an acyclic precursor in a single step, the reaction has significant synthetic promise. The end product of the type 2 intramolecular Diels-Alder (type 2 IMDA) cycloaddition is an anti-Bredt alkene with a bridgehead double bond. Therefore, the reaction offers an easy strategy to explore this unique group of compounds (13).

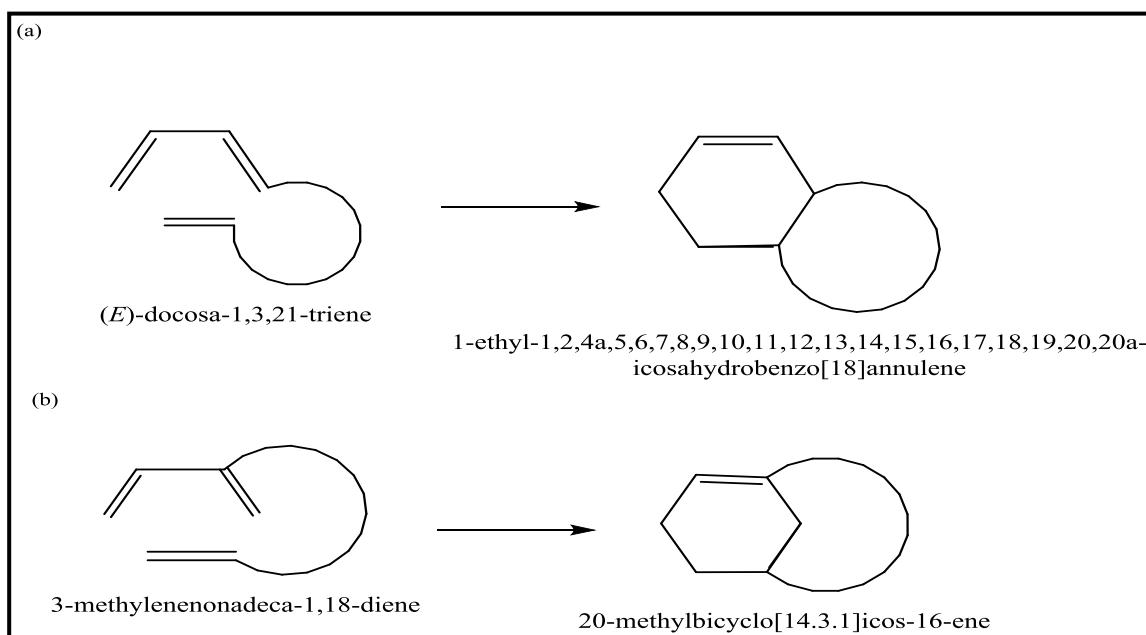


**Figure (1-1): Types of intramolecular Diels-Alder reaction**



### 1.2.1.4. Hetero-Diels-Alder Reaction

The hetero-Diels-Alder reaction is one of the most powerful ways for the production of optically active six-membered containing heteroatoms (such as oxygen, nitrogen, or sulfur) mono- and polycyclic hetero cycles, Figure (1-8), (64) with huge synthetic applications in natural or synthetic compounds with a broad variety of biological activity (60,66). The concurrent development of two carbon-carbon or carbon-heteroatom bonds produces the formation of up to four stereogenic centers in just one step from achiral dienes and dienophiles, causing this method one of the most interesting and attractive processes in asymmetric chemical synthesis. Recently, the Diels-Alder reaction has been expanded to include molecules with C=P, C=N, and C=O functional groups (67). At the same time, the phospho D-A reaction became somewhat less attention than the asymmetric carbo-, oxa-, and aza-Diels-Alder reactions, Although, Its possible use to produce P-chiral cyclic phosphines for application in asymmetric homogeneous catalysis as well as new pharmaceuticals (68).

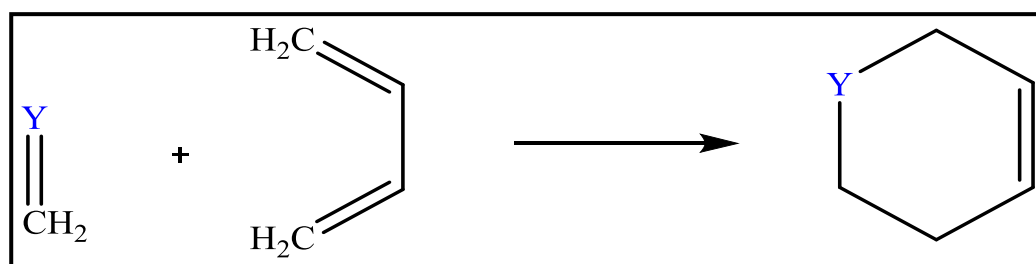


**Figure (1-8): The cycloaddition of 1,3-butadiene and hetero-dienophile D-A Reactions**

### 1.2.1.5. Tandem or Cascade Diels-Alder Reaction

Cascade techniques are considered as an enabling approach to chemical synthesis. The construction of multiple carbon-carbon bonds in a single chemical step in the same reaction vessel provides an extremely efficient approach for the synthesis of complex molecular structures, generating bridged or polycyclic structures containing multiple adjacent stereocenters, without having to isolate intermediates before each subsequent reaction in the pathway (79).

In the context of multiple chemical reactions, “tandem” can therefore be taken to indicate two reactions which follow one another. The diene of the D-A reaction can often be difficult to handle since certain dienes are prone to rapid decomposition or polymerization when isolated. As a result, extensive research has been focused on the production and in situ applications of specific dienes. The cascades can be further classified into (a) reaction sequences in which both diene-dienophile pairs are present in the starting compounds and (b) a necessarily “sequential” pathway in which the first cycloaddition produces a new diene or dienophilic alkene which can then undergo a second cycloaddition reaction (80). As well as Cascade reactions are frequently referred to as domino reactions for the reason that each step of the sequence depends on the functionality produced directly in the previous step (81).

In addition cascade cycloadditions are a subset of tandem cycloadditions that require neither the addition of reagents or the alteration of reaction conditions (82).

### 1.2.1.6. The Retro Diels-Alder Reaction

The retro-Diels-Alder reaction involves the cleavage of a cyclic molecule to regenerate the starting diene and dienophile rather than creating a cyclic product by the coordinated cycloaddition of a diene and a dienophile (V<sup>3</sup>) Figure (1-9). The D-A reaction and the rD-A reaction were initially observed at about the same time. Due to the challenging reaction conditions involved, the reverse reaction still gets relatively little focus (V<sup>4</sup>). Even with its limited popularity, the rD-A reaction has developed into a valuable instrument and is still the method of choice for creating a variety of reactive olefin or metastable molecules. Due to the endothermic requirements of rD-A, high temperatures are sometimes used, which causes the products sometimes break down. A rD-A reaction can only occur under certain circumstances, such as flash-vacuum pyrolysis (FVP), shock tube, photochemical (laser) activation, and gamma radiation. Even though there are many benefits to these techniques, it is common for the final products to change (V<sup>5</sup>).

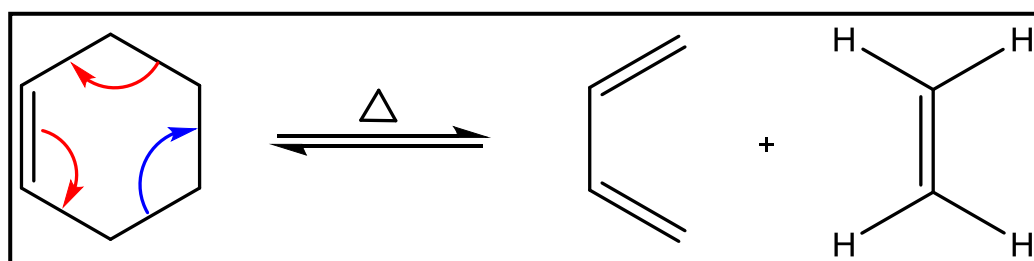


**Figure (1-9): The Retro Diels–Alder reaction**

## 1.2.2. Catalyzing of Diels-Alder Reaction

### 1.2.2.1. Chemical Catalysis

Chemical catalysis in Diels-Alder processes can occur through a variety of mechanisms and with different catalysts:

#### 1.2.2.1.1. Lewis Acid Catalysis:

Lewis acids such as transition metal complexes (e.g., aluminum, tin, titanium) and other metal salts (e.g., Boron trifluoride, copper sulfate zinc chloride) (16) can catalyze. Diels-Alder reactions occur through interaction with the dienophile. These LA-catalyzed cycloadditions are not just quicker than their un-catalyzed counterparts, however, also more regio and stereoselective. According to the Frontier Molecular Orbital (FMO) theory and the large number of mechanistic studies on these chemical reactions, it is recently commonly known that the donor-acceptor interaction generated between the dienophile and the LA-catalyst produces an excellent stability of the dienophile. LUMO, which is eventually turned into a smaller HOMODiene-LUMODienophile energy gap, as a result, to a lower reaction barrier as compared to the uncatalyzed reaction (17).

#### 1.2.2.1.2. Brønsted Acid Catalysis

Brønsted acids can catalyze Diels-Alder reactions by protonating either the diene or dienophile. This facilitates their contact while also decreasing the reaction's activation energy and controlled the regio-, chemo-, and stereoselectivities (18). The enhancement of D–A reactions by acid catalysts

is commonly described using frontier molecular orbital (FMO) theory. When an acid catalyst exists, it can significantly reduce the HOMO-LUMO energy gap by coordinating with positions of high electron density (<sup>9</sup>).

Traditional homogeneous protonic acids (Brønsted acids) such HOAc, H<sub>3</sub>PO<sub>4</sub>, HCl, HNO<sub>3</sub>, and H<sub>2</sub>SO<sub>4</sub> have significantly improved catalytic performance. However, these liquid acids used in homogenous industrial catalytical processes are often poisonous and corrosive, have a high regeneration or quenching cost, and produce a huge number of undesirable byproducts and wastes. Otherwise, solid Brønsted acid catalysts are gaining popularity due to their low corrosivity, ease of handling, and high activity and selectivity (<sup>10</sup>).

### 1.2.2.1.3. Metal Catalysis

Transition metal complexes, particularly those based on ruthenium, palladium, or rhodium, as well as chiral ligands, such salen and oxazoline, may accelerate the production of stereoisomeric cyclic molecules when coordinated with metal ions such as Cr(III), Ni(II), Cu(II), Mg(II), and Ti(IV). Lanthanides and other metal salts can catalyze Diels-Alder processes by a variety of mechanisms, including oxidative addition, ligand exchange, or substrate coordination (<sup>11</sup>). These catalysts allow for extremely regio- and stereocontrolled cycloadditions. Selective catalysis with transition metal complexes typically necessitates the transfer of structural information from another ligand to a transition metal center. Recent research has shown that these complexes can influence site selectivity by improving additions and cycloadditions to diens' distant  $\pi$ -bonds (<sup>12</sup>).

### 1.2.2.1.4. Organocatalysts

Some organic compounds can catalyze Diels-Alder reactions using hydrogen bonding or other non-covalent interactions. As an example, chiral amines and amino acids have been utilized as organocatalysts in enantioselective Diels-Alder reactions (<sup>13</sup>).

### 1.2.2.2. Biological catalysis

#### 1.2.2.2.1. D-A Reactions Catalyzed by Antibodies

For over a decade, scientists have recognized that the immune system is a abundant source of unique and highly effective catalysts for typical chemical synthesis reactions. Antibodies chosen specifically to bind the transition state (T.S) of a particular process and increase its rate are known as catalytic antibodies (<sup>14</sup>). The main aim is to generate monoclonal antibodies that are specifically designed to bind a hapten molecule that mimics the reaction's T.S. via using small molecules known as haptens, Figure (1-10). The hapten is logically designed for a specific targeted chemical reaction, hoping that the reaction will be catalyzed by the antibody it elicits. As well as several groups have successfully produced unique antibodies for the catalysis of the D-A reaction using mammalian immune systems (<sup>15</sup>). This method was quickly dropped in favor of computational design and artificial metalloenzymes, even though catalytic antibodies in D-A reactions showed promising results. This strategy's limit to a single scaffold is one of its drawbacks. Furthermore, the synthesis of certain monoclonal antibodies through mammalian vaccination and the challenging

synthetic availability of hapten molecules seem to be significant obstacles to the development of antibody-based D-Aases (V).

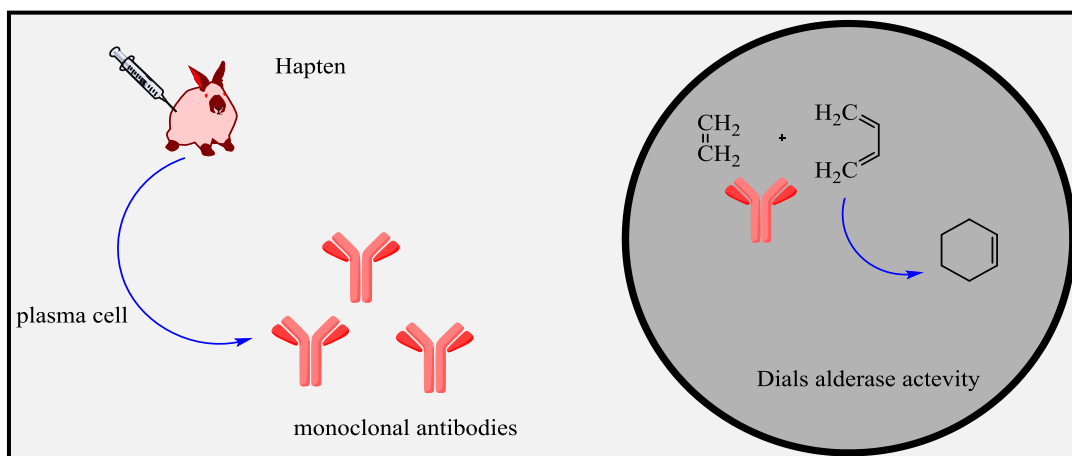


**Figure (1-10): Strategy used for the generation of catalytic monoclonal antibodies**

### 1.2.2.2.2. De novo computational enzyme design

Several research teams have now successfully designed enzyme functions computationally from beginning for a variety of chemical reactions with different mechanisms (86). The computational enzyme design technique may utilize any given scaffold that has known structures, making it ideal for directed evolution. Recent years have seen significant advancements in computational enzyme design due to the creation of methods for accurate protein structure modeling, protein stability prediction, and protein-ligand interaction prediction (87-89). This integrated strategy has been proven for several reactions, including the retro-aldol reaction, Kemp elimination, and Diels-Alder reactions. The first step in the

computational design process is to create a minimum active site shape with specific protein residues to stabilize the predicted T.S for the desired reaction by non-covalent interactions (also known as theozyme). Next, a protein that can be further improved is computationally picked and adapts to the TS while protecting it from the surrounding medium technology (90–93), but instead of using a synthetic hapten to choose a protein template, a computationally produced TS is employed. Despite of the fact that de novo design of active sites for basic reactions has been accomplished with some promising results, attempts to develop enzyme catalysts for energetically demanding processes such as hydrolysis and Claisen rearrangements have encountered challenges.

In case, such approach can avoid the combinatorial explosion was caused by fitting active sites in scaffolds but the geometrical links between the transition state and the catalytic residues that enable catalysis can't always be achieved experimentally. In these instances, the enzyme will show no activity in the new process, there for, The complex active site model for reactions was presented to generate preorganized active sites for actual design, This model include not just the transition state and catalytic residues, nevertheless the residues that stabilize them (94).

### **1.2.2.2.3. D-A Reactions Catalyzed by Artificial Metalloenzymes**

The term "metalloenzyme" refers to a biocatalyst that contains transition metal (or zinc) ions as a cofactor in a protein scaffold. Metal ions are anchored in the protein core by amino acid residue coordination or as a



metal complex cofactor such as heme. Metalloenzymes can show powerful catalytic activity in water under milder condition, allowing them to mediate a variety of bioreactions in *vivo* (metabolism, respiratory chain, etc, ) because their highly organized protein structure may provide a precise catalytic site by controlling the orientation and position of its cooperating amino acid residues. Otherwise, The chiral environment offered by L-amino acid residues, as well as the restricted region within the protein core, contribute to these processes' stereo- and regioselectivity (94). Artificial metalloenzymes based on protein scaffolds have been created through chemical modification, genetic mutation, or metal cofactor substitution of natural metalloenzymes. additionally, The association of a synthetic metal complex and a protein is another useful way for creating artificial metalloenzymes (95-99).

In order to localize metallocofactors within the host protein-provided well-defined second coordination sphere environment, four complementary techniques have been proposed, Figure (1-11).

- 1- Covalent anchoring: Similar to well-known bioconjugation methods, covalent anchoring is a high-yielding, irreversible interaction between an amino acid side-chain on the protein scaffold and cofactors with reactive functional groups (V) Figure (1-11a).
- 2- Supramolecular anchoring: takes advantage of the great affinity that certain proteins have for a small number of substrates, natural cofactors, or noncovalent inhibitors. These are sometimes covalently modified with the cofactor to preserve a high affinity, which

guarantees the cofactor's quantitative localization within the host protein (•••) Figure (1-11b).

- Ƴ- Dative anchoring: The mechanism of dentate anchoring is based on the coordination of a coordinately unsaturated metal center with a nucleophilic amino acid residue (Cys, His, Ser, Asp, Glu, etc.). Covalent or supramolecular approaches are frequently enhanced by this kind of metal activation and anchoring (•••) Figure (1-11c).
- ξ- Metal Substitution: Metal substitution is based on the carefully designed active site of natural metalloenzymes and the unique reactivity of non native metals. The ArM's repertoire can include new-to-nature reactivities after the metal is substituted (•••) Figure (1-11d).

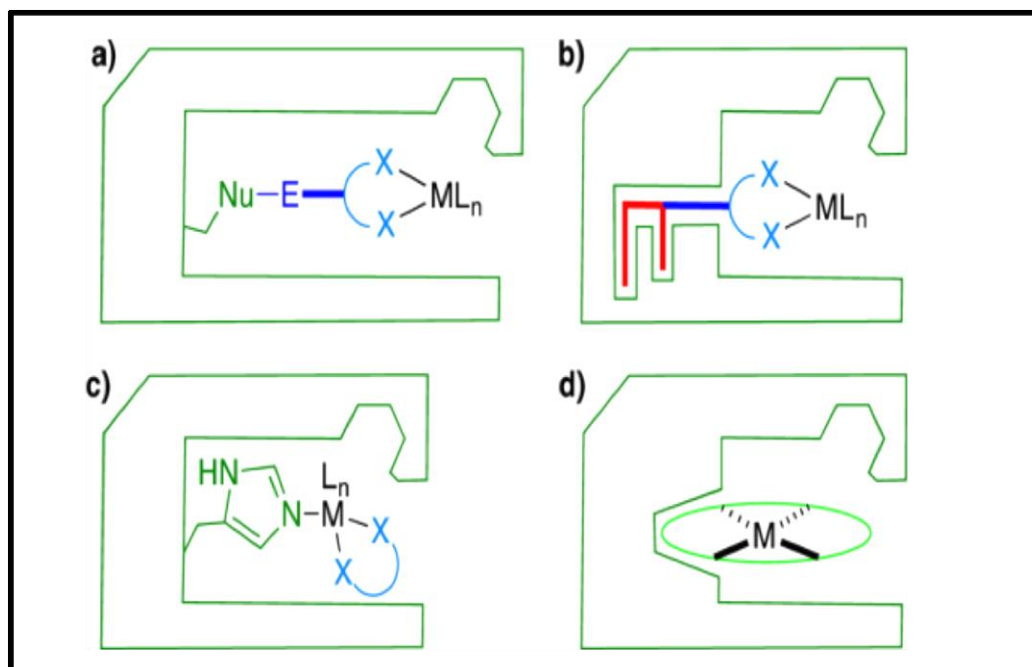


**Figure (1-11): Protein scaffold, an abiotic cofactor can be stably localized using four different anchoring techniques. (a) covalent, (b) supra molecular, (c) dative, (d) metal substitution (16).**

Selecting the right scaffold is a major challenge in creating an artificial metalloenzyme. Even more in many situations, artificial D-Aases incorporating metal showed reduced selectivity when compared to other DAases without any optimization. However, it should be mentioned that no optimization procedures have been done to DAases that contain metal. Artificial metalloenzymes have been widely created to catalyze redox reactions, which frequently require a redox-active metal center, in addition to the D-A reaction (101)(16). While artificial metalloenzymes have been optimized through the application of evolutionary techniques, metallo-D-Aases have not been subjected to similar strategies (102, 103).

#### 1.2.2.2.4. Natural Diels-Alderases

Biosynthetic enzymes produce unique activities, increasing the structural diversity of natural products and promoting host organisms. There has been a lot of interest in research on Diels-Alderases (DAs), which are functionally distinct enzymes that catalyze [ $\xi + \eta$ ] cycloaddition processes in addition, the Diels-Alder reaction. Initial research indicates that these DAs originated from a predecessor that acted as an oxidocyclase (OC) dependent on flavin adenine dinucleotide (FAD) that catalyzes the oxidative cyclization processes of phenolic compounds (104). However, only a few such enzymes

have been found. Genome mining has shown to be an effective technique for identifying new Diels-Alderase from microbial natural product biosynthesis pathways since the discovery of the first stand-alone Diels-Alderase, SpnF, in 2011 (105). On the other hand, since plants have large genomes and few biosynthetic gene groups, it is more difficult to find Diels-Alderase from them using genome mining techniques. There are at least nine biosynthetic systems have been found to contain natural enzymes that are believed to act as the primary cyclase in biosynthetic transformations that mimic Diels-Alder-type structures or biosynthetic formal [4+2] cycloadditions (22). Approximately 100 diverse Diels-Alder (D-A)-type cycloadducts have been identified in natural compounds, including polyketides, alkaloids, isoprenoids, and phenylpropanoids. So far, a variety of enzymes have been identified to catalyze Diels-Alder (D-A) processes. These include the monofunctional D-As PyrE3 (106) and SdnG (107), as well as the multifunctional D-As EupfF (108), LepI (109), and SpnF, (110, 111). The previously documented D-As belong to numerous protein families, including polyketide synthases, lipocalins, malate synthases, FAD-dependent oxidases, and SAM-dependent methyltransferases (112).

#### 1.2.2.2.4.1. **Moraceae family**

Mulberry tree is one of the common plant of the genus *Morus* which is widely grown in China and Japan. In addition, Moraceous plants are a great resource for isolating stilbenes, 3-arylbenzofurans, flavonoids, and a new family of D-A type natural compounds, which contains over 100 members with a variety of biological activities, including antiphlogistic, diuretic, expectorant, laxative (113), anti-diabetic and (114, 115) anti-microbial

properties<sup>(116)</sup> and inhibitory effects on digestive enzymes (pancreatic lipase,  $\alpha$ -amylase and  $\alpha$ -glucosidase) <sup>(117)</sup>. The studies showed The callus of *Morus alba* cells contains two FAD-dependent enzymes that are crucial to the biosynthesis process: *Morus alba* moracin C oxidase (MaMO) and *Morus alba* Diels-Alderase (MaDA), which resemble berberine bridge enzymes (BBE). Among these, MaMO catalyzes the diene-producing oxidative dehydrogenase process, which is followed by the intermolecular Diels-Alder reaction that produces the D-A product. In contrast with many BBE-like enzymes, which normally require FAD as a cofactor to catalyze several oxidation processes <sup>(118)</sup>, MaDA have ability to catalyze non-redox D-A reactions of different dienophiles and different types of natural and artificial polyphenolic dienes <sup>(119)</sup>. The enzymic reserches contributed to employ Diels-Alderase enzymes for unique endo- or exo-selective in the chemoenzymatic synthesis of a wide variety of synthetic and natural DAAs <sup>(120)</sup>. Since the previously isolated MaDA did not catalyze the D-A conversion to DAAs with an exo-configuration, it only showed endo-selectivity. Moreover, it was shown that the MaDA enzymes had great enantioselectivity when it came to catalyzing the Diels–Alder reaction, producing only enantiopure products (with ee > 98%) with high stereoselectivity <sup>(121,122)</sup>.

### 1.2.3. Aim and Objectives of Study

- 1- This study aims to apply the friendly environmental method to Synthesis new organic compounds by Diels-Alder reactions between anthracene derivatives as dines and pyrrole derivatives as dienophiles which have pharmaceutical application, in presence of alba Diels-Alderase (MaDA) as catalyst.
- 2- The objective of the project is achieve endo-selectivity for the product.
- 3- This work includes monitoring the kinetics of the enzymatic Diels-Alder reactions. During this study, all the conditions which may impact on the enzymatic reaction such as the temperature, and the concentration of substrate will be studied. The appropriate mechanism for this enzymatic reaction will be suggested

*Chapter Two*

*Materials and Methods*

## 2. Materials and Methods

This study was conducted in the laboratory of postgraduate, University of Karbala, College of Science, Department of Chemistry. The melting point measurements were performed in University of Karbala, College of Education. The mass-spectroscopy measurements were performed using LC-MS Agilent Infinity 1260, in the laboratory of Institution of Science Institute of Organic Chemistry, N.D. Zelinsky Russian Academy of Science, Moscow, Russia. The Nuclear Magnetic Resonance (NMR) were carried out using Avance III 400 MHz NMR spectrometer, in the laboratory of postgraduate, Department of Chemistry, College of Science, University of Basra, Basra, Iraq. All substrate and enzyme were provided by Hunan Chemfish Pharmaceutical Co., Ltd, Tokyo, Japan.

### 2.1. Chemical and Materials

The materials and chemicals used in this study are listed in Table (2-1):

Table (2-1): Chemicals and their origin

No.	Materials	Company
1-	1-Methyl-1 <i>H</i> -pyrrole-2,5-dione (97%)	Hunan chemfish Pharmaceutical
2-	1-Propyl-1 <i>H</i> -pyrrole-2,5-dione (98%)	Hunan chemfish Pharmaceutical
3-	2-(2,5-Dioxo-2,5-dihydro-1 <i>H</i> - pyrrol-1-yl) acetic acid (97%)	Hunan chemfish Pharmaceutical



٤-	٩,١٠-Diphenylanthracene (٩٨٪)	Hunan chemfish Pharmaceutical
٥-	٩-Anthraceneboronic acid (٩٨٪)	Hunan chemfish Pharmaceutical
٦-	٩-Anthracenemethanol (٩٨٪)	Hunan chemfish Pharmaceutical
٧-	Absolute Ethanol	Romil \ UK
٨-	Acetone	Romil \ UK
٩-	Acetonitrile	Romil \ UK
١٠-	Deionized water	
١١-	Diethyl ether	Romil \ UK
١٢-	Dimethyl formamide	Romil \ UK
١٣-	Dimethyl sulfoxide (DMSO)	Romil \ UK
١٤-	Isopropanol	Romil \ UK
١٥-	Methanol	Romil \ UK
١٦-	Morus alba Diels-Alderase	Hunan chemfish pharmaceutical
١٧-	Propanol	Romil \ UK
١٨-	Tetrahydrofuran (THF) ( ٩٩٪)	HIMEDIA

### 2.1.1 Instrument and Equipment:

All the instruments and equipments that used in this study are summarized in Table (2-2)

**Table (2-2): The devices and their Suppliers**

No.	The device	Supplier
1-	Avance III 400 MHz NMR spectrometer	N.D Zelinsky Russian
2-	Electronic Balance	220-ε\ KERN \UK
3-	Fourier transform infrared (FTIR)	Shimadzu (400 S) \ Japan
4-	Hot plate stirrer	Lab Tech \ Korea
5-	Mass spectrometer	N.D Zelinsky Russian
6-	Oven	Memmert \ Germany
7-	pH-meter	
8-	Schlink line	Newcastle University Workshop \ UK
9-	Spectrophotometer	FAIT HFUL \771\ China
10-	UV-Visible spectrophotometer	UV-1800\Shimadzu \ Japan
11-	Vacuum pump	TW -1.0 A\ China

## 2.2. Subjects and Methods

### 2.2.1. Preparation of *Morus alba* Diels-Alderase (MaDA)

The (0.1g, 10.1U/mg) of MaDA enzyme was dissolved in 10 mL of deionized water at pH around (6.1-6.4).

### 2.3. Preparation and Monitoring the Kinetic Parameters of Meso 9-(hydroxymethyl)-10-methyl-9,10-dihydro-12H,14H-9,10-(epiethane[1,1,2]triazolanoethane[1,2,2]triazyl)anthracene-12,14-dione (P1)

#### 2.3.1 Preparation of Meso 9-(hydroxymethyl)-10-methyl-9,10-dihydro-12H,14H-9,10-(epiethane[1,1,2]triazolanoethane[1,2,2]triazyl)anthracene-12,14-dione (P1)

The experiment of D-A reaction was carried out in an inert environment in the presence of nitrogen as an inert gas and completely isolated from the atmosphere using the Schlink line technique. 0.5 mL of MaDA was added to mixture of 1 mmol of both anthracen-9-ylmethanol (D1) and 1-methyl-1H-pyrrole-2,5-dione (Dp1) dissolved in 50 mL of tetrahydrofuran (THF). The mixture was stirred for 1.0 hour at 40°C. The color of the mixture was light brown and gradually converts into pale yellow precipitate as shown in Figure(2-1).



**Figure (2-1): An image showing the change in the color of the reaction mixture from light brown to pale yellow**

At the end of the reaction, the main product was isolated from the solvent by an air-vacuum filter filled with nitrogen. The product separated on the filter surface while the solvent separated down the filter to the reactor as indicated in Figure (2-2a) and purified by using recrystallization method by using Ethanol as solvent. The purity of this product and the other compounds have been prepared was checked using thin layer chromatography method by using n-hexane and ethyl acetate, Figure (2-2b).

The main yield of the reaction was (94%). All isolated products were isolated and characterized by nuclear magnetic resonance (NMR), FTIR, Mass, and UV/Vis. spectroscopies. The scheme of the formation of D-A reaction for P<sub>1</sub> shown in Figure (2-3).

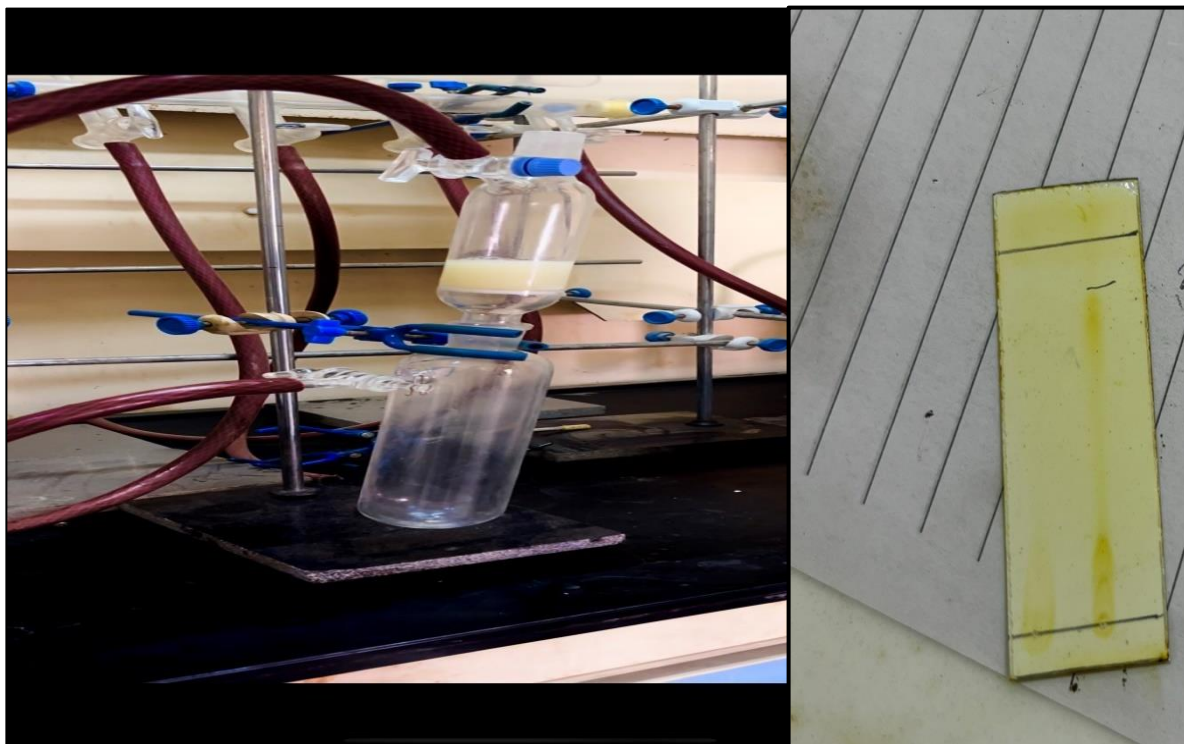


**Figure (2-2): (a) The filtration technique which was used to separate the reaction products from the solvent, where the pale yellow ppt. on the filter surface is the product, while the solvent in the reactor, (b) The TLC technique.**

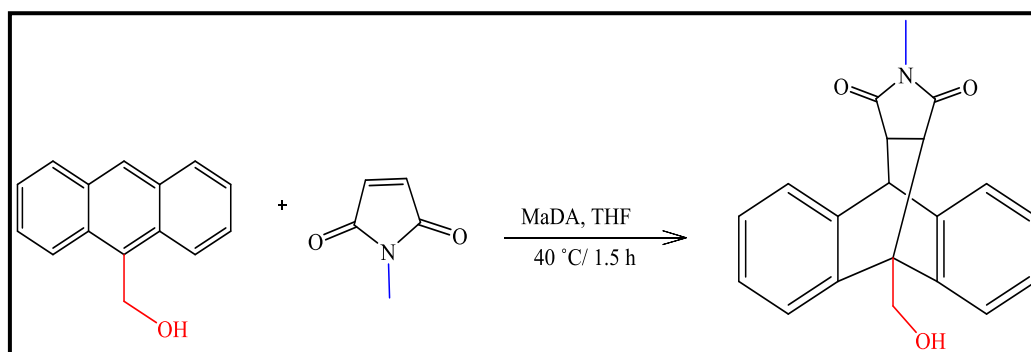


**Figure (2-3): The main product P, of D-A reaction**

Furthermore, the solubility of P<sub>1</sub> was listed in the Table (۲-۳):

**Table (۲-۳): The solubility of P<sub>1</sub>**

Solvent	Solubility
Acetone	Soluble
Acetonitrile	Soluble
DMF	Soluble
DMSO	Soluble
Ethanol	Partially soluble
Ether	Insoluble
Isopropanol	Partially soluble
Methanol	Partially soluble
Propanol	Partially soluble
THF	Soluble

### ۲.۳.۲. Preparation of P<sub>1</sub> Solutions:

The ۱ mM stock P<sub>1</sub> solution was prepared by dissolving (۰.۰۰۷۹ g) of P<sub>1</sub> in ۲۰ mL of THF, the set of different concentrations solutions were prepared (۰.۰۰۰, ۰.۰۱, ۰.۰۲, ۰.۰۳, ۰.۰۴, ۰.۰۵) mM.

### 2.3.3. Determination the appropriate concentration for Anthracen-9-ylmethanol and 1-Methyl-1*H*-pyrrole-2,5-dione (P<sub>1</sub>) (Michaelis-Menten Equation)

The experiments of reaction between anthracen-9-ylmethanol(D<sub>1</sub>) and 1-methyl-1*H*-pyrrole-2,5-dione (Dp<sub>1</sub>) in the presence of the MaDA as a catalyst for each of the concentrations (0.1, 0.2, 0.3, 0.4, 0.5) mM, at a temperature of (30) °C and specific enzymatic activity (0.1 U/mg) of the MaDA enzyme, where the color of the reaction mixture was brown, The reaction was followed up by withdrawing 1 mL of the mixture every 5 minutes and measuring its absorbance by spectrophotometer analyzer after fixing the wavelength at 370 nm, and continue until almost constant readings of absorbance are obtained. Then, after observing the results, the ideal substrates concentration were reached at the concentration (0.5 mM) for (D<sub>1</sub>) and (0.2 mM) for (Dp<sub>1</sub>) that provides the optimum data during work. In addition, for drawing the Michaelis –Menten equation to find the Michaelis constant (K<sub>m</sub>), or the velocity at which the Michaelis-Menten equation's maximum velocity equals half.

### 2.3.4. Determination of Optimal MaDA Enzyme Activity for P<sub>1</sub>

Furthermore, the enzymatic experiments of P<sub>1</sub> were carried out under completely emptied conditions of atmospheric air as well and in the presence of nitrogen as an inert gas with the presence of MaDA by applying different specific activities of MaDA (0.1, 0.2, 0.3, 0.4, and 0.5) U/mg after stabilizing

the concentration of the substrates at 1.0mM of D<sub>1</sub> and 0.5mM Dp<sub>1</sub>, The temperature at 30°C and, apply the same steps in the previous enzymatic experiments and following the absorbance readings after fixing the wavelength at 370 nm. (1.0) U/mg is the appropriate enzymatic activity for this reaction.

### 2.3.5. Thermodynamic Study for P<sub>1</sub>

After determining the appropriate concentration for both D<sub>1</sub> and Dp<sub>1</sub> and the specific activity of MaDA, the rate of the reaction was monitored at different temperatures (10, 20, and 30) °C, by mix 1.0 mM of D<sub>1</sub> and 0.5 mM of Dp<sub>1</sub> with (1.0) U/mg of MaDA for each experience. the absorbance was monitored every 5 minutes until get stable or nearly close readings. It was found that 20°C is the best temperature suitable for the enzymatic reaction. In addition, the change in enthalpy ( $\Delta H$ ), the change in Gibbs free energy ( $\Delta G$ ), and the change in entropy ( $\Delta S$ ) have been measured.

### 2.4. Preparation and Monitoring the Kinetic Parameters of

Meso 9-(hydroxymethyl)-13-propyl-9,10-dihydro-12H,14H-9,10-

(epiethane[1,1,2]triazolanoethane[1,2,2]triazyl)anthracene-12,14-dione (P<sub>1</sub>)

2.4.1. Preparation of Meso 9-(hydroxymethyl)-13-propyl-9,10-dihydro-12H,14H-9,10-



**(epiethane[1,1,2]triazanoethane[1,2,2]triazyl)anthracene-1,2,3-dione (P<sub>7</sub>)**

The experiment of D-A reaction between anthracen-9-ylmethanol (D<sub>1</sub>) and 1-propyl-1*H*-pyrrole-2,5-dione (Dp<sub>7</sub>) performed by using the same methodology mentioned above and under the same conditions, Figure (2-4). The color of the mixture was light brown and gradually converts into pale yellow precipitate. The product purified by using recrystallization method using acetone and the main yield of the reaction was (93%).

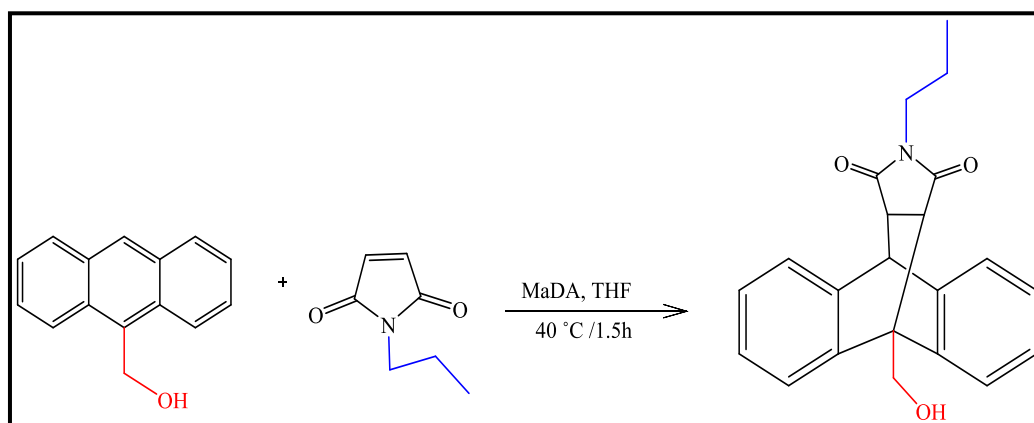


**Figure (2-4): The main product P<sub>7</sub> of D-A reaction**

Furthermore, the solubility of P<sub>7</sub> was listed in Table (2-4):

**Table (2-4): The solubility of P<sub>7</sub>**

Solvent	Solubility
Acetone	Partially soluble
Acetonitrile	Partially soluble
DMF	Soluble

DMSO	Soluble
Ethanol	Insoluble
Ether	Insoluble
Isopropanol	Partially soluble
Methanol	Insoluble
Propanol	Partially soluble
THF	Soluble

#### 2.4.2. Preparation of P<sub>r</sub> Solutions:

The 1 mM stock P<sub>r</sub> solution was prepared by dissolving (0.0086g) of P<sub>r</sub> in 20 ml of THF, the set of different concentrations solutions were prepared (0.005, 0.01, 0.02, 0.03, 0.04, 0.05) mM.

#### 2.4.3. Determination the appropriate concentration for anthracen-9-ylmethanol (D<sub>r</sub>) and 1-propyl-1H-pyrrole-2,5-dione (Dp<sub>r</sub>) (Michaelis-Menten Equation)

The experiments of reaction between anthracen-9-ylmethanol (D<sub>r</sub>) and 1-propyl-1H-pyrrole-2,5-dione (Dp<sub>r</sub>) carried out under the same conditions with the same methods as previously mentioned and specific enzymatic activity (0.1) U/mg of the MaDA enzyme, where the color of the reaction mixture was brown. Then, after observing the results, after fixing the wavelength at 360 nm, and continue until almost constant readings of absorbance are obtained. the ideal substrates concentration were reached at

the concentration (0.0 mM) for ( $D_1$ ) and (0.5 mM) for ( $D_{p_1}$ ) that provides the optimum data during work. In addition for drawing the Michaelis-Menten equation to find the Michaelis constant ( $K_m$ ), or the velocity at which the Michaelis-Menten equation's maximum velocity equals half.

#### **2.4.4. Determination of Optimal MaDA Enzyme Activity for $P_1$**

In addition, the enzymatic studies of  $P_1$  were carried out under fully emptied conditions of atmospheric air, as well as in the presence of nitrogen as an inert gas with the presence of MaDA by applying varies MaDA specific activities (0.1, 0.2, 0.3, 0.4, and 0.5) U/mg. After stabilizing the substrate concentrations at 0.0 mM  $D_1$  and 0.5 mM  $D_{p_1}$ , the temperature at (30)°C, the previous enzymatic tests was repeated, and take absorbance values after setting the wavelength at 360 nm. (0.4) U/mg is the correct enzymatic activity for this process.

#### **2.4.5. Thermodynamic Study for $P_1$**

After determining the appropriate concentration for both  $D_1$  and  $D_{p_1}$  and the activity of MaDA, the rate of the reaction was monitored at different temperatures (10, 20, and 30) °C, by mix 0.0 mM of  $D_1$  and 0.5 mM of  $D_{p_1}$  with (0.4) U/mg of MaDA for each experience. the absorbance was monitored every 0 minutes until getting stable or nearly close readings. It was found that 30°C is the best temperature suitable for the enzymatic reaction. In addition, the change in enthalpy ( $\Delta H$ ), the change in Gibbs free energy ( $\Delta G$ ), and the change in entropy ( $\Delta S$ ) have been measured.

**2.5. Preparation and Monitoring the Kinetic Parameters of Meso 9-(hydroxymethyl)-12,14-dioxo-9,10-dihydro-13H-9,10-(epiethane[1,1,2]triazolanoethane[1,2,2]triazyl)anthracen-13-yl)acetic acid (P<sub>r</sub>)**

**2.5.1. Preparation of Meso 9-(hydroxymethyl)-12,14-dioxo-9,10-dihydro-13H-9,10-(epiethane[1,1,2]triazolanoethane[1,2,2]triazyl)anthracen-13-yl)acetic acid (P<sub>r</sub>)**

The experiment of D-A reaction between anthracen-9-ylmethanol (D<sub>1</sub>) and 2-(2,5-dioxo-2,5-dihydro-1H-pyrrol-1-yl)acetic acid (Dp<sub>r</sub>) were performed by using the same methodology mentioned above and under the same conditions, Figure(2-5). The color of the mixture was light brown and gradually converts into pale yellow precipitate. The product purified by using recrystallization method using Ethanol and the main yield of the reaction was (57%).

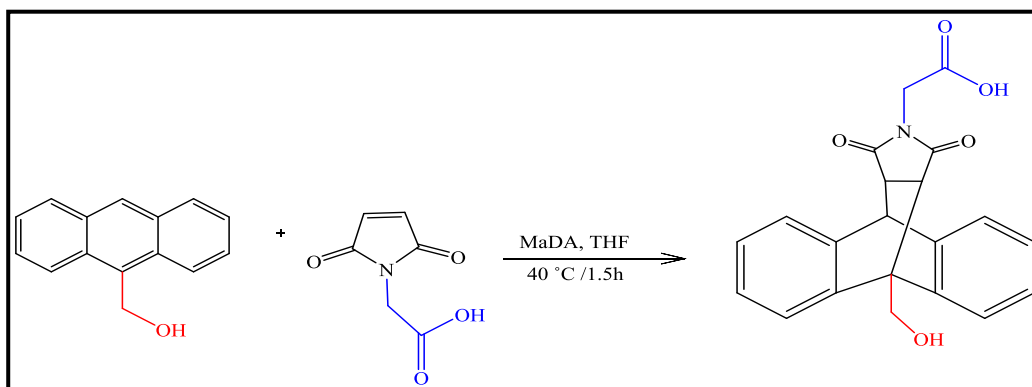


**Figure (2-5): The main product P<sub>r</sub> of D-A reaction**

Furthermore, the solubility of P<sub>r</sub> was listed in Table (2-5):

**Table (2-5): The solubility of P<sub>r</sub>.**

Solvent	Solubility
Acetone	Soluble
Acetonitrile	Insoluble
DMF	Soluble
DMSO	Soluble
Ethanol	Partially soluble
Ether	Insoluble
Isopropanol	Partially soluble
Methanol	Soluble
Propanol	Partially soluble
THF	Soluble

**2.5.2. Preparation of P<sub>r</sub> Solutions:**

The 1 mM stock P<sub>r</sub> solution was prepared by dissolving (0.009g) of P<sub>r</sub> in 20 ml of THF, the set of different concentrations solutions were prepared (0.005, 0.01, 0.02, 0.03, 0.04, 0.05) mM

### 2.0.3. Determination of appropriate concentration for anthracen-9-ylmethanol ( $D_1$ ) and 2-(2,6-dioxo-2,6-dihydro-1H-pyrrol-1-yl)acetic acid ( $D_{P_1}$ ) (Michaelis-Menten Equation)

The experiments of reaction between anthracen-9-ylmethanol ( $D_1$ ) and 2-(2,6-dioxo-2,6-dihydro-1H-pyrrol-1-yl)acetic acid ( $D_{P_1}$ ) carried out under the same conditions with the same methods as previously mentioned and specific enzymatic activity (0.1) U/mg of the MaDA enzyme, where the color of the reaction mixture was brown. Then, after observing the results, after fixing the wavelength at 360 nm, and continue until almost constant readings of absorbance are obtained. The ideal substrates concentration were reached at the concentration (0.3 mM) for ( $D_1$ ) and (0.2 mM) for ( $D_{P_1}$ ) that provides the optimum data during work. In addition for drawing the Michaelis-Menten equation to find the Michaelis constant ( $K_m$ ), or the velocity at which the Michaelis-Menten equation's maximum velocity equals half.

### 2.0.4. Determination of Optimal MaDA Enzyme Activity for $P_1$

In addition, the enzymatic studies of  $P_1$  were carried out under fully emptied conditions of atmospheric air, as well as in the presence of nitrogen as an inert gas with the presence of MaDA by applying varies MaDA activities (0.1, 0.2, 0.3, 0.4, and 0.5) U/mg. After stabilizing the substrate concentrations at 0.3 mM  $D_1$  and 0.2  $D_{P_1}$ , the temperature at (30)°C, the

previous enzymatic tests was repeated, and take absorbance values after setting the wavelength at 360 nm. (1.0) U/mg is the correct enzymatic activity for this process.

### 2.5.5. Thermodynamic Study for P<sub>r</sub>

After determining the appropriate concentration for both D<sub>1</sub> and Dp<sub>r</sub> and the activity of MaDA, the rate of the reaction was monitored under the same conditions and using the same approach as previously described, by mix 0.3 mM of D<sub>1</sub> and 0.2 mM of Dp<sub>r</sub> with (1.0) U/mg of MaDA for each experience. The absorbance was monitored every 5 minutes until getting stable or nearly close reading. It was found that 30°C is the best temperature suitable for the enzymatic reaction. In addition, the change in enthalpy ( $\Delta H$ ), the change in Gibbs free energy ( $\Delta G$ ), and the change in entropy ( $\Delta S$ ) have been measured.

### 2.6. Preparation and Monitoring the Kinetic Parameters of Meso(13-methyl-12,14-dioxo-9,10-(epiethane[1,1,2]triazanoethane[1,2,2]triazyl)anthracen-9(10H)-yl)boronic acid (P<sub>4</sub>)

#### 2.6.1. Preparation of Meso (13-methyl-12,14-dioxo-9,10-(epiethane[1,1,2]triazanoethane[1,2,2]triazyl)anthracen-9(10H)-yl)boronic acid (P<sub>4</sub>)

The experiment of D-A reaction between anthracen-9-ylboronic acid (D<sub>1</sub>) and 1-methyl-1H-pyrrole-2,5-dione (Dp<sub>1</sub>) performed by using the same

methodology mentioned above and under the same conditions, Figure (٢-٦). The color of the mixture was light brown and gradually converts into pale yellow precipitate. The product purified by using recrystallization method using Ethanol and the main yield of the reaction was (٦٠%).

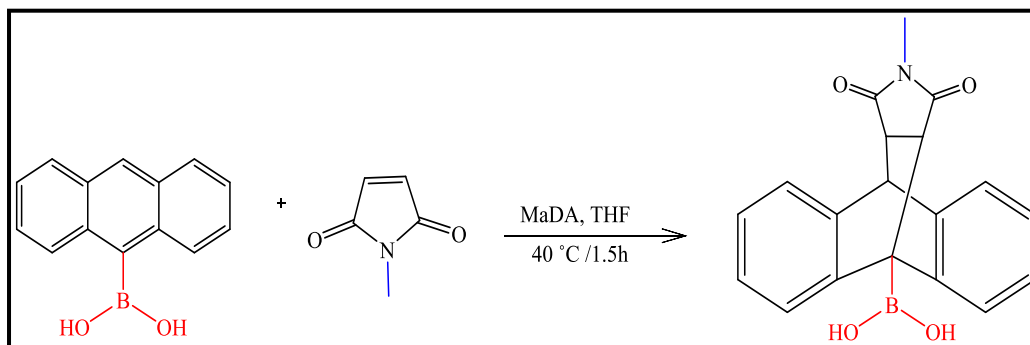


**Figure (٢-٦): The main product  $P_4$  of D-A reaction**

Furthermore, the solubility of  $P_4$  was listed in the Table (٢-٦):

**Table (٢-٦): The solubility of  $P_4$**

Solvent	Solubility
Acetonitrile	Partially soluble
Acetone	Soluble
DMF	Soluble
DMSO	Soluble
Ethanol	Soluble
Ether	Insoluble
Isopropanol	Partially soluble
Methanol	Soluble
Propanol	Partially soluble



THF	Soluble
-----	---------

### 2.6.2. Preparation of $P_4$ Solutions:

The 1 mM stock  $P_4$  solution was prepared by dissolving (0.0083 g) of  $P_4$  in 10 mL of THF, the set of different concentrations solutions were prepared (0.000, 0.01, 0.02, 0.03, 0.04, 0.05) mM.

### 2.6.3. Determination the appropriate concentration for Anthracen-9-ylboronic acid ( $D_1$ ) and 1-Methyl-1H-pyrrole-2,5-dione ( $Dp_1$ ) (Michaelis-Menten Equation)

The experiments of reaction between anthracen-9-ylboronic acid ( $D_1$ ) and 1-methyl-1H-pyrrole-2,5-dione ( $Dp_1$ ) carried out under the same conditions with the same methods as previously mentioned and enzymatic activity (0.1) U/mg of the MaDA enzyme, where the color of the reaction mixture was brown. Then, after observing the results, after fixing the wavelength at 360 nm, and continue until almost constant readings of absorbance are obtained. The ideal substrates concentration were reached at the concentration (0.0 mM) for ( $D_1$ ) and (0.0 mM) for ( $Dp_1$ ) that provides the optimum data during work. In addition, for drawing the Michaelis-Menten equation to find the Michaelis constant ( $K_m$ ), or the velocity at which the Michaelis-Menten equation's maximum velocity equals half.

### **2.6.4. Determination of Optimal MaDA Enzyme Activity for P<sub>ε</sub>**

In addition, the enzymatic studies of P<sub>ε</sub> were carried out under fully emptied conditions of atmospheric air, as well as in the presence of nitrogen as an inert gas with the presence of MaDA by applying varies MaDA specific activities (0.1, 0.2, 0.3, 0.4, and 0.5)U/mg. After stabilizing the substrate concentrations at 0.5mM D<sub>γ</sub> and 0.5 Dp<sub>γ</sub>, The temperature at (30)°C, repeat the previous enzymatic tests, and take absorbance values after setting the wavelength at 360 nm. (0.2) U/mg is the correct enzymatic specific activity for this process.

### **2.6.5 Thermodynamic Study for P<sub>ε</sub>**

After determining the appropriate concentration for both D<sub>γ</sub> and Dp<sub>γ</sub> and the activity of MaDA, the rate of the reaction was monitored under the same conditions and using the same approach as previously described, by mix 0.5 mM of D<sub>γ</sub> and 0.5 mM of Dp<sub>γ</sub> with (0.2) U/mg of MaDA for each experiment. the absorbance was monitored every 5 minutes until getting stable or nearly close readings. It was found that 30°C is the best temperature suitable for the enzymatic reaction. In addition, the change in enthalpy (ΔH), the change in Gibbs free energy (ΔG), and the change in entropy (ΔS) have been measured.

## 2.7. Preparation and Monitoring the Kinetic Parameters of Meso(1,3-dioxo-2-propyl-2,3-epiethane[1,1,2]triazanoethane[1,2,2]triazyl)anthracen-9(10H)-ylboronic acid (P.)

### 2.7.1. Preparation of Meso (1,3-dioxo-2-propyl-2,3-epiethane[1,1,2]triazanoethane[1,2,2]triazyl)anthracen-9(10H)-ylboronic acid (P.)

The experiment of D-A reaction between anthracen-9-ylboronic acid (D<sub>v</sub>) and 1-propyl-1*H*-pyrrole-2,5-dione (Dp<sub>v</sub>) performed by using the same methodology mentioned above and under the same conditions, Figure(2-7). The color of the mixture was light brown and gradually converts into pale yellow precipitate. The product purified by using recrystallization method using Ethanol and the main yield of the reaction was (50%).

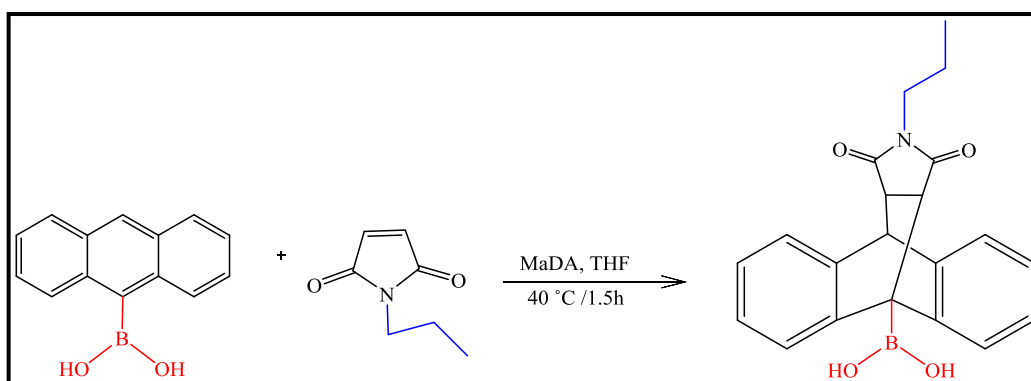


Figure (2-7): The main product P. of D-A reaction

Furthermore, the solubility of P<sub>o</sub> was listed in Table (2-7):

**Table (2-7): The solubility of P<sub>o</sub>.**

Solvent	Solubility
Acetone	Soluble
Acetonitrile	Partially soluble
DMF	Soluble
DMSO	Soluble
Ethanol	Soluble
Ether	Insoluble
Isopropanol	Partially soluble
Methanol	Soluble
Propanol	Partially soluble
THF	Soluble

### 2.7.2. Preparation of P<sub>o</sub> Solutions:

The 1 mM stock P<sub>o</sub> solution was prepared by dissolving (0.009 g) of P<sub>o</sub> in 20 mL of THF, the set of different concentrations solutions were prepared (0.000, 0.01, 0.02, 0.03, 0.04, 0.05) mM

### 2.7.3. Determination of appropriate concentration for Anthracen-9-ylboronic acid ( $D_r$ ) and $\gamma$ -propyl- $\gamma$ H-pyrrole-2,5-dione ( $Dp_r$ ) (Michaelis-Menten Equation)

The experiments of reaction between anthracen-9-ylboronic acid ( $D_r$ ) and  $\gamma$ -propyl- $\gamma$ H-pyrrole-2,5-dione ( $Dp_r$ ) carried out under the same conditions with the same methods as previously mentioned and specific enzymatic activity (0.1) U/mg of the MaDA enzyme, where the color of the reaction mixture was brown. Then, after observing the results, after fixing the wavelength at 360 nm, and continue until almost constant readings of absorbance are obtained. the ideal substrates concentration were reached at the concentration (0.0 mM) for ( $D_r$ ) and (0.0 mM) for ( $Dp_r$ ) that provides the optimum data during work. In addition for drawing the Michaelis-Menten equation to find the Michaelis constant ( $K_m$ ), or the velocity at which the Michaelis-Menten equation's maximum velocity equals half.

### 2.7.4. Determination of Optimal MaDA Enzyme Activity for P.

In addition, the enzymatic studies of P. were carried out under fully emptied conditions of atmospheric air, as well as in the presence of nitrogen as an inert gas with the presence of MaDA by applying varies MaDA specific activities (0.1, 0.2, 0.3, 0.4, and 0.5) U/mg. After stabilizing the substrate concentrations at 0.0mM  $D_r$  and 0.0  $Dp_r$ , The temperature at (30)°C, the previous enzymatic tests was repeated, and take absorbance

values after setting the wavelength at 360 nm. (0.0) U/mg is the correct enzymatic activity for this process.

### 2.7.0 Thermodynamic Study for P.

After determining the appropriate concentration for both D<sub>r</sub> and Dp<sub>r</sub> and the activity of MaDA, the rate of the reaction was monitored under the same conditions and using the same approach as previously described, by mix 0.0 mM of D<sub>r</sub> and 0.0 mM of Dp<sub>r</sub> with (0.0) U/mg of MaDA for each experience. When you continue to follow the absorbance readings every 0 minutes until you get stable or nearly close readings. It was found that 30°C is the best temperature suitable for the enzymatic reaction. In addition, the change in enthalpy ( $\Delta H$ ), the change in Gibbs free energy ( $\Delta G$ ), and the change in entropy ( $\Delta S$ ) have been measured.

### 2.8. Preparation and Monitoring the Kinetic Parameters of Meso (9-(dihydroxyboranyl)-1,2,4-dioxo-9,10-dihydro-13H-9,10-(epiethane[1,1,2]triazolanoethane[1,2,2]triazol)anthracen-13-yl)acetic acid (P<sub>r</sub>)

#### 2.8.1. Preparation of Meso (9-(dihydroxyboranyl)-1,2,4-dioxo-9,10-dihydro-13H-9,10-(epiethane[1,1,2]triazolanoethane[1,2,2]triazol)anthracen-13-yl)acetic acid (P<sub>r</sub>)

The experiment of D-A reaction between anthracen-9-ylboronic acid (D<sub>r</sub>) and 2-(2,6-dioxo-2,6-dihydro-1H-pyrrrol-1-yl) acetic acid (Dp<sub>r</sub>) was

performed by using the same methodology mentioned above and under the same conditions, Figure (٢-٨). The color of the mixture was light brown and gradually converts into pale yellow precipitate. The product purified by using recrystallization method using Ethanol and the main yield of the reaction was (٩٤%).

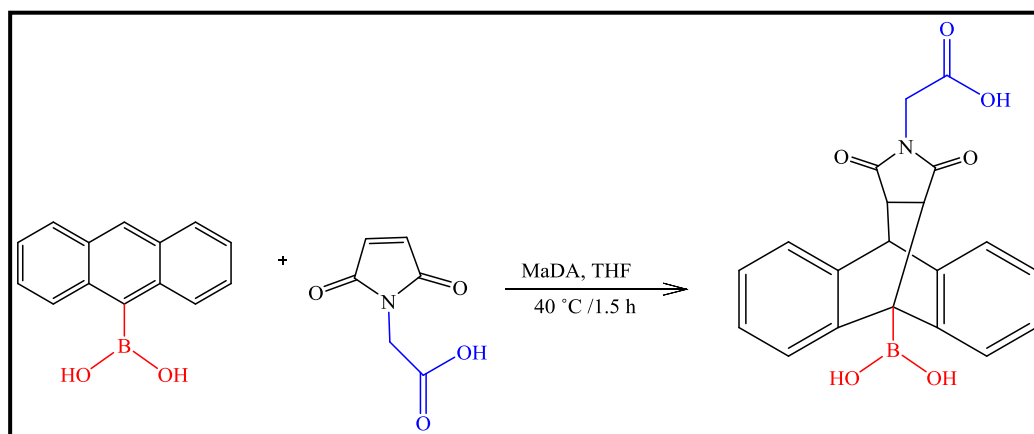


**Figure (٢-٨): The main product P<sub>7</sub> of D-A reaction**

Furthermore, the solubility of P<sub>7</sub> was listed in Table (٢-٨):

**Table (٢-٨): The solubility of P<sub>7</sub>**

Solvent	Solubility
Acetone	Soluble
Acetonitrile	Partially soluble
DMF	Soluble
DMSO	Soluble
Ethanol	Soluble
Ether	Insoluble
Isopropanol	Partially soluble
Methanol	Soluble

Propanol	Partially soluble
THF	Soluble

### 2.8.2. Preparation of P<sub>1</sub> Solutions:

The 1 mM stock P<sub>1</sub> solution was prepared by dissolving (0.009 g) of P<sub>1</sub> in 10 mL of THF, the set of different concentrations solutions were prepared (0.005, 0.01, 0.02, 0.03, 0.04, 0.05) mM.

### 2.8.3. Determination of appropriate concentration for Anthracen-9-ylboronic acid (D<sub>1</sub>) and 2-(2,6-dioxo-2,6-dihydro-1H-pyrrol-1-yl) acetic acid (Dp<sub>1</sub>) (Michaelis-Menten Equation)

The experiments of reaction between anthracen-9-ylboronic acid (D<sub>1</sub>) and 2-(2,6-dioxo-2,6-dihydro-1H-pyrrol-1-yl) acetic acid (Dp<sub>1</sub>) carried out under the same conditions with the same methods as previously mentioned and enzymatic activity (0.1) U/mg of the MaDA enzyme, where the color of the reaction mixture was brown. Then, after observing the results, after fixing the wavelength at 360 nm, and continue until almost constant readings of absorbance are obtained. The ideal substrates concentration were reached at the concentration (0.1 mM) for (D<sub>1</sub>) and (0.1 mM) for (Dp<sub>1</sub>) that provides the optimum data during work. In addition, for drawing the Michaelis-Menten equation to find the Michaelis constant (K<sub>m</sub>), or the velocity at which the Michaelis-Menten equation's maximum velocity equals half.



### 2.8.4. Determination of Optimal MaDA Enzyme Activity for $P_1$

In addition, the enzymatic studies of  $P_1$  were carried out under fully emptied conditions of atmospheric air, as well as in the presence of nitrogen as an inert gas with the presence of MaDA by applying varies MaDA specific activities (0.1, 0.2, 0.3, 0.4, and 0.5) U/mg. After stabilizing the substrate concentrations at 0.1 mM  $D_1$  and 0.1  $Dp_1$ , The temperature at 30°C, repeat the previous enzymatic tests, and take absorbance values after setting the wavelength at 360 nm. (0.4) U/mg is the correct enzymatic activity for this process.

### 2.8.5 Thermodynamic Study for $P_1$

After determining the appropriate concentration for both  $D_1$  and  $Dp_1$  and the activity of MaDA, the rate of the reaction was monitored under the same conditions and using the same approach as previously described, by mix 0.1 mM of  $D_1$  and 0.1 mM of  $Dp_1$  with (0.4) U/mg of MaDA for each experience. the absorbance was monitored every 5 minutes until getting stable or nearly close readings. It was found that 30°C is the best temperature suitable for the enzymatic reaction. In addition, the change in enthalpy ( $\Delta H$ ), the change in Gibbs free energy ( $\Delta G$ ), and the change in entropy ( $\Delta S$ ) have been measured.

The physical properties of all the products which have been prepared was described in table (۲-۹)

**Table (۲-۹): Physical properties and the yield of D-A products.**

Compound Symbol	Chemical Formula	Mol. wt.	Colour	Melting Point	Yield %
P <sub>۱</sub>	C <sub>۲۱</sub> H <sub>۱۷</sub> NO <sub>۲</sub>	۳۱۹	Pale yellow	۱۶۴- ۱۶۶	۷۴
P <sub>۲</sub>	C <sub>۲۲</sub> H <sub>۲۱</sub> NO <sub>۲</sub>	۳۴۷	Pale yellow	۲۱۴- ۲۱۶	۵۳
P <sub>۳</sub>	C <sub>۲۱</sub> H <sub>۱۷</sub> NO <sub>۵</sub>	۳۶۳	Pale yellow	۱۴۵- ۱۴۷	۵۷
P <sub>۴</sub>	C <sub>۱۹</sub> H <sub>۱۶</sub> BNO <sub>۴</sub>	۳۳۳	Pale yellow	۱۴۳- ۱۴۵	۶۰
P <sub>۵</sub>	C <sub>۲۱</sub> H <sub>۲۰</sub> BNO <sub>۴</sub>	۳۶۱	Pale yellow	۱۹۲- ۱۹۴	۷۰
P <sub>۶</sub>	C <sub>۲۰</sub> H <sub>۱۶</sub> BNO <sub>۶</sub>	۳۷۷	Pale yellow	۱۹۴- ۱۹۶	۹۴

### ۲.۹. preparation of Diels Alder reaction by using ۹,۱۰-diphenylanthracene as diene

The experiment of D-A reaction between 9,10-diphenylanthracene as diene ( $D_1$ ) with three Dienophiles (1-methyl-1*H*-pyrrole-2,5-dione ( $D_{p1}$ ), 1-propyl-1*H*-pyrrole-2,5-dione ( $D_{p2}$ ), 2-(2,5-dioxo-2,5-dihydro-1*H*-pyrrol-1-yl) acetic acid ( $D_{p3}$ ) was performed by using the same methodology mentioned above and under the same conditions. The color of the mixture was yellow and gradually converts into pale yellow precipitate, Figure (2-9). For more information, see appendixes 20, 26, 27.

## 2.1.1. Monitoring of Kinetic Parameters

### 2.1.1.1. Michaelis-Menten Equation

By monitoring the changes in concentrations, the Michaelis-Menten equation was used to determine the appropriate substrate concentration (for each reaction) of ( $D_1 + D_2$ ) ( $D_{p1} + D_{p2} + D_{p3}$ ) at a particular (enzymatic specific activity 0.1, 0.2, 0.3, 0.4, and 0.5 U/mg) respectively and at temperature of 25 °C. The concentrations of each reaction separately were then plotted against the velocity. Determine the derivative's concentration at which the reaction velocity is half based on the information provided which known as the Michaelis constant ( $K_m$ ).

### 2.1.1.2. Determination the product's concentration of D-A reaction

Using Lambert-Beer's law, equation (1), the concentration of the substrate was determined for each experiment at every time, where (C) is the

concentration of the substrate, (b) is the thickness of the cells (1 cm), (A) is the measured absorbance of the reaction mixture while following enzymatic experiments, and ( $\epsilon$ ) is the molar absorption coefficient from the slope of calibration curve for each reaction see appendix 1, 2, 3, 4, and 5.

$$C = A / b \epsilon \quad \text{Eq.....(1)}$$

The product concentration was then measured using the following equation each time:

$$[P] = [S]_T - [S]_0 \quad \text{Eq.....(2)}$$

Where  $[S]_T$  represents the concentration of the substrate at a certain time. Whereas  $[S]_0$  represents the concentration of the substrate at time zero for each experiment.

### 2.1.3. Finding the values of the reaction rate constant and enzymatic reaction rate

It was noted that there is a linear relationship when drawing between the natural logarithm of the product concentration ( $\ln p$ ) and time (t) in minute, so the first-order equation (3) for the reaction can be applied to find the reaction rate constant and the enzymatic reaction rate.

$$\text{Slope} = k (\text{min}^{-1}) = \text{Velocity (V)} \quad \text{Eq.....(3)}$$

### 2.1.4. Calculating the values of $K_m$ and $V_{\text{Max}}$ for each reaction

By applying the Michaelis-Menten equation Eq.(ξ) and establishing the relationship between the substrate concentration [S] and the rate of the enzymatic reaction (V) as well as the line weaver Burk equation (ο) is the relationship between reciprocal of velocity (1/V) and reciprocal of substrate concentration (1/[S]). The values of the maximum velocity (V max) of the enzymatic reaction and a velocity constant were established. For more information, see appendixes ٢,٦,١٠,١٤,١٨, and ٢٢.

$$v = \frac{V_{max}[S]}{K_m + [S]} \quad \text{Eq.....(ξ)}$$

#### Michaelis-Menten equation

$$\frac{1}{v} = \frac{K_m}{V_{max}[S]} + \frac{1}{V_{max}} \quad \text{Eq.....(ο)}$$

#### Line Weaver Burk equation

### ٢.١٠.٥. Achieving the optimal activity for enzyme reaction

The optimal enzyme activity of an enzymatic reaction after which the speed becomes constant was calculated due to binding all substrates to the enzyme by drawing the linear relationship between the enzymatic activity and the related velocity, as in the appendixes ٣,٧,١١,١٥,١٩, and ٢٣.

### ٢.١٠.٦. Determination the optimal temperature for enzymatic action

The optimum temperature was identified by plotting the relationship between each velocity against the temperatures through the bell curve.

### 2.10.7. Calculating the Thermodynamic Parameters $\Delta H$ , $\Delta S$ and $\Delta G$

The slope of the straight-line equation for Arrhenius (VI) between the natural logarithm of the reaction rate constant ( $\ln k$ ) and reciprocal of temperature ( $1/T$ ) was used to calculate the activation energy ( $E_a$ ) necessary for the reaction to occur. For more information, see appendixes 8, 9, 10, 11, 12, and 13.

$$\ln k = \ln A - E_a / RT \quad \text{Eq. ....(VI)}$$

#### Arrhenius equation

The value of ( $\Delta S$ ) and ( $\Delta H$ ) of the reaction can be found through the scheme of Van 't Hoff equation (VII) between ( $\ln k$ ) and ( $1/T$ ), where the slope is represented ( $-\Delta H/R$ ), but the intercept is represented cutting with the y-axis ( $\Delta S/R$ ).

$$\ln keq = -\frac{\Delta H}{TR} + \frac{\Delta S}{R} \quad \text{Eq. ....(VII)}$$

**R = The gas constant (8.314 Joule/mole)**

#### Van 't Hoff equation

***Chapter Three***  
***Results and Discussion***

## 3. Results and Discussion

### 3.1. Characteristics of Meso 9-(hydroxymethyl)-13-methyl-9,10-dihydro-12H,14H-9,10-(epiethane[1,1,2]triazanoethane[1,2,2]triazyl)anthracene-12,14-dione (P<sub>1</sub>)

The Fourier transform infrared (FTIR) spectrum of P<sub>1</sub> Figure (3-1) exhibited a medium broad peak at  $3502\text{ cm}^{-1}$  refer to the OH belong to terminal OH of hydroxymethyl that attached at 10-anthracene. The weak peak at  $3066\text{ cm}^{-1}$  belong to the stretching C-H (SP<sup>2</sup>) for the pyrrole ring. In addition, the two weak peaks at  $2958\text{ cm}^{-1}$ , and  $2877\text{ cm}^{-1}$  belong to C-H(SP<sup>3</sup>) of the methyl, which linked to the pyrrole ring. The two peaks that related to stretching active carbonyl amide groups of pyrrole ring appeared as the weak peak at  $1766\text{ cm}^{-1}$  and the strong sharp peak at  $1693\text{ cm}^{-1}$ . The medium peak at  $1462\text{ cm}^{-1}$  belong to C=C of anthracene rings. The medium peak at  $1207\text{ cm}^{-1}$  attributed to the (C-O) bond of alcohol for the hydroxymethyl. (123-125). All peaks appear in FTIR spectrum for all products seen in table (3-12).



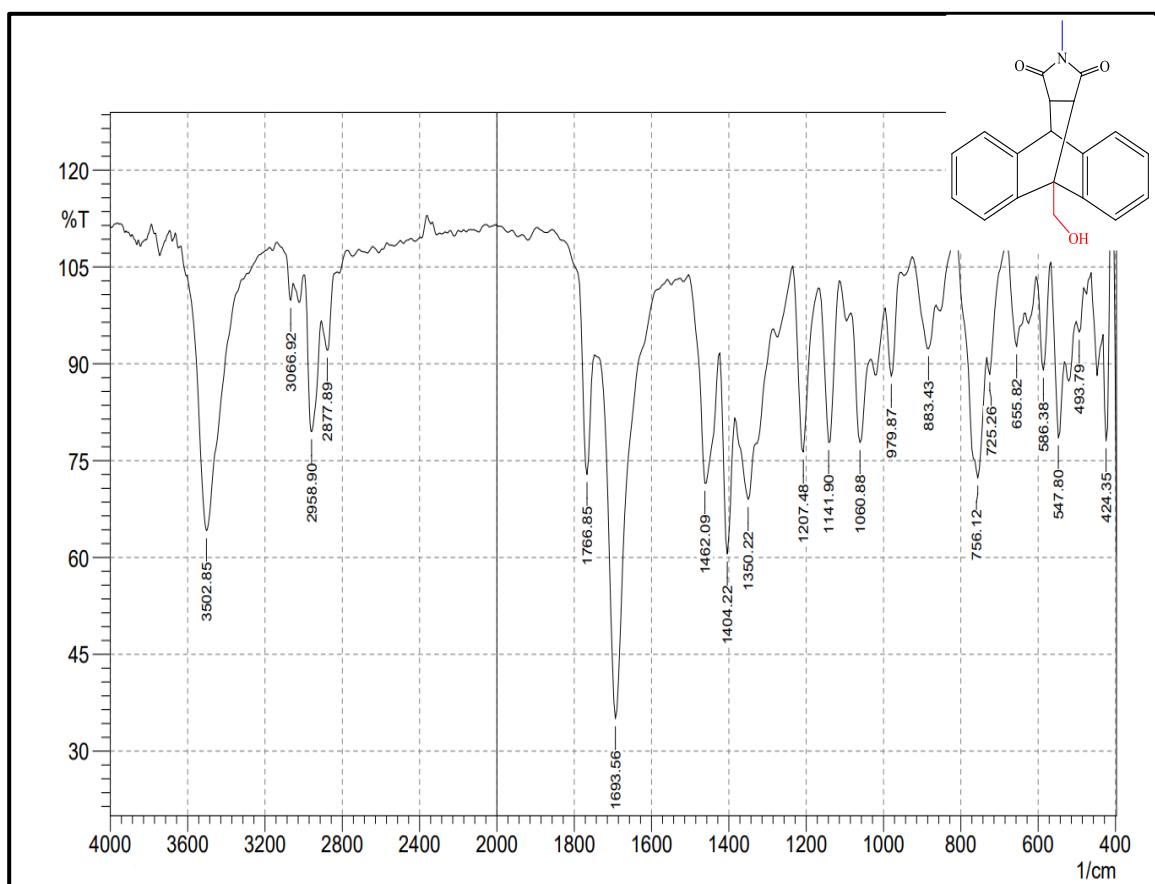


**Figure (3-1): The FTIR spectrum for P<sub>1</sub>**

The <sup>1</sup>H NMR spectrum for P<sub>1</sub> in D<sub>2</sub>O Figure (3-2), display the singlet peak at δ (1.32) ppm belong to protons of CH<sub>3</sub> attached to N of pyrrole ring, while the protons of the two CH groups that attached to carbonyl of pyrrole showed multiplet at δ(2.31-2.34) ppm and at δ (2.46-2.50) ppm, respectively. The multiplet peak at δ (3.20-3.29) ppm belong to CH proton of the 9-H anthracene. The signal of (OH) proton of the 10-methylol anthracene appeared the peak at δ (4.68) ppm, in addition to the triplet peak at δ (0.27-0.30) ppm attributed to the protons of CH<sub>2</sub> that attached to hydroxyl group appear. The multiplet peaks at δ (7.09-7.14) ppm, δ (7.21) ppm, δ (7.42-7.44) ppm, and δ (7.60) ppm belong to protons of aromatic

rings of anthracene (126, 127). All peak appears in  $^1\text{H}$  NMR spectrum for all products seen in table (3-13).

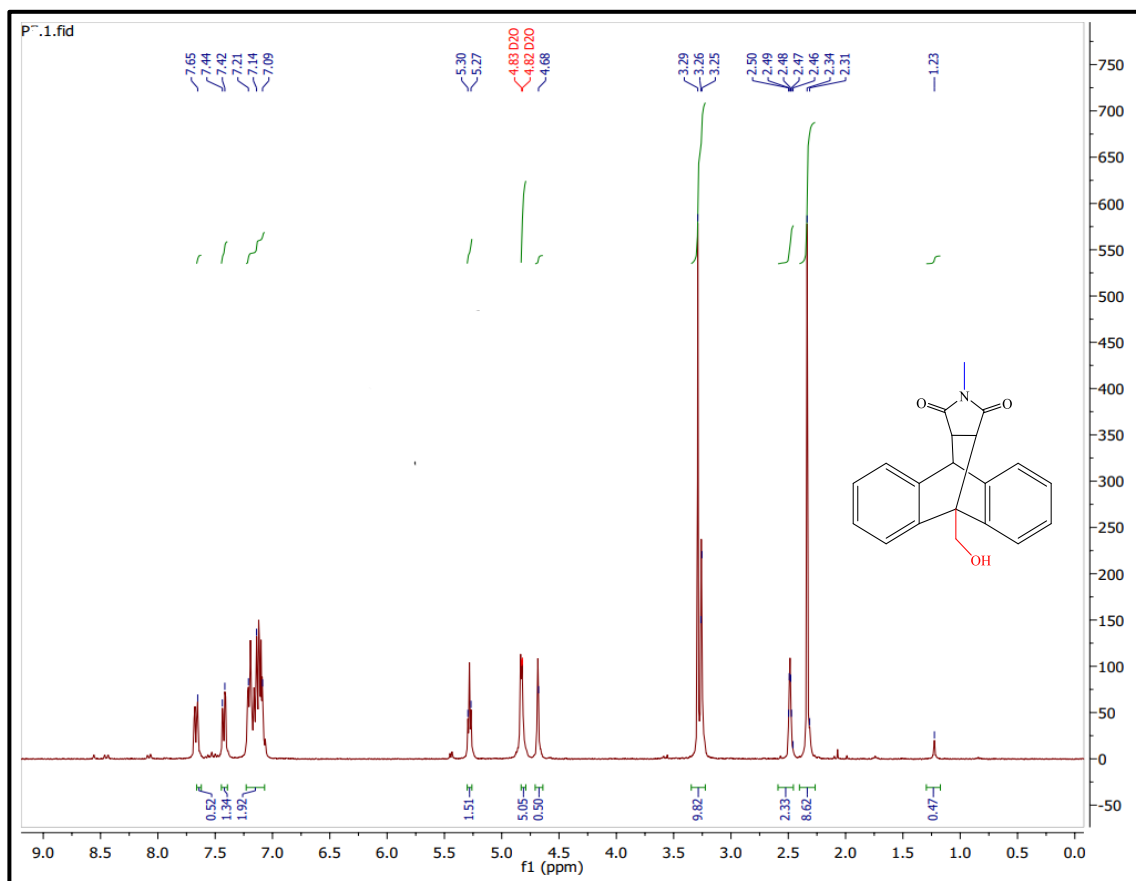


**Figure (3-2): The  $^1\text{H}$  NMR spectrum for P<sub>1</sub>**

The  $^{13}\text{C}$  NMR spectrum of P<sub>1</sub> in DMSO- $d_6$  showed the peak of the carbon atom of methyl group that attaches to N at  $\delta$  (24.30) ppm. The peak at  $\delta$  (40.34) ppm belong to the 10-carbon of anthracene that attached to the 10-hydroxymethyl ( $\text{CH}_2\text{-OH}$ ) group. The peak at  $\delta$  (46.06) ppm belong to 9-carbon of anthracene which closed the cycle with pyrrole. The peaks at  $\delta$  (48.13) ppm and  $\delta$  (49.67) ppm attributed to the two alpha carbons of pyrrole, respectively. The peak at  $\delta$  (58.72) ppm belong to carbon of

hydroxymethyl that attached to the anthracene. The peaks at  $\delta$  (122.80) ppm,  $\delta$  (124.06) ppm,  $\delta$  (125.04) ppm,  $\delta$  (125.27) ppm,  $\delta$  (125.50) ppm,  $\delta$  (126.23) ppm,  $\delta$  (126.57) ppm,  $\delta$  (126.74) ppm,  $\delta$  (127.08) ppm,  $\delta$  (127.34) ppm,  $\delta$  (127.57) ppm,  $\delta$  (127.80) ppm,  $\delta$  (128.10) ppm,  $\delta$  (133.19) ppm,  $\delta$  (134.97) ppm,  $\delta$  (139.76) ppm,  $\delta$  (140.03) ppm,  $\delta$  (140.31) ppm,  $\delta$  (140.59) ppm,  $\delta$  (140.87) ppm,  $\delta$  (145.34) ppm,  $\delta$  (146.06) ppm,  $\delta$  (148.13) ppm,  $\delta$  (149.67) ppm,  $\delta$  (158.72) ppm,  $\delta$  (176.38) ppm, and  $\delta$  (177.04) ppm attributed to the carbons of the anthracene rings. The peaks at  $\delta$  (176.38) ppm and  $\delta$  (177.04) ppm attributed to the carbons of the two carbonyl groups for the pyrrole, respectively, Figure (3-3). All peak appears in  $^{13}\text{C}$ NMR spectrum for all products seen in table (3-14).

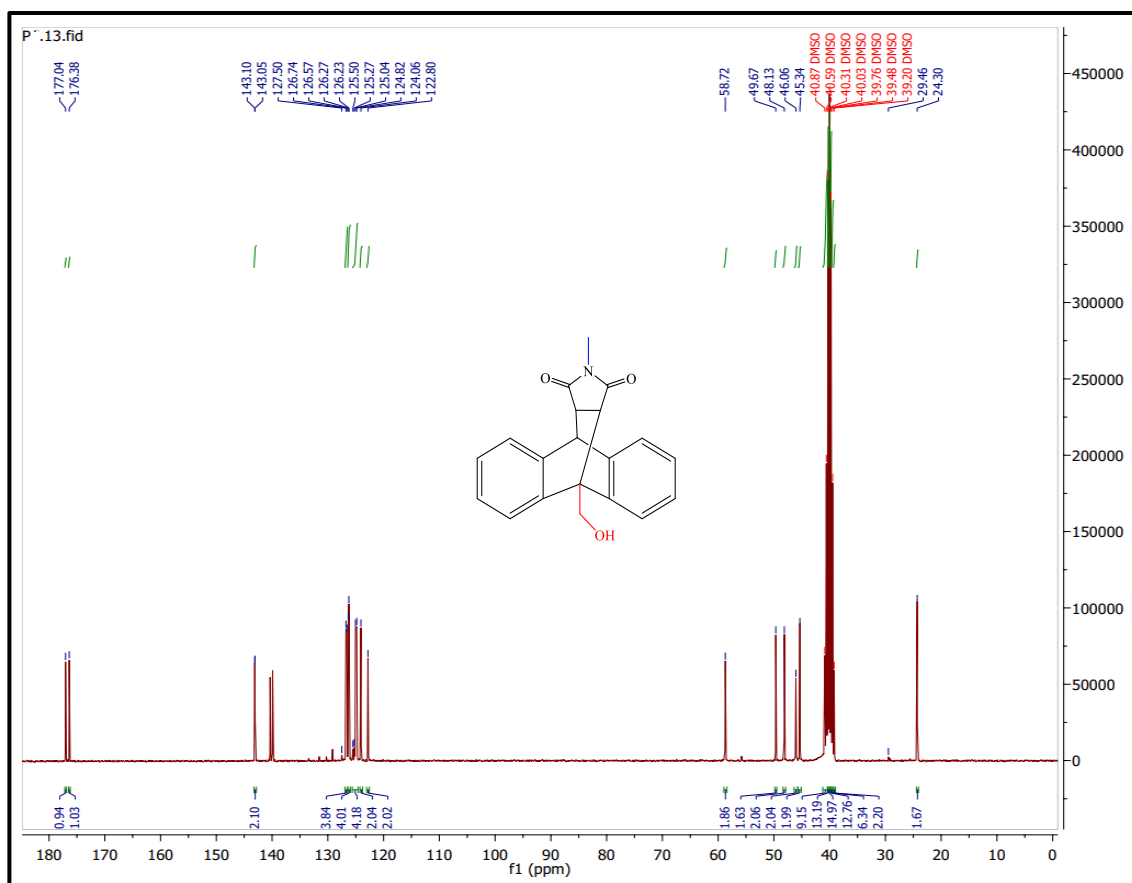


Figure (3-3): The  $^{13}\text{C}$  NMR spectrum of P<sub>1</sub>

The mass spectrum of P<sub>1</sub> appears signal at (320.1) m/z) relative to the molecular ion, the value close to the calculated molecular weight (319.1 g/mole), as shown in Figure (3-4).

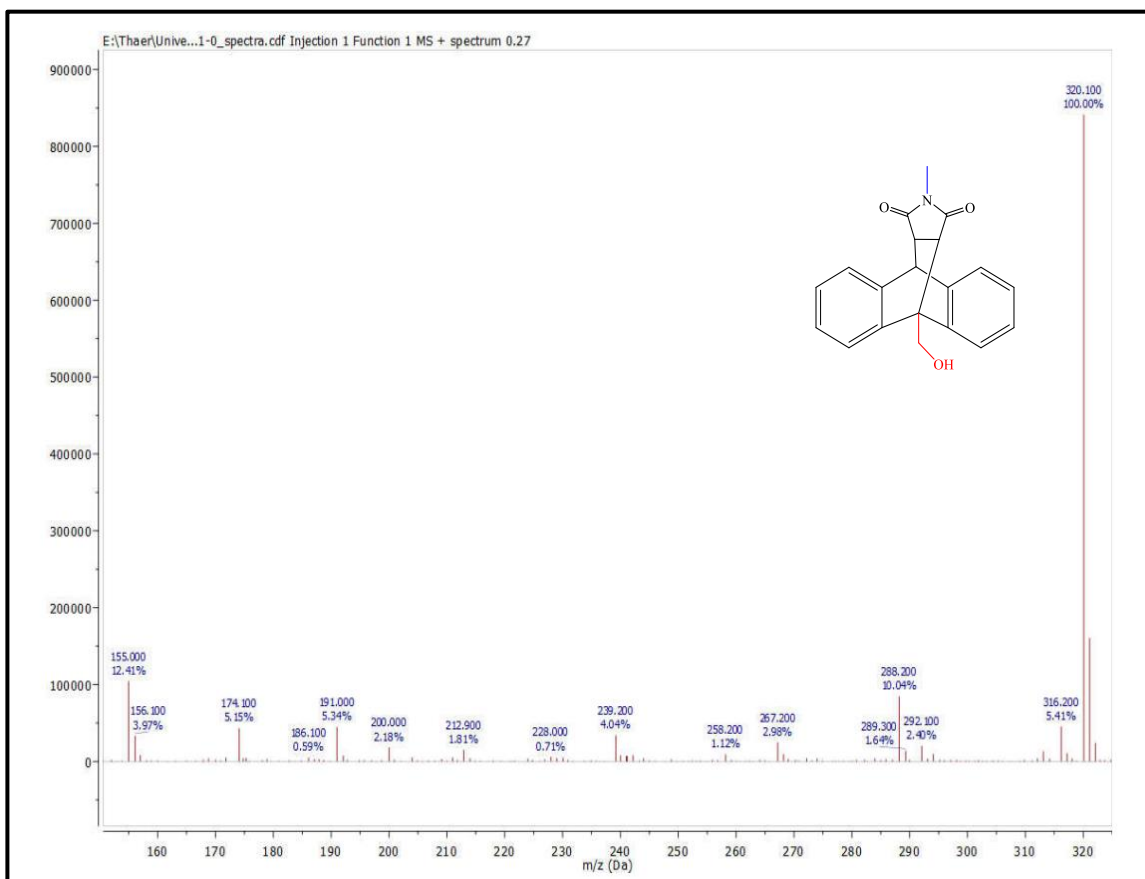
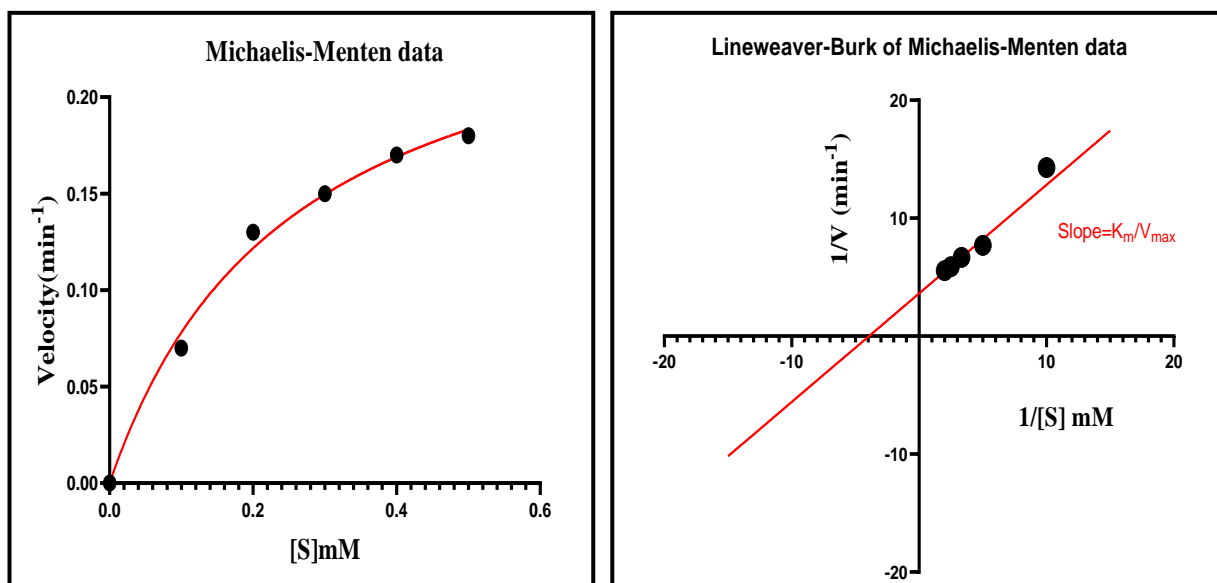


Figure (3-4): The mass spectrum for P<sub>1</sub>

**3.2. Kinetic Study of Meso 9-(hydroxymethyl)-13-methyl-9,10-dihydro-12H,14H-9,10-epiethane[1,1,2]triazolanoethane[1,2,2]triazyl)anthracene-12,14-dione (P<sub>1</sub>)**

**۳.۲.۱. Determine the values of the reaction rate constant (Michaelis-Menten constant) and the maximum velocity of the enzymatic reaction for P<sub>۱</sub>**

From the absorbance readings against the D<sub>۱</sub> concentrations, the corresponding reaction rate was found. After that, the Michaelis-Menten equation was applied by drawing the relationship between the velocity of enzymatic reaction and the concentration of the D<sub>۱</sub> as substrate, as well as the line Weaver-Burk equation was applied by plot the relationship between the reciprocal of the velocity ( $1/V$ ) versus the reciprocal of the concentration ( $1/[S]$ ) to reach the value of the enzymatic reaction rate constant ( $K_m$ ) and the maximum velocity of the enzymatic reaction ( $V_{max}$ ), Figure (۳-۵) and Table (۳-۱).



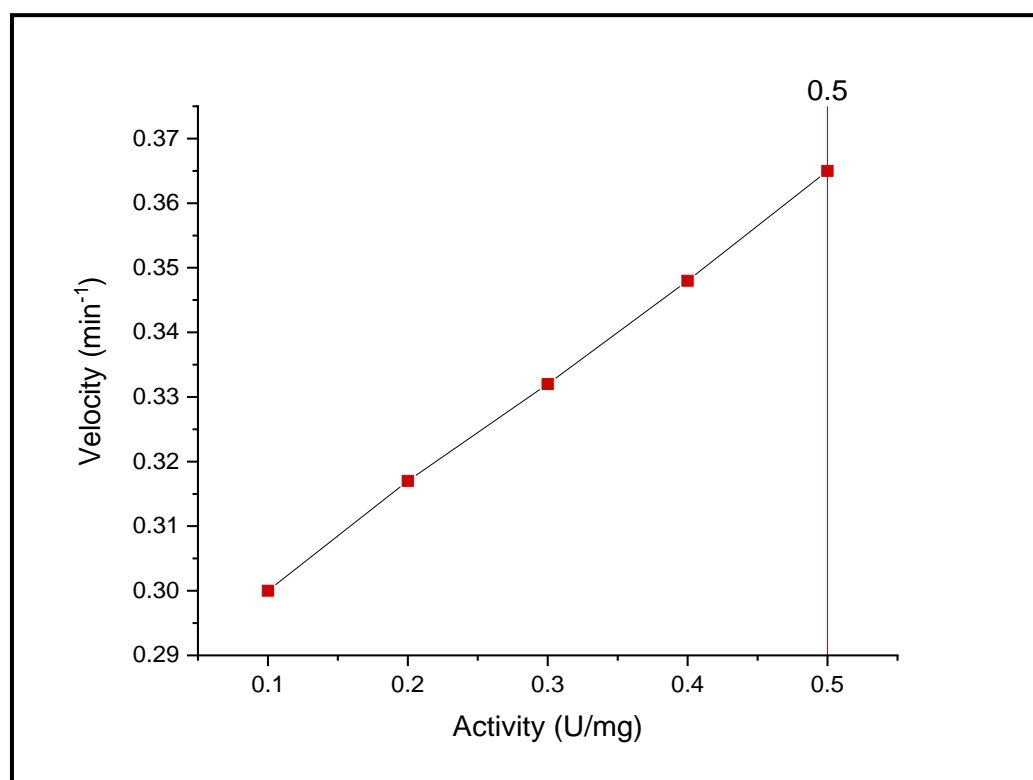
**Figure (۳-۵): Michaelis-Menten diagram and line weaver - Burk diagram of the D-A reaction of P<sub>۱</sub>**

**Table (۳-۱): The Values of  $K_m$  and  $V_{max}$  for the D-A reaction of  $P_1$** 

kinetic Parameters	Michaels Menten plot	line weaver Burk plot
$V_{max}$ ( $\text{min}^{-1}$ )	۰.۲۷۶۴	۰.۲۷۶۴
$K_m$	۰.۲۵۴۱	۰.۲۵۴۱

### ۳.۲.۲. Finding of Enzymatic Activity of $P_1$

The ideal enzymatic specific activity was found by drawing the relationship between the enzyme reaction velocity and the activity, which produced a bell-like shape, Figure (۳-۶).

**Figure (۳-۶): The appropriate enzyme activity of MaDA for  $P_1$**

From the foregoing, the ideal enzymatic activity for this reaction is ( $0.30$  U/mg).

### 3.2.3. Finding Optimum Temperature for $P_1$

The optimum temperature for the D-A reaction of  $P_1$  was determined by plot the velocity of the reaction against the different temperatures ( $15, 25, 40$  C°). The  $25$  C° is the ideal temperature, Figure (3-7).

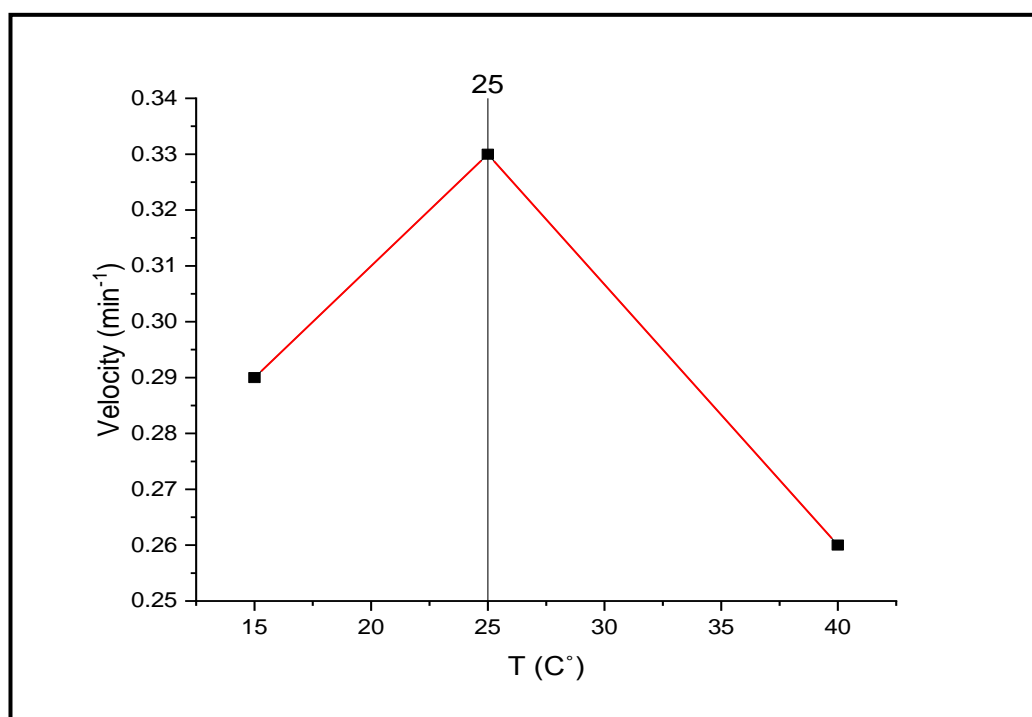
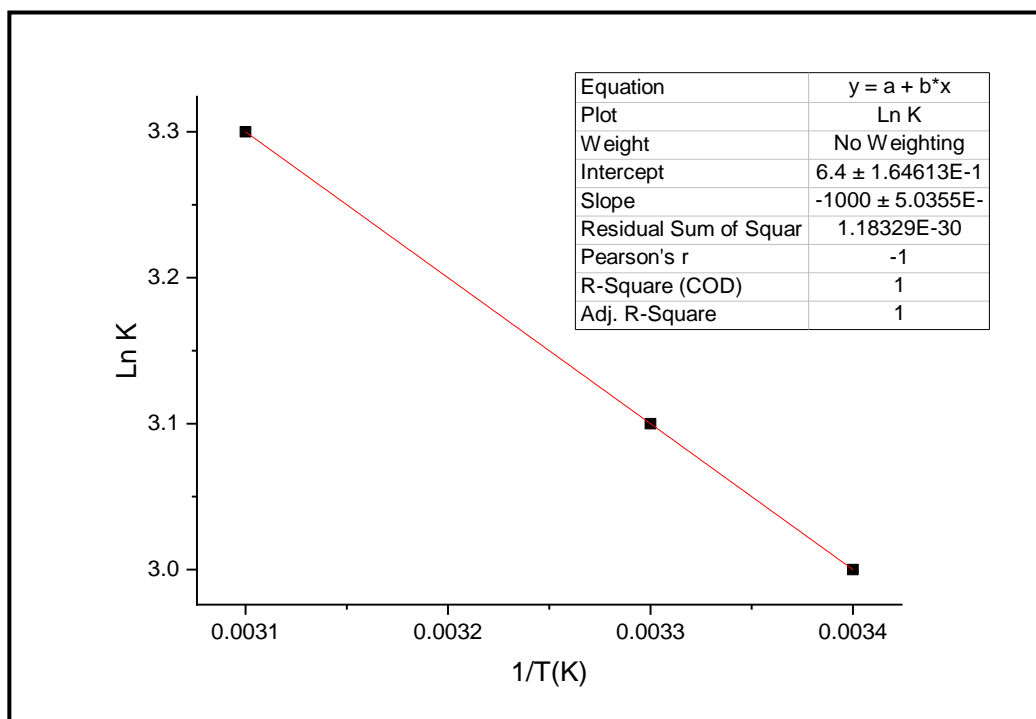


Figure (3-7): The ideal temperature for  $P_1$

### 3.2.4. Finding the Thermodynamic Parameters for $P_1$

By applying the Van't Hoff equation, drawing the relationship between  $\ln K$  against the reciprocal of temperature Figure (3-8). The value of ( $\Delta H$ ) was calculated from the slope and the value of the activation energy ( $\Delta E_a$ ) is

equal to the ( $\Delta H$ ) value of the liquids, while a ( $\Delta S$ ) value was calculated from the intersection with the y-axis. As for the Gibbs free energy, it was found by applying the free Gibbs equation are presented in Table (3-2).



**Figure (3-8): Van't Hoff equation for P<sub>1</sub>**

**Table (3-2): The values of ( $\Delta H$ ), ( $\Delta S$ ) and ( $\Delta G$ ) for P<sub>1</sub>**

$\Delta H$ (J.mol <sup>-1</sup> )	$\Delta S$ (J.K <sup>-1</sup> )	$\Delta G$ (J)
8314	03.209	-7.042

The negative value of the Gibbs free energy indicates that the enzyme reaction is spontaneous. It also has a positive entropy value, making it random. In addition to positive enthalpy value making it endothermic.



**3.3. Characteristics of Meso 9-(hydroxymethyl)-10-propyl-9,10-dihydro-12H,14H-9,10-(epiethane[1,1,2]triazanoethane[1,2,2]triazyl)anthracene-12,14-dione (P<sub>r</sub>)**

The Fourier transform infrared (FTIR) spectrum of P<sub>r</sub> Figure (3-9) showed a medium peak at 3490 cm<sup>-1</sup> belong to terminal OH of hydroxymethyl that attached at 10-anthracene. The weak peak at 3066 cm<sup>-1</sup> attributed to the stretching C-H (SP<sup>3</sup>) for the pyrrole ring. The weak peaks at 2943 cm<sup>-1</sup>, 2897 cm<sup>-1</sup>, and 2839 cm<sup>-1</sup> belong to C-H(SP<sup>3</sup>) of the propyl, which linked to the pyrrole ring. The two stretching peaks related to the active carbonyl for pyrrole ring, appeared as the weak peak at 1766 cm<sup>-1</sup> and the strong sharp peak at 1689 cm<sup>-1</sup>. The weak peak at 1546 cm<sup>-1</sup> belong to C=C of the anthracene rings. The medium peak at 1292 cm<sup>-1</sup> attributed to the (C-O) bond of alcohol for the hydroxymethyl. (123-120). All peak appears in FTIR spectrum for all products seen in table(3-12).

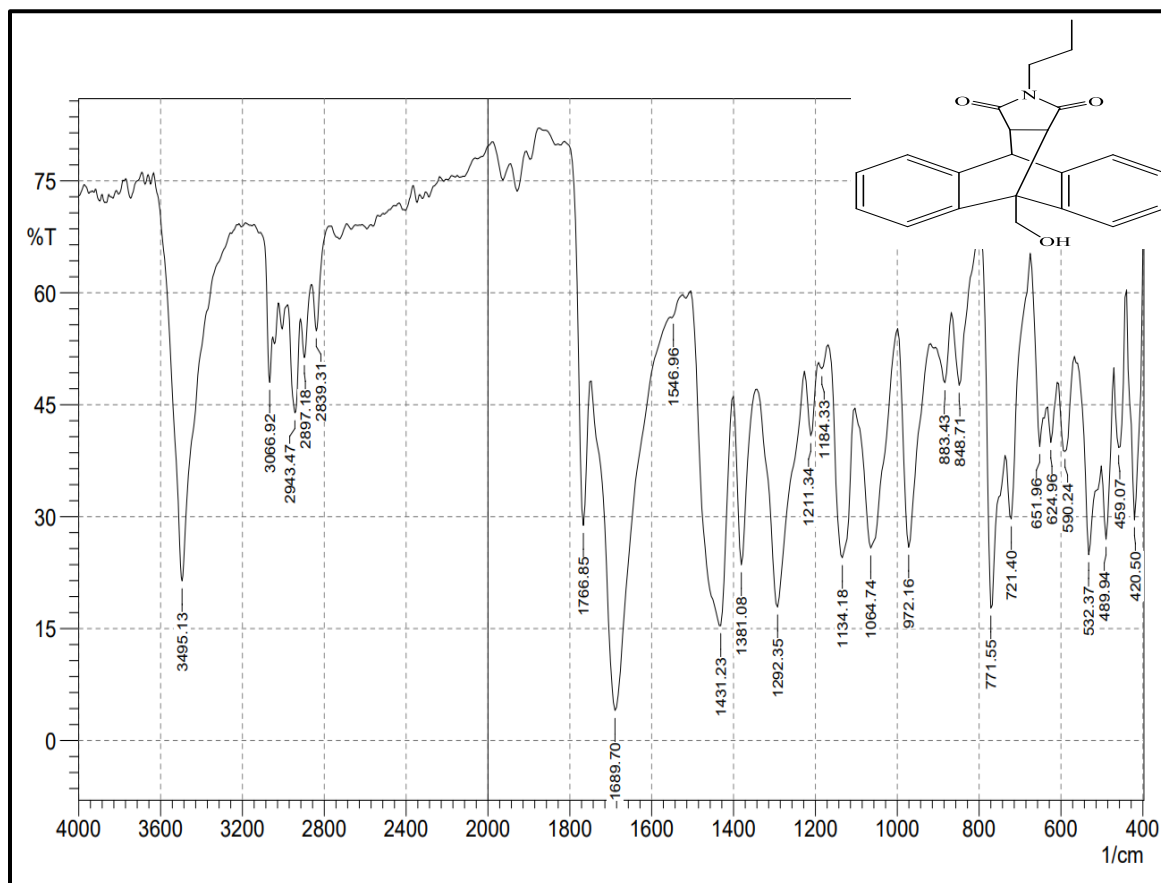


**Figure (3-9): The FTIR spectrum for P7**

The  $^1\text{H}$  NMR spectrum for P7 in  $\text{D}_2\text{O}$  Figure (3-10) display the quartet peak at  $\delta$  (0.36-0.51) ppm attributed to the terminal  $\text{CH}_2$  of propyl group, which attached with pyrrole, the hexate peak at  $\delta$  (0.68-0.71) ppm belong to the protons of middle  $\text{CH}_2$  of propyl, and the triplet peak at  $\delta$  (1.2-1.22) belong to the  $\text{CH}_3$  of propyl that attached to N of pyrrole ring. The protons of the two  $\text{CH}$  groups that attached to carbonyl of pyrrole showed multiplet at  $\delta$  (2.47-2.50) ppm and at  $\delta$  (2.89-2.93) ppm respectively. The multiplet peak at  $\delta$  (3.20-3.29) ppm belong to  $\text{CH}$  proton of the 9-H anthracene. The signal of (OH) proton of the 10-methylol anthracene appeared the peak at  $\delta$

( $\delta$  7.6-7.8) ppm, in addition to the triplet peak at  $\delta$  (0.3-0.35) ppm attributed to the protons of  $\text{CH}_2$  that attached to hydroxyl group. The multiplet peaks at  $\delta$  (7.1-7.15) ppm,  $\delta$  (7.4-7.45) ppm,  $\delta$  (7.6-7.65) ppm, and  $\delta$  (8.0-8.05) ppm belong to protons of aromatic rings of anthracene. (126, 127). All peak appears in  $^1\text{H}$  NMR spectrum for all products seen in table (3-13).

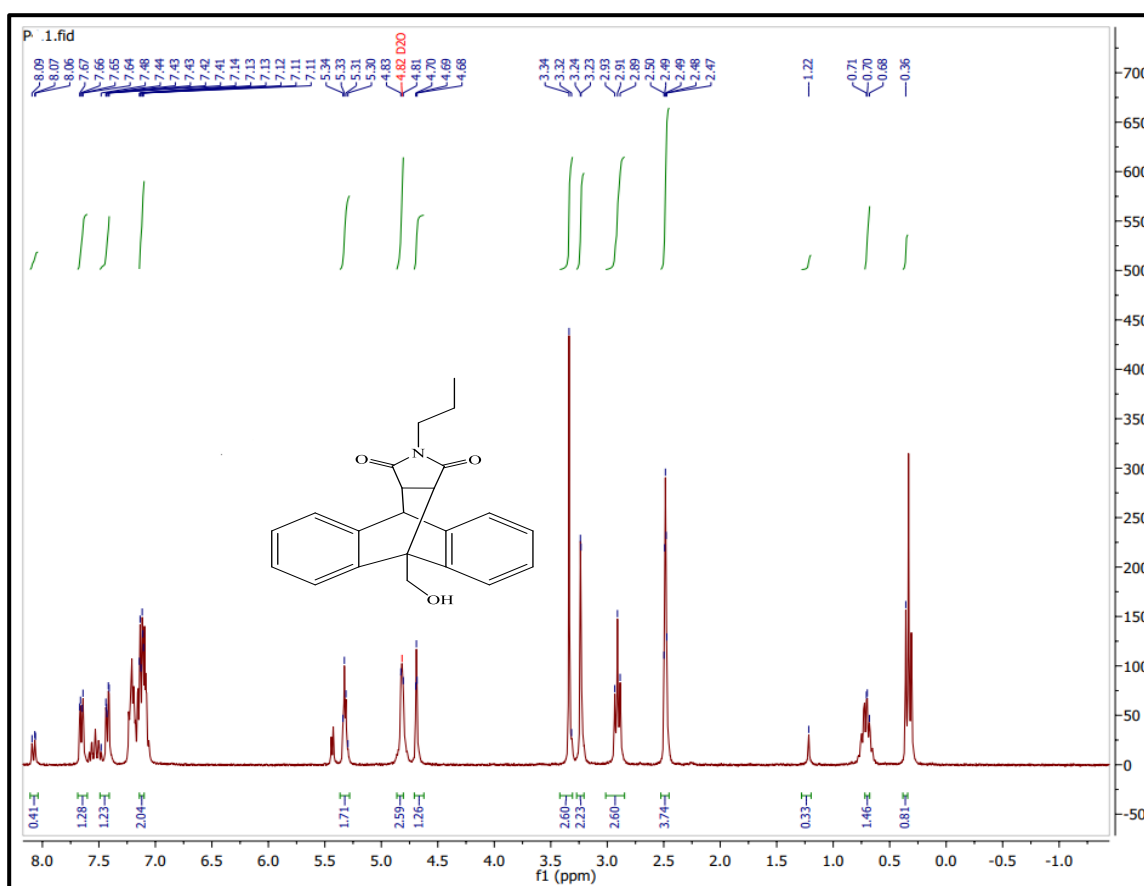


**Figure (3-10): The  $^1\text{H}$  NMR spectrum for P7**

The  $^{13}\text{C}$  NMR spectrum of P7 in  $\text{DMSO-d}_6$  Figure (3-11) showed a peak at  $\delta$  (11.22) ppm attributed to the terminal  $\text{CH}_2$  of propyl that linked with pyrrole, a peak at  $\delta$  (20.46) ppm attributed to the middle  $\text{CH}_2$  of propyl, and

a peak at  $\delta$  (39.06) ppm attributed to the CH<sub>2</sub> of propyl that attached to the N of pyrrole. The peak at  $\delta$  (50.33) ppm belong to the 1'-carbon of anthracene that attached to the 1'-hydroxymethyl (CH<sub>2</sub>-OH) group. The peak at  $\delta$  (50.80) ppm belong to 9'-carbon of anthracene which closed the cycle with pyrrole. The peaks at  $\delta$  (57.84) ppm and  $\delta$  (59.61) ppm attributed to the two alpha carbons of pyrrole, respectively. The peak at  $\delta$  (58.70) ppm belong to carbon of hydroxymethyl that attached at 1'-anthracene. The peaks at  $\delta$  (124.16) ppm,  $\delta$ (124.82) ppm,  $\delta$  (125.53) ppm,  $\delta$  (126.26) ppm,  $\delta$  (126.57) ppm,  $\delta$  (126.73) ppm,  $\delta$  (127.52) ppm,  $\delta$  (129.16) ppm,  $\delta$ (140.49) ppm, and  $\delta$  (143.21) ppm attributed to the carbons of the anthracene rings. The peaks at  $\delta$  (176.36) ppm and  $\delta$ (177.07) ppm attributed to the carbons of the two carbonyl groups for the pyrrole, respectively. All peak appears in <sup>13</sup>C NMR spectrum for all products seen in table (3-14).

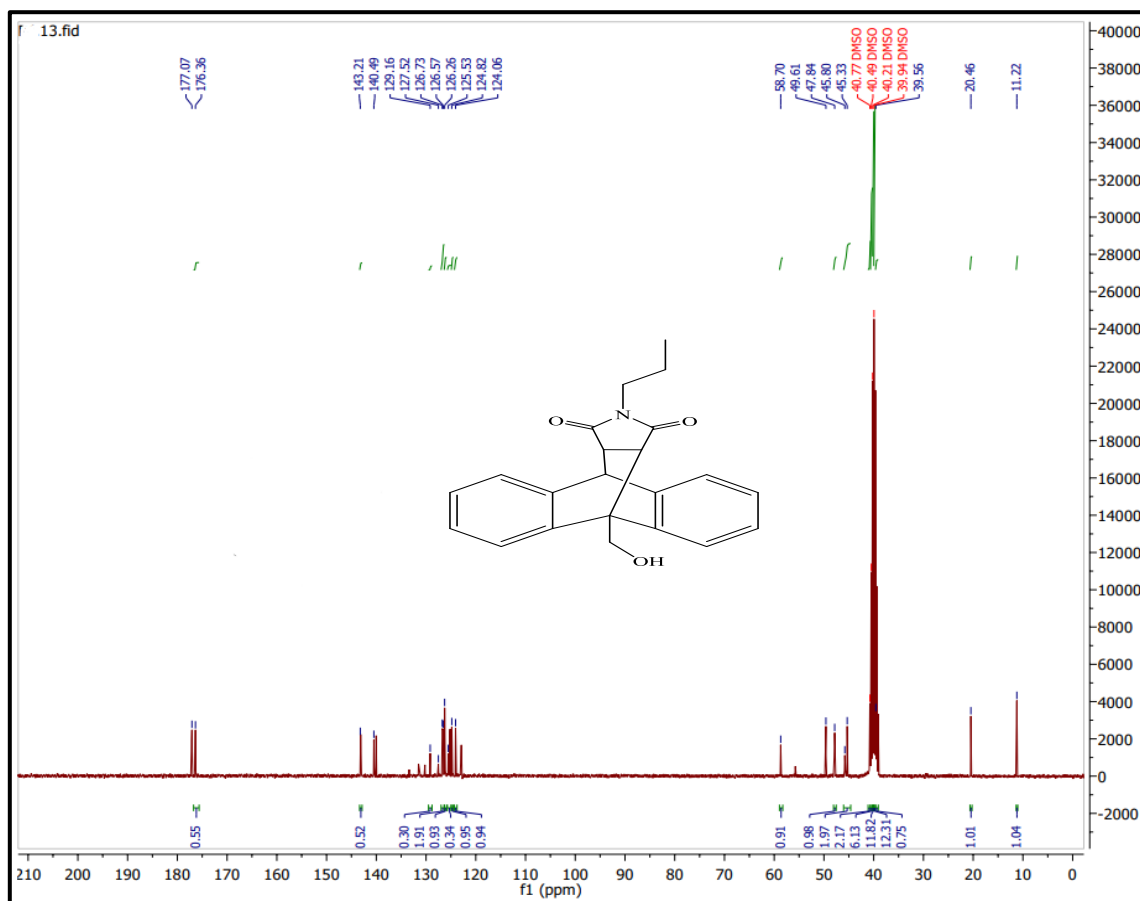


**Figure (3-11): The  $^{13}\text{C}$  NMR spectrum of  $P_7$**

The mass spectrum of  $P_7$  appears signal at (348.3 m/z) relative to the molecular ion, the value close to the calculated molecular weight (347.1 g/mole), as shown in Figure (3-12).

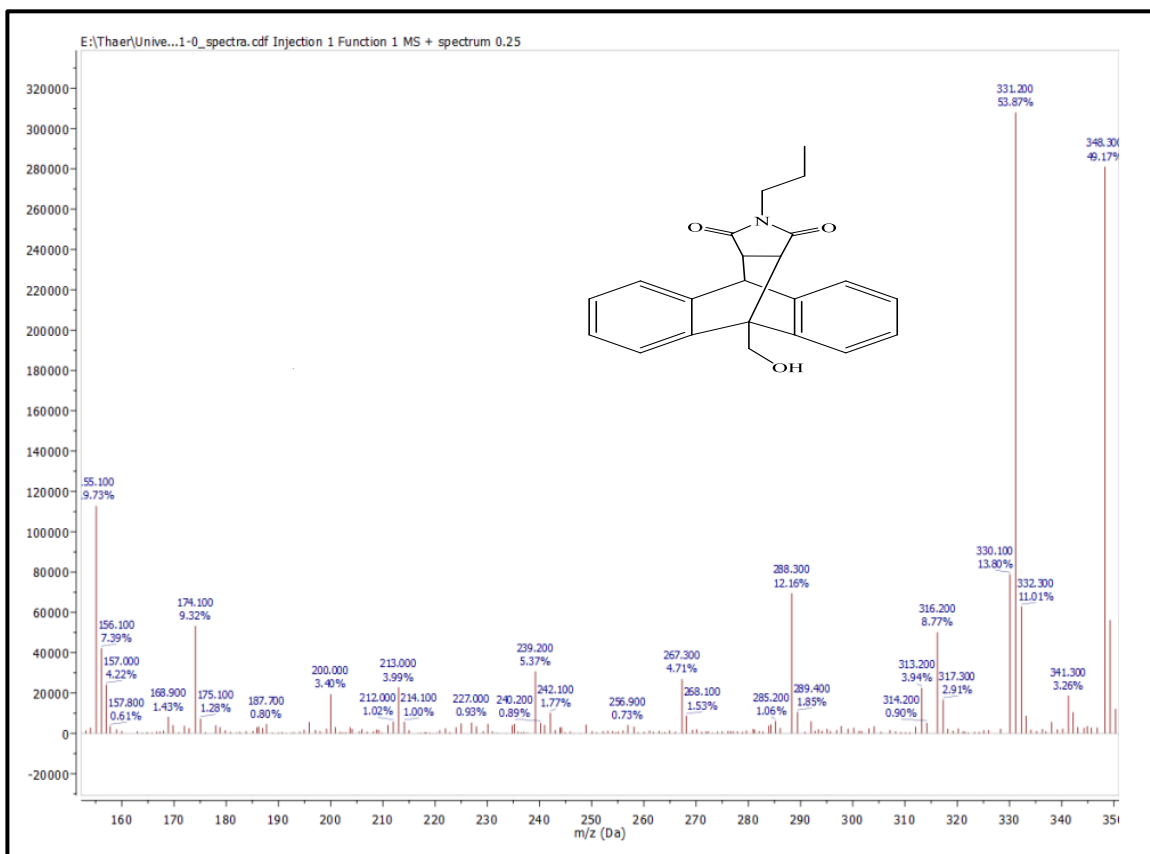
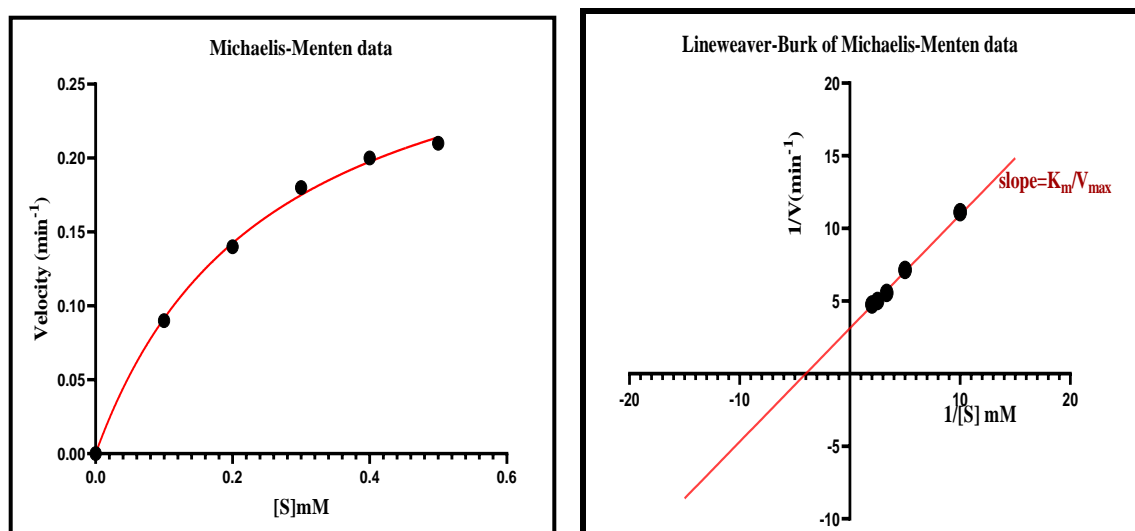


Figure (3-12): The mass spectrum of P7

**3.4. Kinetic Study of Meso -(hydroxymethyl)-1-propyl-9,10-dihydro-12H,14H-9,10-epiethane[1,1,2]triazolanoethane[1,2,2]triazylanthracene-12,14-dione (P7)**

**3.4.1. Determine the values of the reaction rate constant (Michaelis-Menten constant) and the maximum velocity of the enzymatic reaction for P7**

From the absorbance readings against the  $D_1$  concentrations, the corresponding reaction rate was found. After that, the Michaelis-Menten equation was applied by drawing the relationship between the velocity of enzymatic reaction and the concentration of the  $D_1$  as substrate, as well as the line Weaver-Burk equation was applied by plot the relationship between the reciprocal of the velocity ( $1/V$ ) versus the reciprocal of the concentration ( $1/[S]$ ) to reach the value of the enzymatic reaction rate constant ( $K_m$ ) and the maximum velocity of the enzymatic reaction ( $V_{max}$ ), Figure (3-13) and Table (3-3).



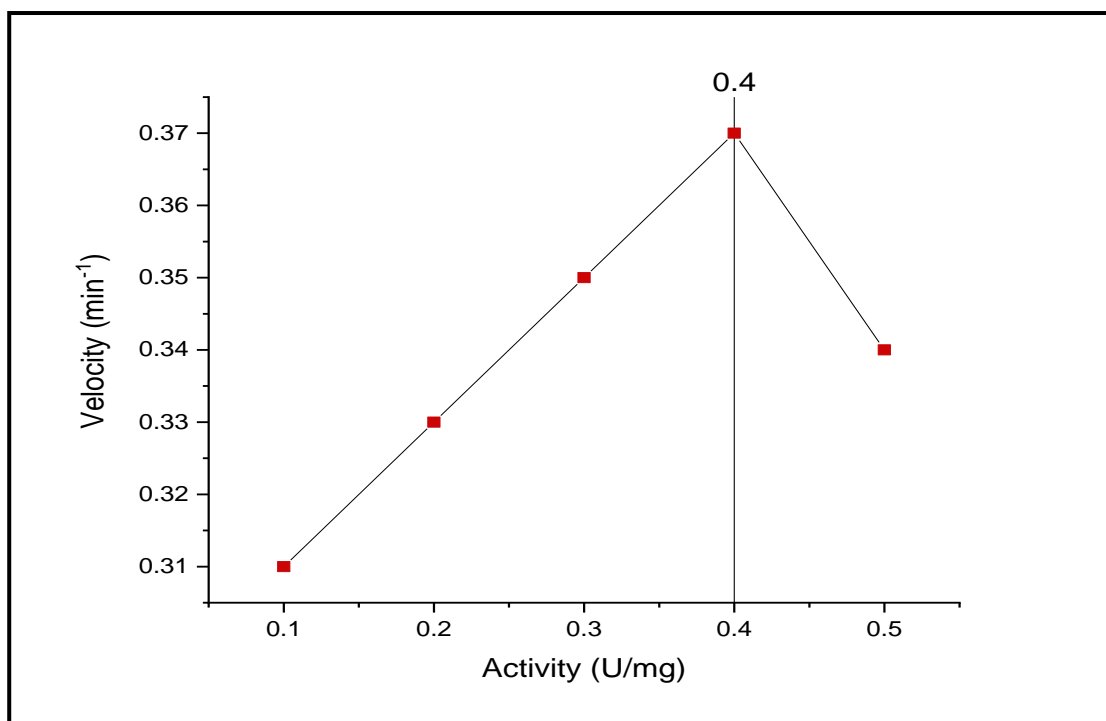
**Figure (3-13): Michaelis-Menten diagram and line weaver - Burk diagram of the D-A reaction of P<sub>7</sub>**

**Table (٣-٣): The Values of  $K_m$  and  $V_{max}$  for the D-A reaction of  $P_7$** 

kinetic Parameters	Michaels Menten plot	line weaver Burk plot
$V_{max}$ ( $\text{min}^{-1}$ )	٠.٣٢١٨	٠.٣٢١٨
$K_m$	٠.٢٥١٧	٠.٢٥١٧

### ٣.٤.٢. Finding of Enzymatic Activity of $P_7$

The ideal enzymatic activity was found by drawing the relationship between the enzyme reaction velocity and the activity, which produced a bell-like shape, Figure (٣-١٤).

**Figure (٣-١٤): The appropriate enzyme activity of MaDA for  $P_7$** 

From the foregoing, the ideal enzymatic activity for this reaction is (٠.٤ U/mg).



### 3.4.3. Finding Optimum Temperature for P<sub>γ</sub>

The optimum temperature for the D-A reaction of P<sub>γ</sub> was determined by plot the velocity of the reaction against the different temperatures (15, 25, 40 C°). The 25 C° is the ideal temperature, Figure (3-15).

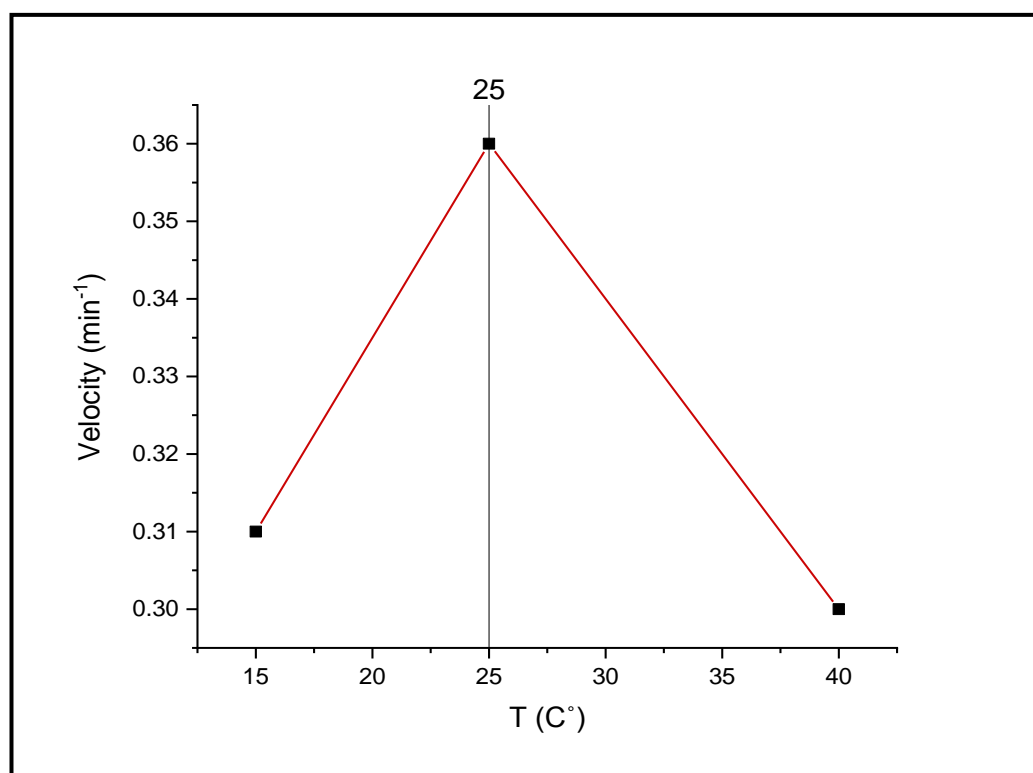
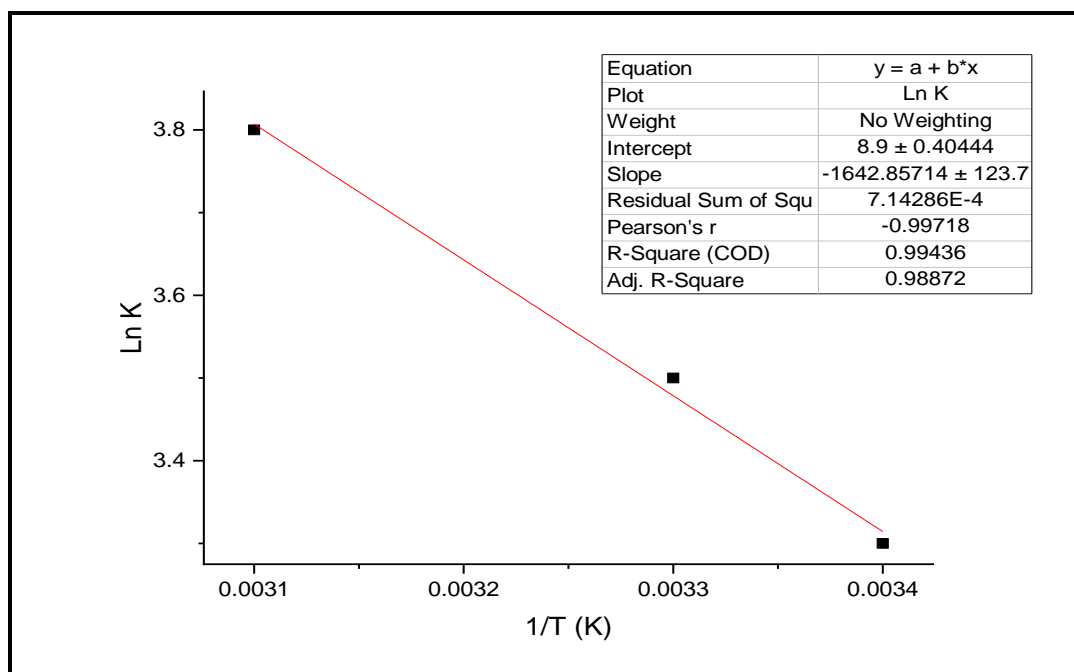


Figure (3-15): Image showing the ideal temperature for P<sub>γ</sub>

### 3.4.4. Finding the Thermodynamic Parameters for P<sub>γ</sub>

By applying the Van't Hoff equation, drawing the relationship between  $\ln K$  against the reciprocal of temperature Figure (3-16). The value of ( $\Delta H$ ) was calculated from the slope and the value of the activation energy ( $\Delta E_a$ ) is equal to the ( $\Delta H$ ) value of the liquids, while a ( $\Delta S$ ) value was calculated

from the intersection with the y-axis. As for the Gibbs free energy, it was found by applying the free Gibbs equation, Table(3-4).



**Figure (3-16): Van't Hoff equation for P<sub>1</sub>**

**Table (3-4): The values of ( $\Delta H$ ), ( $\Delta S$ ) and ( $\Delta G$ ) for P<sub>1</sub>**

$\Delta H$ (J.mol <sup>-1</sup> )	$\Delta S$ (J.K <sup>-1</sup> )	$\Delta G$ (J)
13608.713	73.994	-1391.499

The negative value of the Gibbs free energy indicates that the enzyme reaction is spontaneous. It also has a positive entropy value, making it random. In addition to positive enthalpy value making it endothermic. From above result, we can see that this reaction is the most thermally preferred.

**3.5. Characteristics of Meso (9-(hydroxymethyl)-1,2,4-dioxo-9,10-dihydro-13H-9,10-(epiethane[1,1,2]triazanoethane[1,2,2]triazyl)anthracen-13-yl)acetic acid (P<sub>r</sub>)**

The Fourier transform infrared (FTIR) spectrum of P<sub>r</sub> Figure (3-17) showed a medium broad peak at 3417 cm<sup>-1</sup> belonging to OH for both the acetyl linked to the pyrrole and the terminal OH of hydroxymethyl attached at 10-anthracene. The weak peak at 3093 cm<sup>-1</sup> refer to the stretching C-H (SP<sup>3</sup>) for the pyrrole ring. The weak peaks at 2951 cm<sup>-1</sup> and 2912 cm<sup>-1</sup> attributed to C-H (SP<sup>3</sup>) of acetyl. The weak peak at 1766 cm<sup>-1</sup> and the strong peak at 1697 cm<sup>-1</sup> attributed to the stretching active carbonyl amide of pyrrole. The weak peak at 1516 cm<sup>-1</sup> belong to C=C of the anthracene rings. The medium peak at 1234 cm<sup>-1</sup> attributed to the (C-O) bond of alcohol for the hydroxymethyl. (123-125). All peak appears in FTIR spectrum for all products seen in table (3-12).

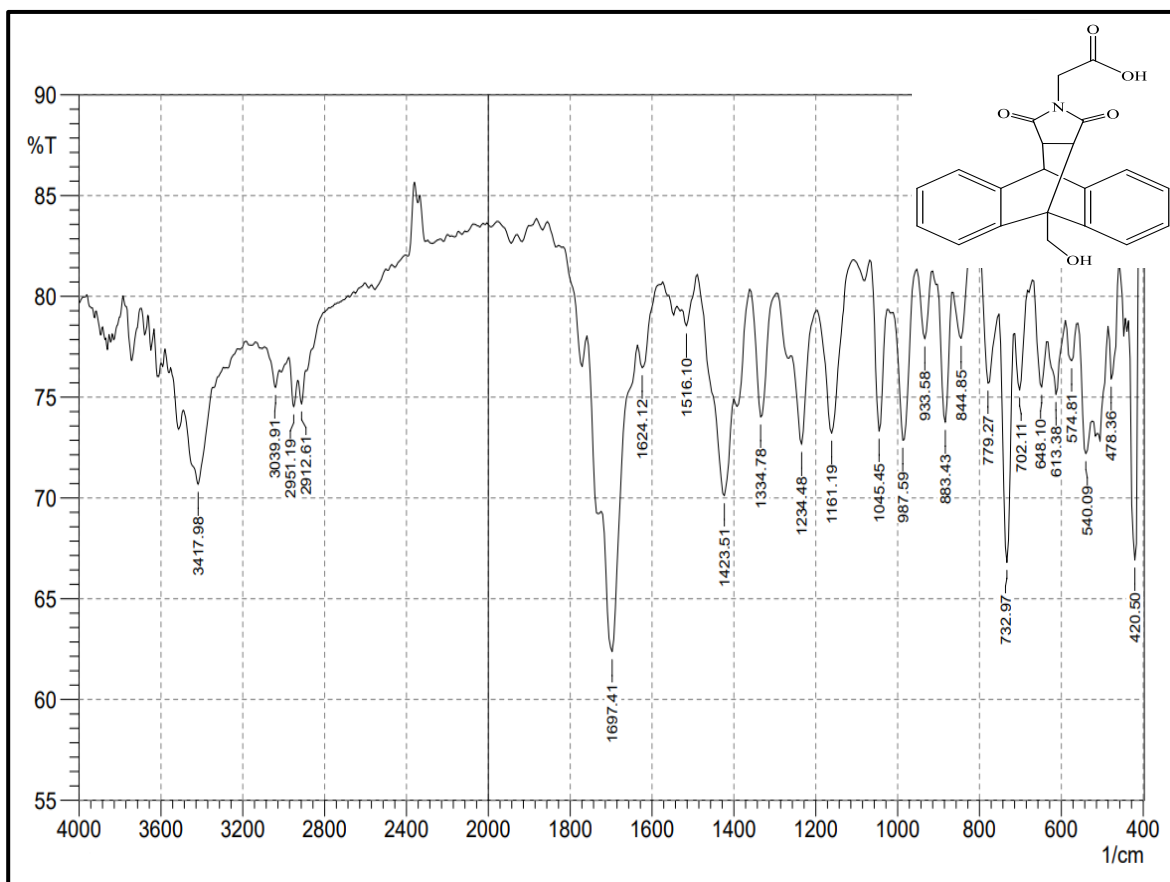


**Figure (3-17): The FTIR spectrum for P<sub>7</sub>**

The <sup>1</sup>H NMR spectrum for P<sub>7</sub> in D<sub>2</sub>O (Figure 3-18) displays the singlet peak at δ (1.21) ppm attributed to the CH<sub>3</sub> of acetyl group, which is attached to the N of pyrrole. The protons of the two CH groups attached to the carbonyl of pyrrole showed a multiplet at δ (7.48-7.60) ppm. The multiplet peak at δ (7.26-7.5) ppm belongs to the CH proton of the 9-H anthracene. The signal of the (OH) proton of the 10-methyl anthracene appeared as a peak at δ (8.50) ppm, in addition to the triplet peak at δ (9.30-9.43) ppm attributed to the protons of CH<sub>2</sub> attached to the hydroxyl group. The signal peak at δ (8.05) ppm is attributed to the (OH) of acetyl attached to pyrrole. The multiplet peaks at δ (7.14-7.18) ppm, δ (7.64-7.66) ppm, and δ (8.43-8.56) ppm are also observed.

ppm belong to protons of aromatic rings of anthracene. (126, 127). All peak appears in  $^1\text{H}$  NMR spectrum for all products seen in table(3-13).

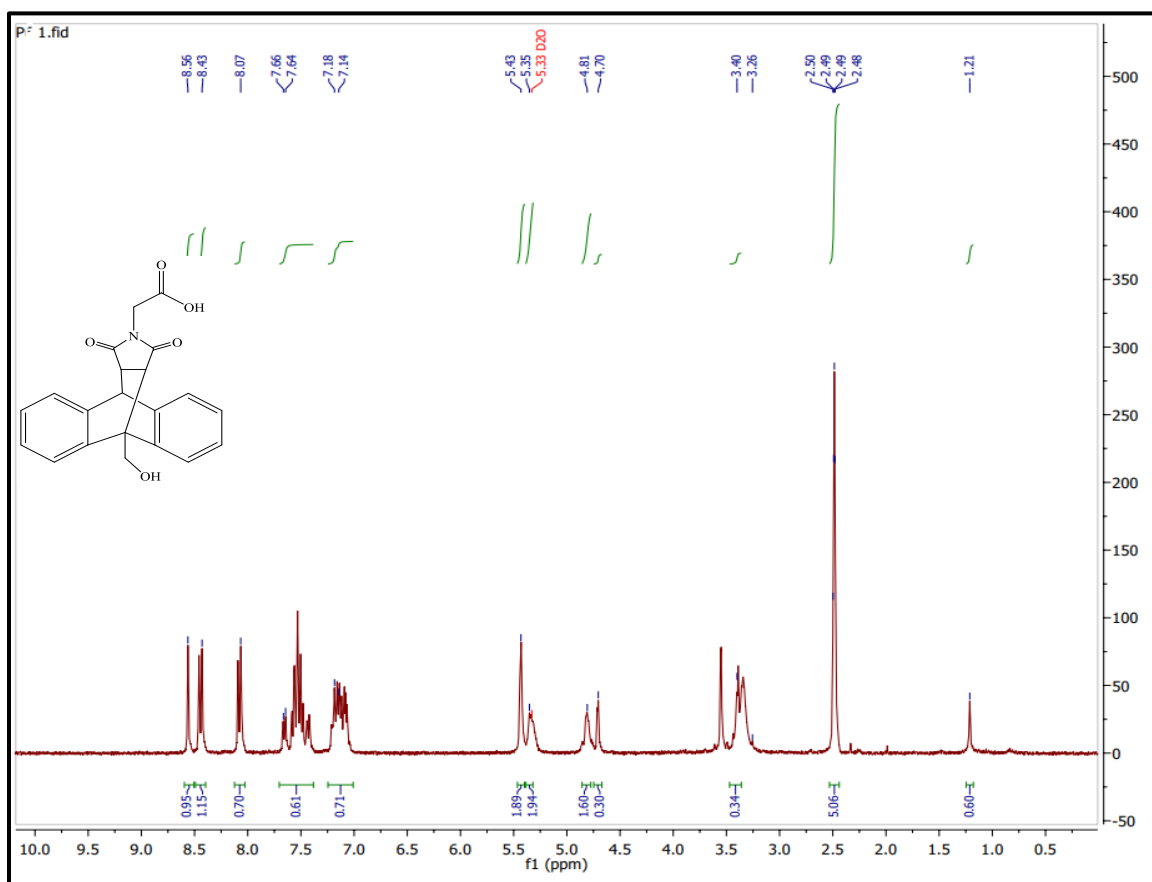


**Figure (3-18): The  $^1\text{H}$  NMR spectra for P7**

The  $^{13}\text{C}$  NMR spectrum of P7 in  $\text{CDCl}_3$  Figure (3-19) showed the peak at  $\delta$  (39.10) ppm attributed to the  $\text{CH}_3$  of acetyl group, which attached with the N of pyrrole. The peak at  $\delta$  (39.60) ppm belong to the  $\alpha$ -carbon of anthracene that attached to the  $\alpha$ -hydroxymethyl ( $\text{CH}_2\text{-OH}$ ) group. The peaks at  $\delta$  (50.20) ppm and  $\delta$  (50.80) ppm attributed to the two alpha carbons of pyrrole, respectively. The peak at  $\delta$  (60.70) ppm belong to the

carbon of hydroxymethyl that attached at 1'-anthracene. The peak at  $\delta$  (176.64) ppm belong to 9'-carbon of anthracene which closed the cycle with pyrrole. The peaks at  $\delta$  (120.14) ppm,  $\delta$  (120.26) ppm,  $\delta$  (126.24) ppm,  $\delta$  (126.71) ppm,  $\delta$  (129.17) ppm,  $\delta$  (129.21) ppm,  $\delta$  (130.73) ppm,  $\delta$  (143.12) ppm,  $\delta$  (143.23) ppm,  $\delta$  (143.17) ppm,  $\delta$  (138.73) ppm,  $\delta$  (125.26) ppm,  $\delta$  (125.14) ppm,  $\delta$  (130.21) ppm,  $\delta$  (126.74) ppm, and  $\delta$  (125.26) ppm attributed to the carbons of the anthracene rings. The peak at  $\delta$  (168.04) ppm belong to the carbon of the carbonyl for the acetyl that attached to the pyrrole. The peaks at  $\delta$  (176.36) ppm and  $\delta$  (177.07) ppm attributed to the carbons of the two carbonyl groups for the pyrrole ring, respectively. All peak appears in  $^{13}\text{C}$  NMR spectrum for all products seen in table(3-14).

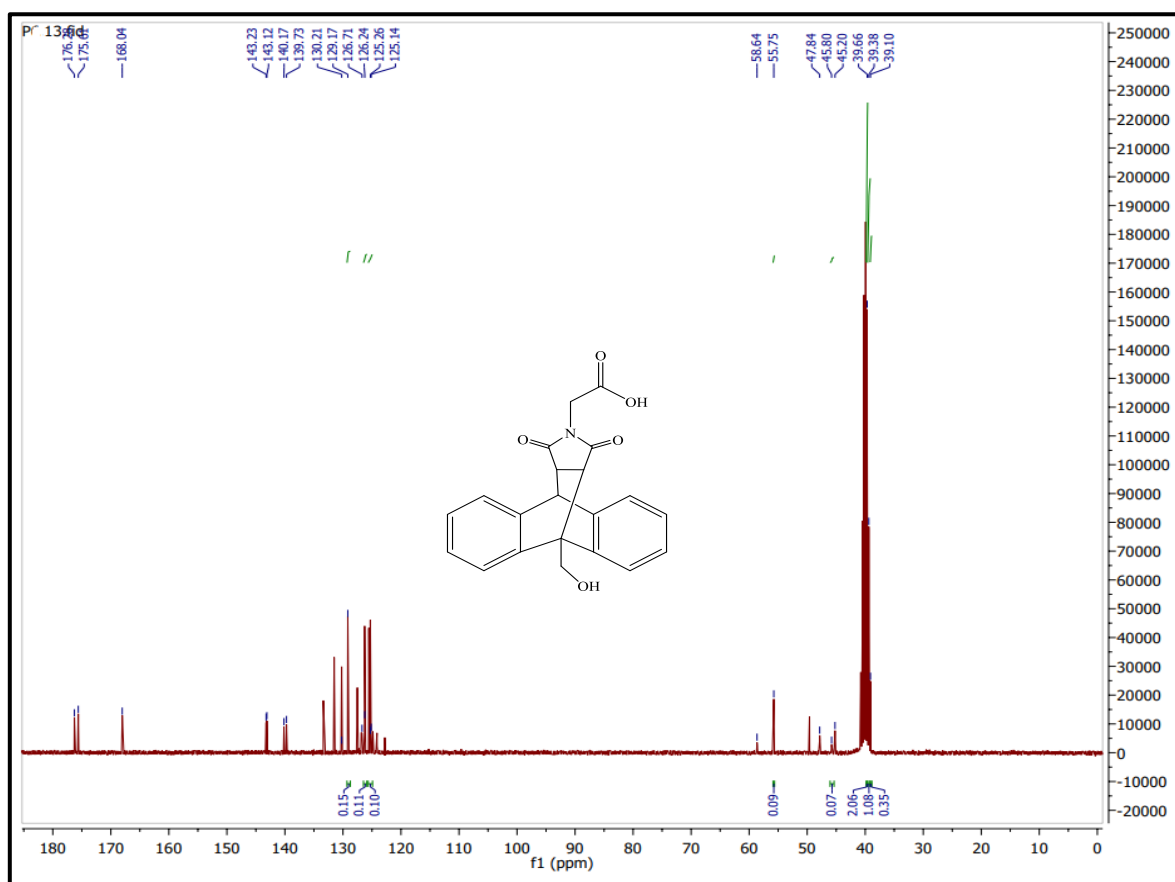


Figure (3-14): The  $^{13}\text{C}$  NMR spectrum of P7

The mass spectrum of P<sub>r</sub> appears signal at (364.1) m/z) relative to the molecular ion, the value close to the calculated molecular weight (363.1 g/mole), as shown in Figure (3-20).

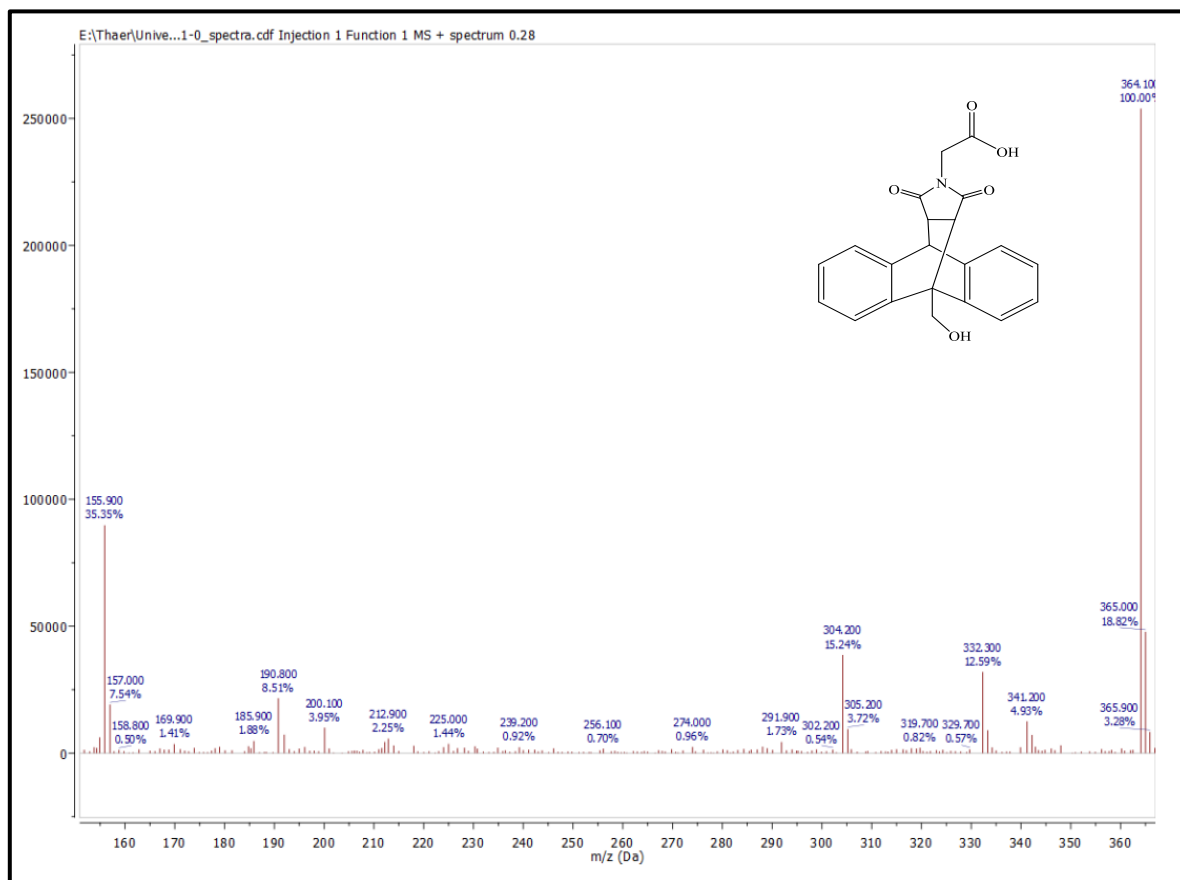
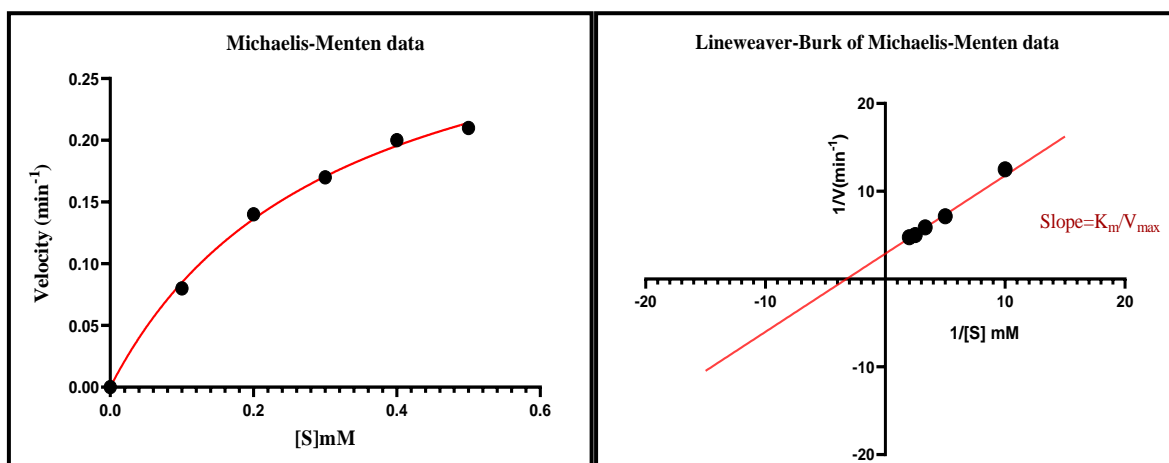


Figure (3-20): The mass spectrum of P<sub>r</sub>

**3.6. Kinetic Study of Meso (9-(hydroxymethyl)-1,2,14-dioxo-9,10-dihydro-13H-9,10-(epiethane[1,1,2]triazolanoethane[1,2,2]triazol)anthracen-13-yl)acetic acid (P<sub>r</sub>)**

**3.6.1. Determine the values of the reaction rate constant (Michaelis-Menten constant) and the maximum velocity of the enzymatic reaction for P<sub>r</sub>**

The Michaelis-Menten and Line Weaver-Burk equations were applied. The values of the maximum velocity of the enzymatic reaction and the reaction rate constant were as shown in the, Figure (3-21), and in Table (3-5).



**Figure (3-21): Michaelis-Menten diagram and line weaver - Burk diagram of the D-A reaction of P<sub>r</sub>**

**Table (3-5): The Values of K<sub>m</sub> and V<sub>max</sub> for the D-A reaction of P<sub>r</sub>**

kinetic Parameters	Michaels Menten plot	line weaver Burk plot
V <sub>max</sub> (min <sup>-1</sup> )	0.3463	0.3463
K <sub>m</sub>	0.3087	0.3087



### ۳.۶.۲. Finding of Enzymatic Activity of P<sub>r</sub>

The ideal enzymatic specific activity was found by drawing the relationship between the enzyme reaction velocity and the activity Figure, (۳-۲۲).

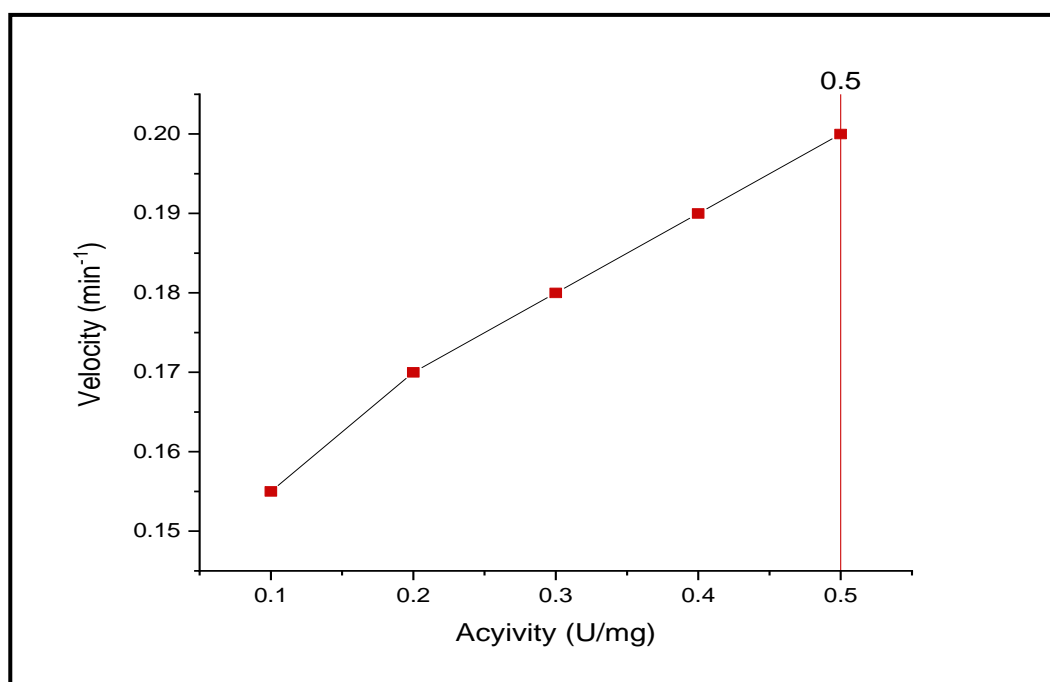


**Figure (۳-۲۲): The appropriate enzyme activity of MaDA for P<sub>r</sub>**

From the foregoing, the ideal enzymatic specific activity for this reaction is (۰.۵ U/mg).

### 3.6.3. Finding Optimum Temperature for P<sub>r</sub>

The optimum temperature for the D-A reaction of P<sub>r</sub> was determined by plot the velocity of the reaction against the different temperatures (15, 25, 40 C°). The 25 C° is the ideal temperature, Figure (3-23).

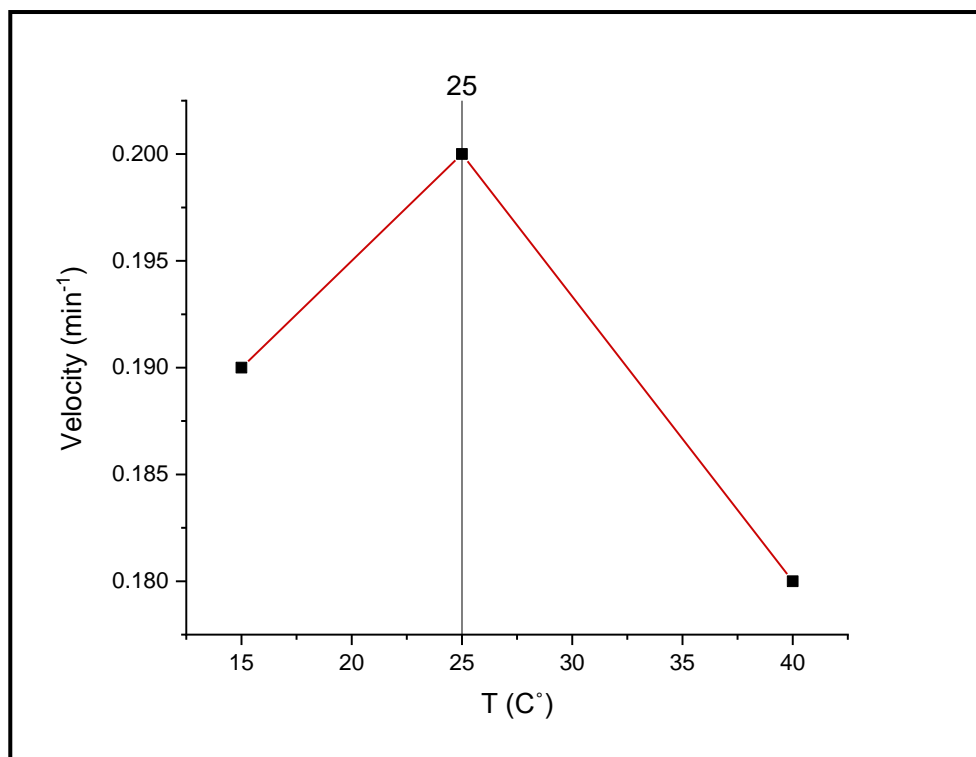
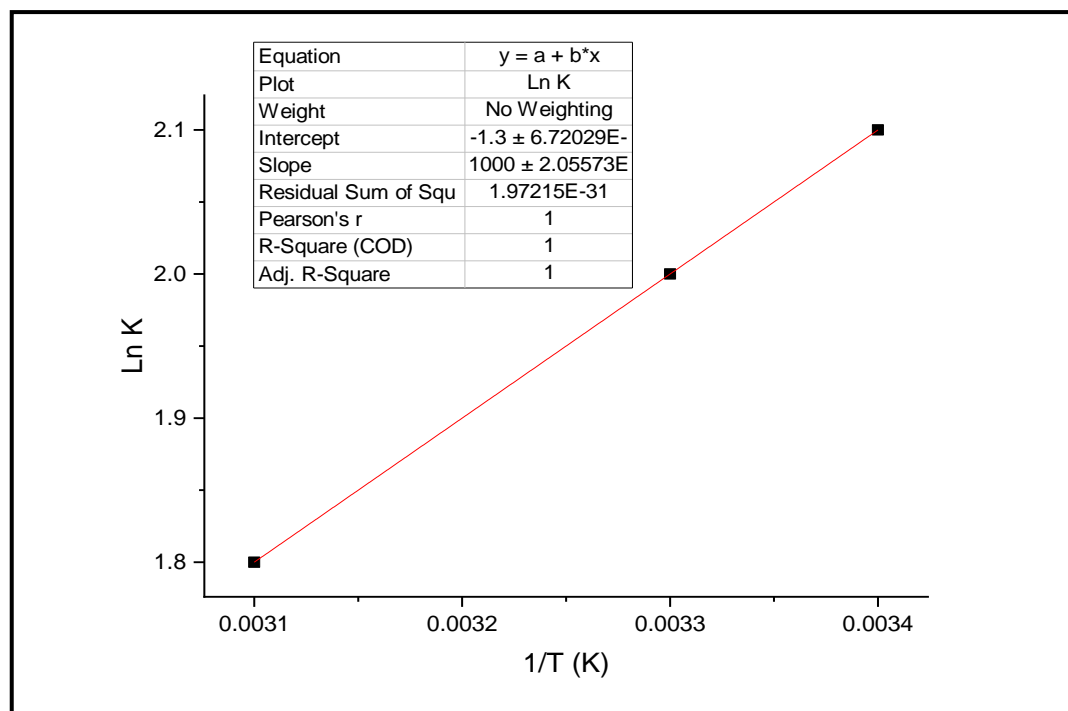


Figure (3-23): Image showing the ideal temperature for P<sub>r</sub>

### 3.6.4. Finding the Thermodynamic Parameters for P<sub>r</sub>

By creating a Van't Hoff diagram Figure (3-24), which graphs the values of (ln K) against the inverse of the temperature, and by following the previously mentioned processes, the values of the change in  $\Delta H$ ,  $\Delta S$ , and  $\Delta G$  are presented in Table (3-5).



**Figure (3-24): Van't Hoff equation for P<sub>r</sub>**

**Table (3-25): The values of ( $\Delta H$ ), ( $\Delta S$ ) and ( $\Delta G$ ) of P<sub>r</sub>**

$\Delta H$ (J.mol <sup>-1</sup> )	$\Delta S$ (J.K <sup>-1</sup> )	$\Delta G$ (J)
-8314	-10.808	-0.93216

The negative value of the Gibbs free energy indicates that the enzyme reaction is spontaneous. It also has a negative entropy value, making it nonrandom. In addition to negative enthalpy value making it exothermic.

### 3.7. Characteristics of Meso (1<sup>3</sup>-methyl-1<sup>2</sup>,1<sup>4</sup>-dioxo-9,1<sup>0</sup>- (epiethane[1,1,2]triazanoethane[1,2,2]triazyl)anthracen- 9(1<sup>0</sup>H)-yl)boronic acid (P<sub>4</sub>)

The FTIR spectrum for this product P<sub>4</sub> Figure (3-20) exhibited the strong a broad peak at 3333 cm<sup>-1</sup> and the medium broad peak at 3279 cm<sup>-1</sup> attributed to the two OH of the boric acid that linked at 1<sup>0</sup>-anthracene. The weak peak at 3074 cm<sup>-1</sup> belong to the stretching C-H (SP<sup>3</sup>) for the pyrrole ring. In addition, the weak peak at 2900 cm<sup>-1</sup> belong to C-H (SP<sup>3</sup>) of the methyl, which linked to the pyrrole ring. The two peaks that related to stretching active carbonyl amide groups of pyrrole ring appeared as the weak peak at 1766 cm<sup>-1</sup> and the strong sharp peak at 1680 cm<sup>-1</sup>. The weak peak at 1000 cm<sup>-1</sup> belong to C=C of anthracene rings. Furthermore, peak at 1384, 1346 cm<sup>-1</sup> belong to B-O (1<sup>2</sup>3-1<sup>2</sup>0). All peak appears in FTIR spectrum for all products seen in table(3-12).

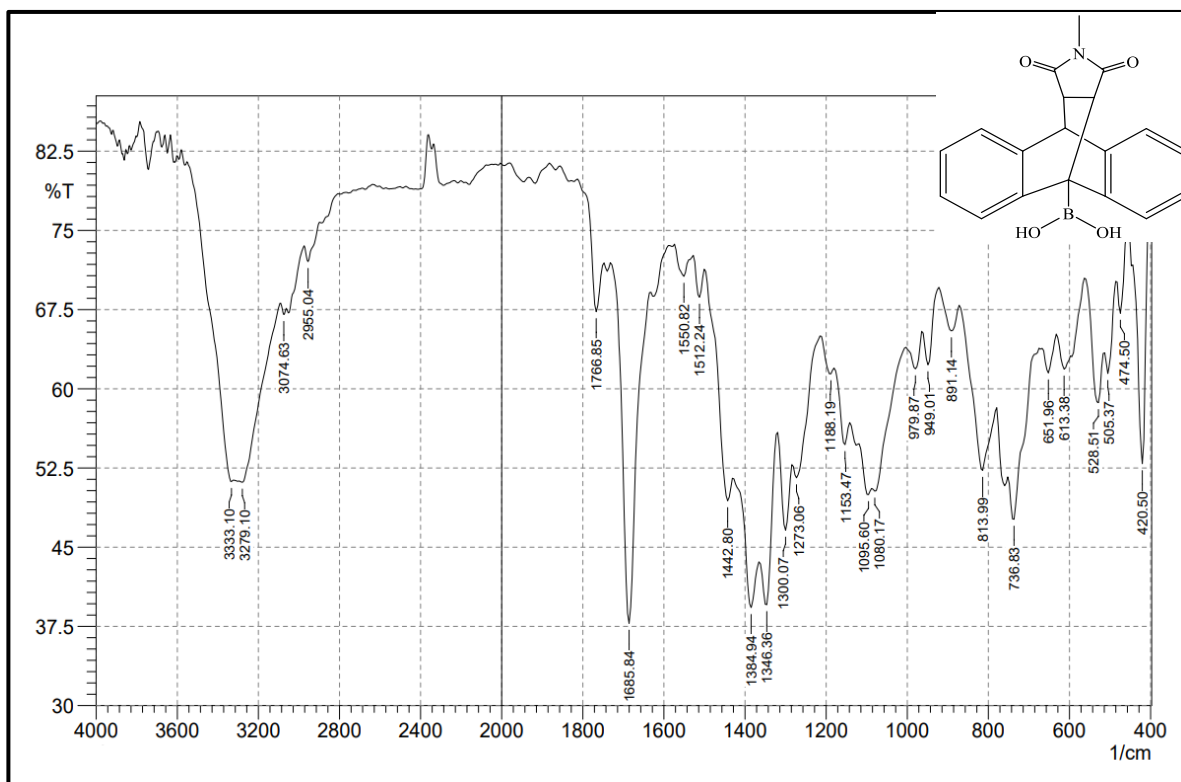


**Figure (3-25): The FTIR spectrum for P<sub>4</sub>**

The <sup>1</sup>H NMR spectrum for P<sub>4</sub> in D<sub>2</sub>O Figure (3-26) display the singlet peak at δ (1.22) ppm belong to protons of CH<sub>2</sub> attached to N of pyrrole ring, while the protons of the two CH groups that attached to carbonyl of pyrrole showed multiplet at δ (2.29-2.31) ppm and at δ (2.47-2.50) ppm, respectively. The multiplet peak at δ (3.16-3.34) ppm belong to CH proton of the 9-H anthracene. The signal of protons of the two (OH) groups of the boronic acid-anthracene appear the peaks at δ (8.45) ppm and δ (8.80) ppm, respectively. The multiplet peaks at δ (7.00-7.02) ppm, δ (7.12-7.14) ppm, and δ (8.00-8.02) ppm belong to protons of aromatic rings of anthracene. (26, 27). All peak appears in <sup>1</sup>H NMR spectrum for all products seen in table(3-13).

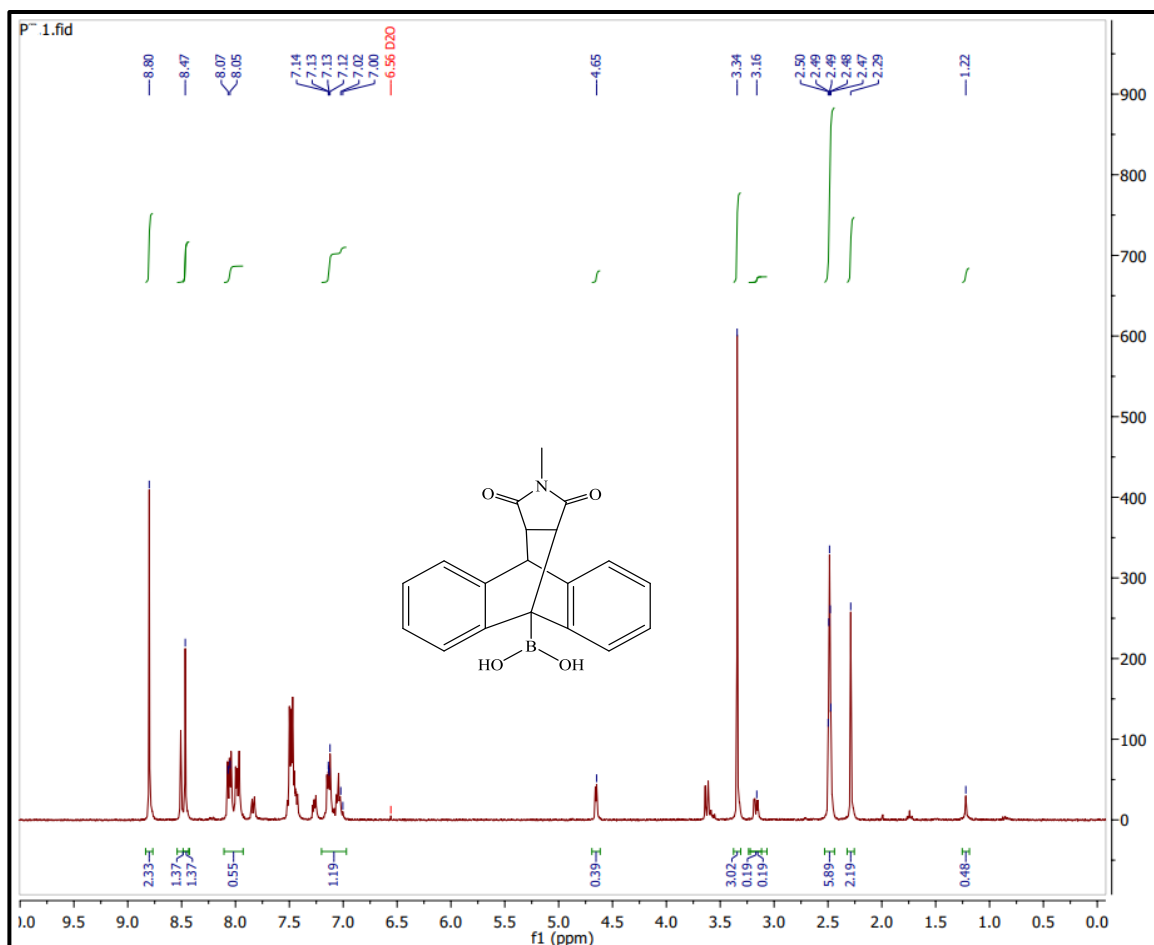


**Figure (3-26): The  $^1\text{H}$  NMR spectrum for  $\text{P}_z$**

The  $^{13}\text{C}$  NMR spectrum of  $\text{P}_z$  in  $\text{DMSO-d}_6$  Figure (3-27) showed the peak of the carbon atom of methyl group that attaches to N at  $\delta$  (24.24) ppm. The peak at  $\delta$  (40.84) ppm belong to the  $\beta$ -carbon of anthracene that attached to the boric acid. The peak at  $\delta$  (47.80) ppm belong to  $\alpha$ -carbon of anthracene which closed the cycle with pyrrole. The peak at  $\delta$  (48.01) attributed to the two alpha carbons of pyrrole. The peaks at  $\delta$  (120.46) ppm,  $\delta$  (120.60) ppm,  $\delta$  (120.72) ppm,  $\delta$  (126.07) ppm,  $\delta$  (126.37) ppm,  $\delta$  (127.07) ppm,  $\delta$  (128.89) ppm,  $\delta$  (129.00) ppm,  $\delta$  (131.22) ppm,  $\delta$  (140.02) ppm,  $\delta$  (141.78) ppm,  $\delta$  (143.69) ppm, and  $\delta$  (144.41) ppm attributed to the

carbons of the anthracene rings. The peaks at  $\delta$  (177.42) ppm and  $\delta$  (177.42) ppm attributed to the carbons of the two carbonyl groups for the pyrrole ring, respectively. All peak appears in  $^{13}\text{C}$ NMR spectrum for all products seen in table (3-14).

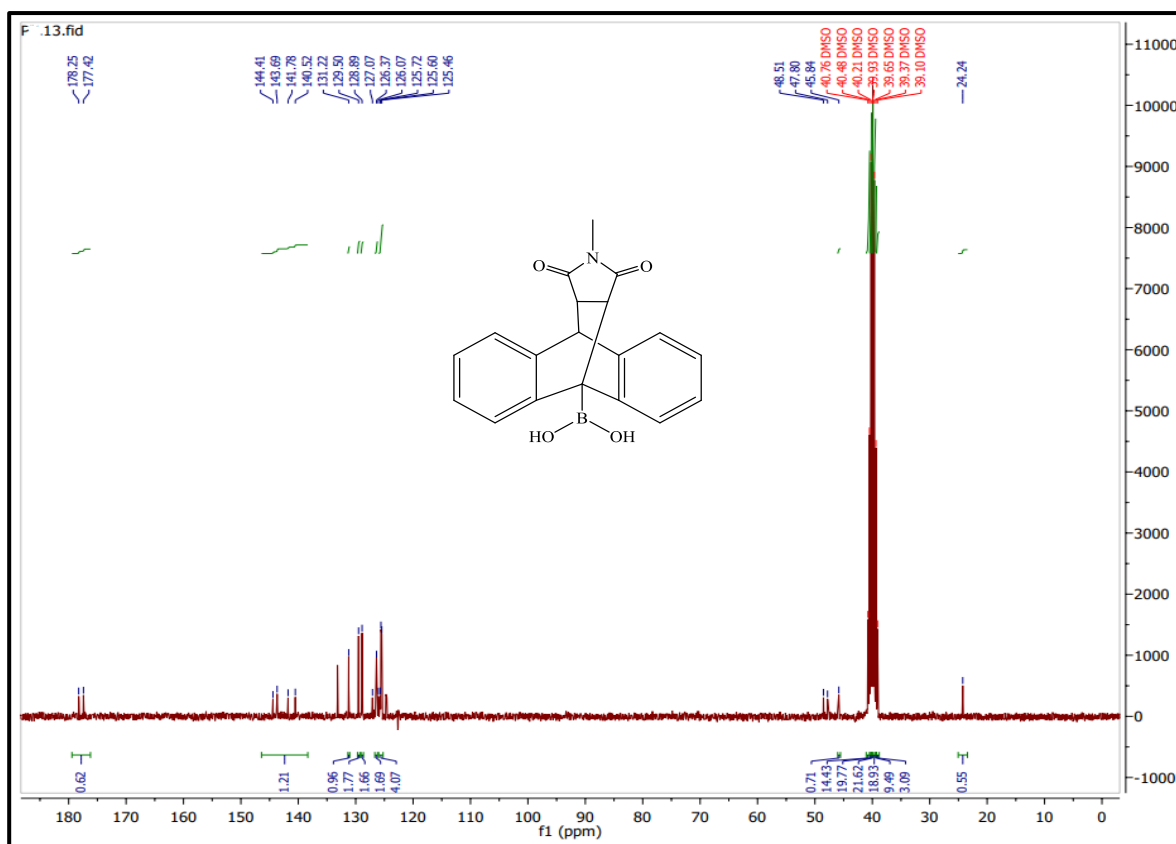


Figure (3-27): The  $^{13}\text{C}$  NMR spectra for  $\text{P}_4$

The mass spectrum of  $\text{P}_4$  appears signal at (332.3 m/z) relative to the molecular ion, the value close to the calculated molecular weight (333.1 g/mole), as shown in Figure (3-28).

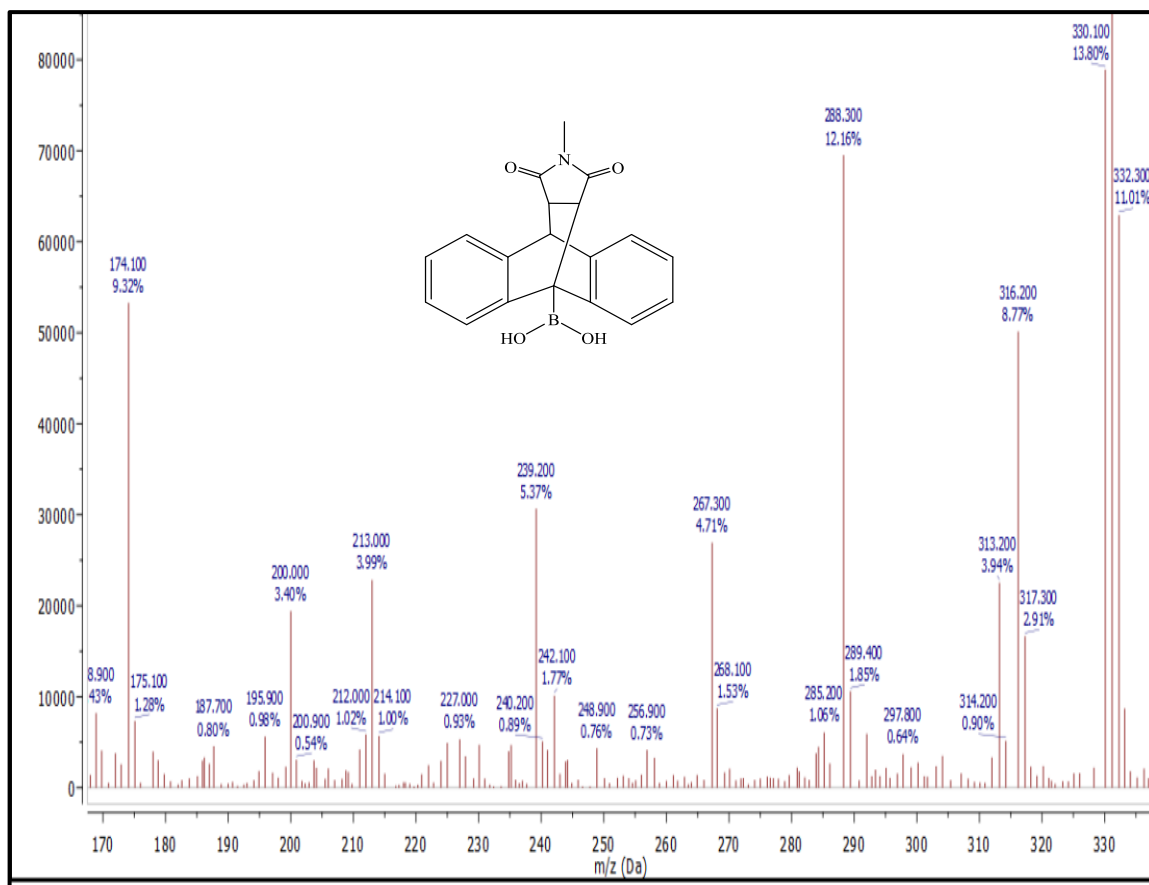


Figure (3-28): The mass spectrum of P4

3.8. Kinetic Study of Meso (1-methyl-1,2,3-dioxo-9,10-epiethane[1,1,2]triazanoethane[1,2,2]triazyl)anthracen-9(10H)-yl)boronic acid (P4)

3.8.1. Determine the values of the reaction rate constant (Michaelis Menten constant) and the maximum velocity of the enzymatic reaction for P4

From the absorbance readings against the  $D_T$  concentrations, the corresponding reaction rate was found. After that, the Michaelis-Menten



equation was applied by drawing the relationship between the velocity of enzymatic reaction and the concentration of the D<sub>r</sub> as substrate, as well as the line Weaver-Burk equation was applied by plot the relationship between the reciprocal of the velocity ( $1/V$ ) versus the reciprocal of the concentration ( $1/[S]$ ) to reach the value of the enzymatic reaction rate constant ( $K_m$ ) and the maximum velocity of the enzymatic reaction ( $V_{max}$ ). Figure (3-29) and Table(3-6)

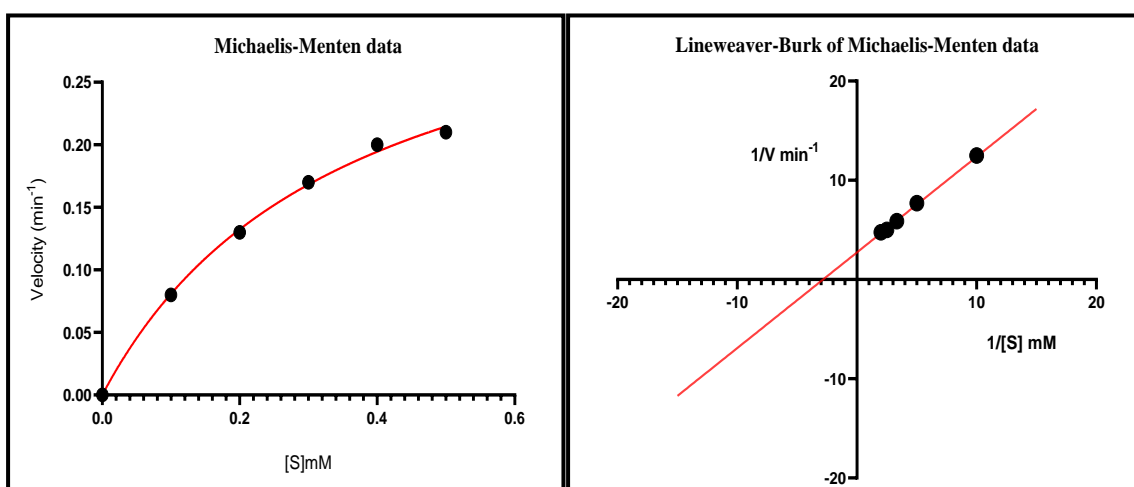


**Figure (3-29): Michaelis-Menten diagram and line weaver - Burk diagram of the D-A reaction of P<sub>4</sub>**

**Table (3-6): The Values of  $K_m$  and  $V_{max}$  for the D-A reaction of P<sub>4</sub>**

kinetic Parameters	Michaels Menten plot	line weaver Burk plot
$V_{max}$ ( $\text{min}^{-1}$ )	0.2609	0.2609
$K_m$	0.3027	0.3027

From the above-mentioned and depending on the value of the Michaelis-Menten constant ( $K_m$ ), the affinity between the substrate (D<sub>r</sub>) and the

enzyme (MaDA) in this reaction is the least value among the other interactions mentioned.

### ۳.۸.۲. Finding of Enzymatic Activity of P<sub>۴</sub>

The ideal enzymatic activity was found by drawing the relationship between the enzyme reaction speed and the specific activity, which produced a bell-like shape, Figure (۳-۳۰).

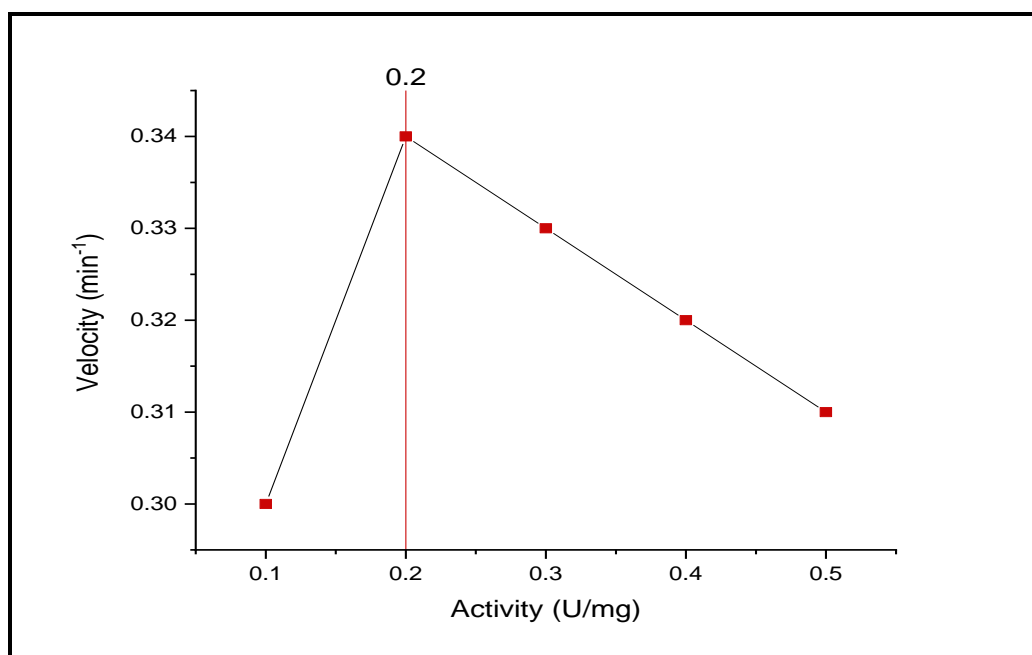


**Figure (۳-۳۰): The appropriate enzyme activity of MaDA for P<sub>۴</sub>**

From the foregoing, the ideal enzymatic specific activity for this reaction is (۰.۲ U/mg).

### 3.8.3. Finding Optimum Temperature for $P_4$

The optimum temperature for the D-A reaction of  $P_4$  was determined by plot the velocity of the reaction against the different temperatures ( $15, 25, 40$ ,  $^{\circ}\text{C}$ ). The  $25^{\circ}\text{C}$  is the ideal temperature, Figure (3-31).

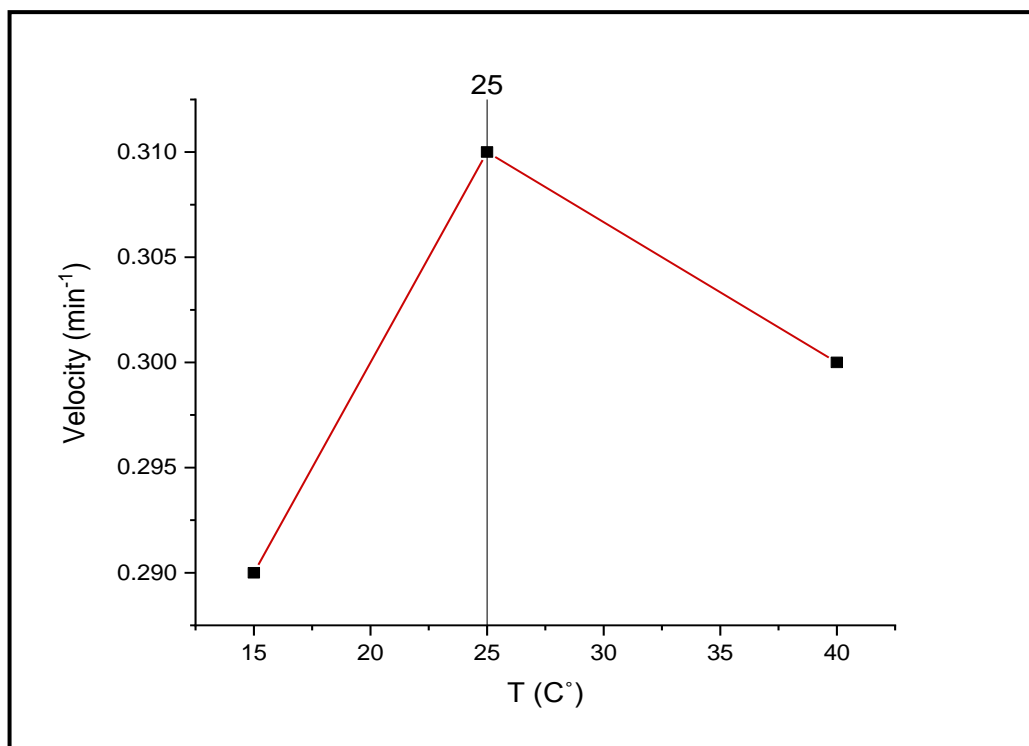
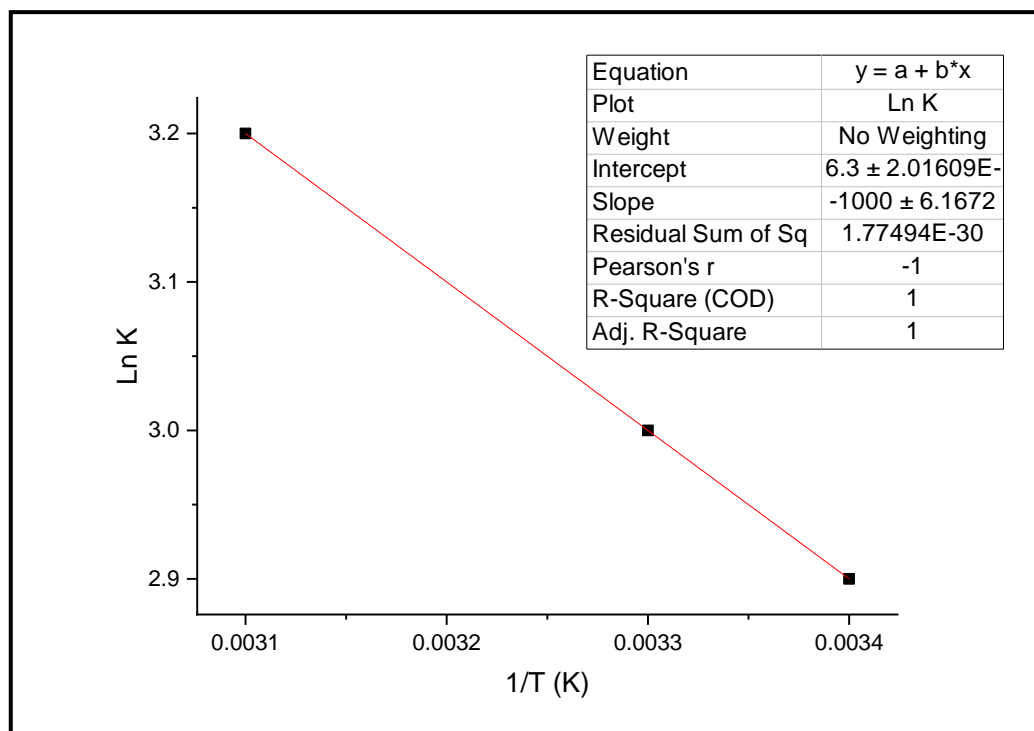


Figure (3-31): Image showing the ideal temperature for  $P_4$ .

### 3.8.4. Finding the Thermodynamic Parameters for $P_4$

By creating a Van't Hoff diagram Figure (3-32), which graphs the values of  $(\ln K)$  against the inverse of the temperature, and by following the previously mentioned processes, the values of the change in  $\Delta H$ ,  $\Delta S$ , and  $\Delta G$  are presented in Table (3-7).



**Figure (3-32): Van't Hoff equation for P<sub>4</sub>**

**Table (3-33): The values of ( $\Delta H$ ), ( $\Delta S$ ) and ( $\Delta G$ ) for P<sub>4</sub>**

$\Delta H$ (J.mol <sup>-1</sup> )	$\Delta S$ (J.K <sup>-1</sup> )	$\Delta G$ (J)
8314	52.378	-7294.644

The negative value of the Gibbs free energy indicates that the enzyme reaction is spontaneous. It also has a positive entropy value, making it random. In addition to positive enthalpy value making it endothermic

### 3.9. Characteristics of Meso (1,3-dioxo-2-propyl-9,10-(epiethane[1,1,2]triazanoethane[1,2,2]triazyl)anthracen-9(10H)-yl)boronic acid (P.)

The FTIR spectrum for this product P. Figure (3-33) appeared the strong a broad peak at  $3329\text{ cm}^{-1}$  attributed to the two OH of the boric acid that linked at 10-anthracene. The weak peak at  $3001\text{ cm}^{-1}$  attributed to the stretching C-H ( $\text{SP}^3$ ) for the pyrrole ring. The weak peaks at  $2943\text{ cm}^{-1}$ ,  $2878\text{ cm}^{-1}$ , and  $2880\text{ cm}^{-1}$  belong to C-H ( $\text{SP}^3$ ) of the propyl, which linked to the pyrrole ring. The two stretching peaks related to the active carbonyl for pyrrole ring, appeared as the weak peak at  $1763\text{ cm}^{-1}$  and the strong sharp peak at  $1681\text{ cm}^{-1}$ . The weak peak at  $1004\text{ cm}^{-1}$  belong to C=C of the anthracene rings. The peaks at  $1392, 1360\text{ cm}^{-1}$  belong to B-O (123-120). All peak appears in FTIR spectrum for all products seen in table(3-12).

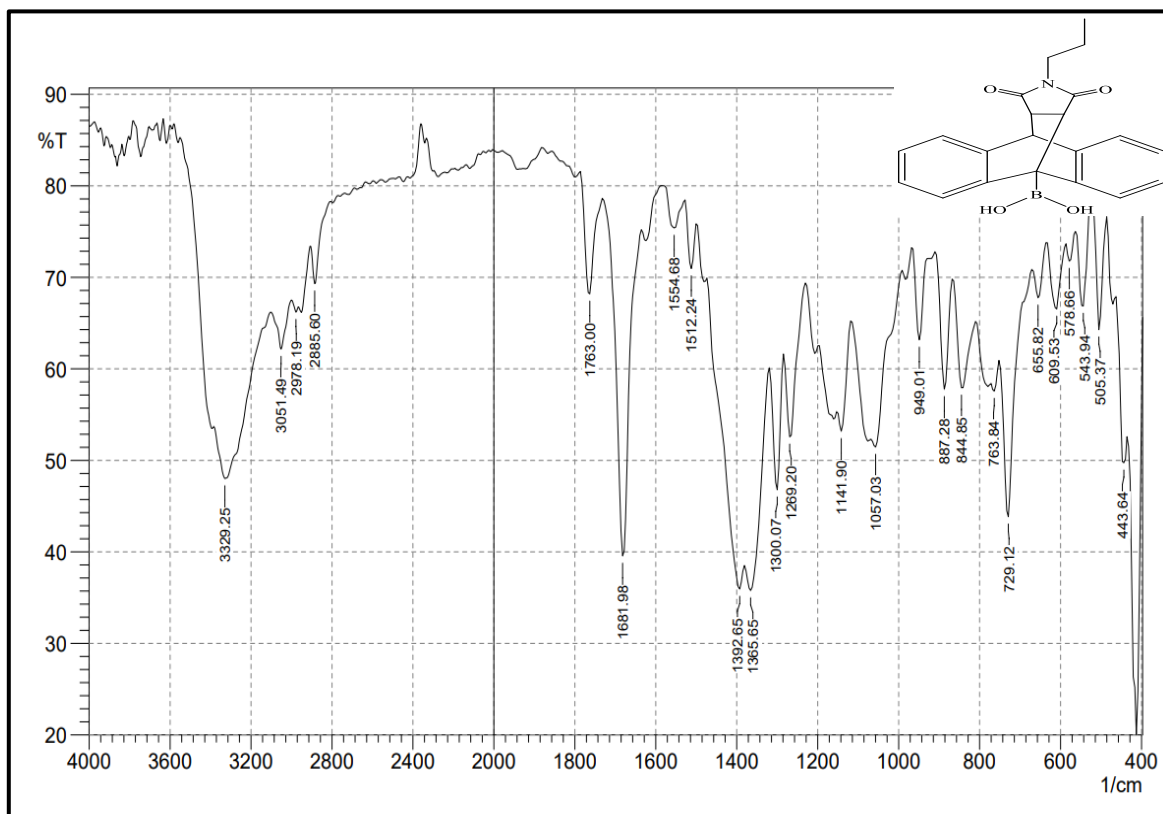


**Figure (3-33): The FTIR spectrum for P.**

The <sup>1</sup>H NMR spectrum for P, in D<sub>2</sub>O Figure (3-34) display the quartet peak at δ (0.41-0.43) ppm attributed to the terminal CH<sub>3</sub> of propyl group, which attached with pyrrole, the hexate peak at δ (0.67-0.72) ppm belong to the protons of middle CH<sub>2</sub> of propyl, and the triplet peak at δ (1.21-1.22) belong to the CH<sub>2</sub> of propyl that attached to N of pyrrole ring. The protons of the two CH groups that attached to carbonyl of pyrrole showed multiplet at δ (1.72-1.76) ppm and at δ (2.48-2.50) ppm, respectively. The multiplet peak at δ (3.30-3.62) ppm belong to CH proton of the 9-H anthracene. The signal of protons of the two (OH) groups of the 10-boronic acid-anthracene appear the peaks at δ (8.47) ppm and δ (8.80) ppm, respectively. The multiplet peaks at δ (7.12-7.10) ppm, δ (7.40-7.50) ppm, and δ (8.03-8.08) ppm belong to protons of aromatic rings of anthracene. (126, 127). All peak appears in <sup>1</sup>H NMR spectrum for all products seen in table (3-13).

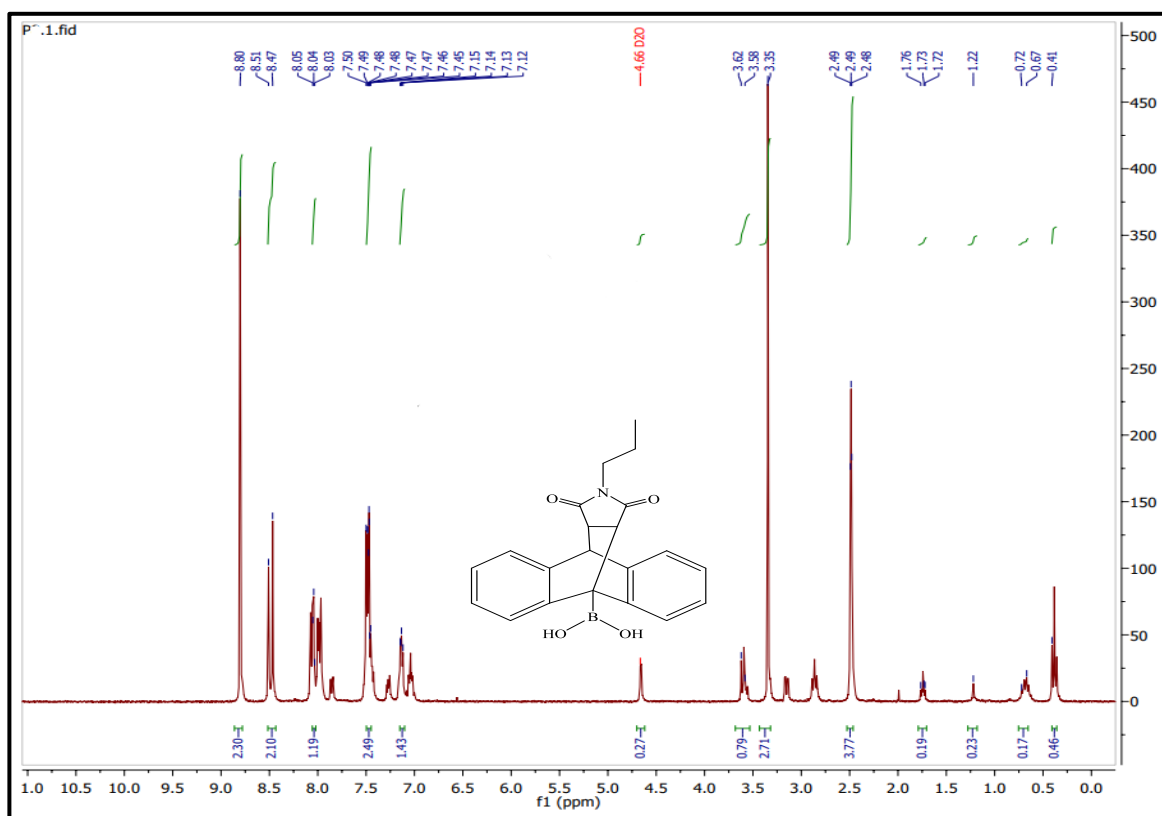
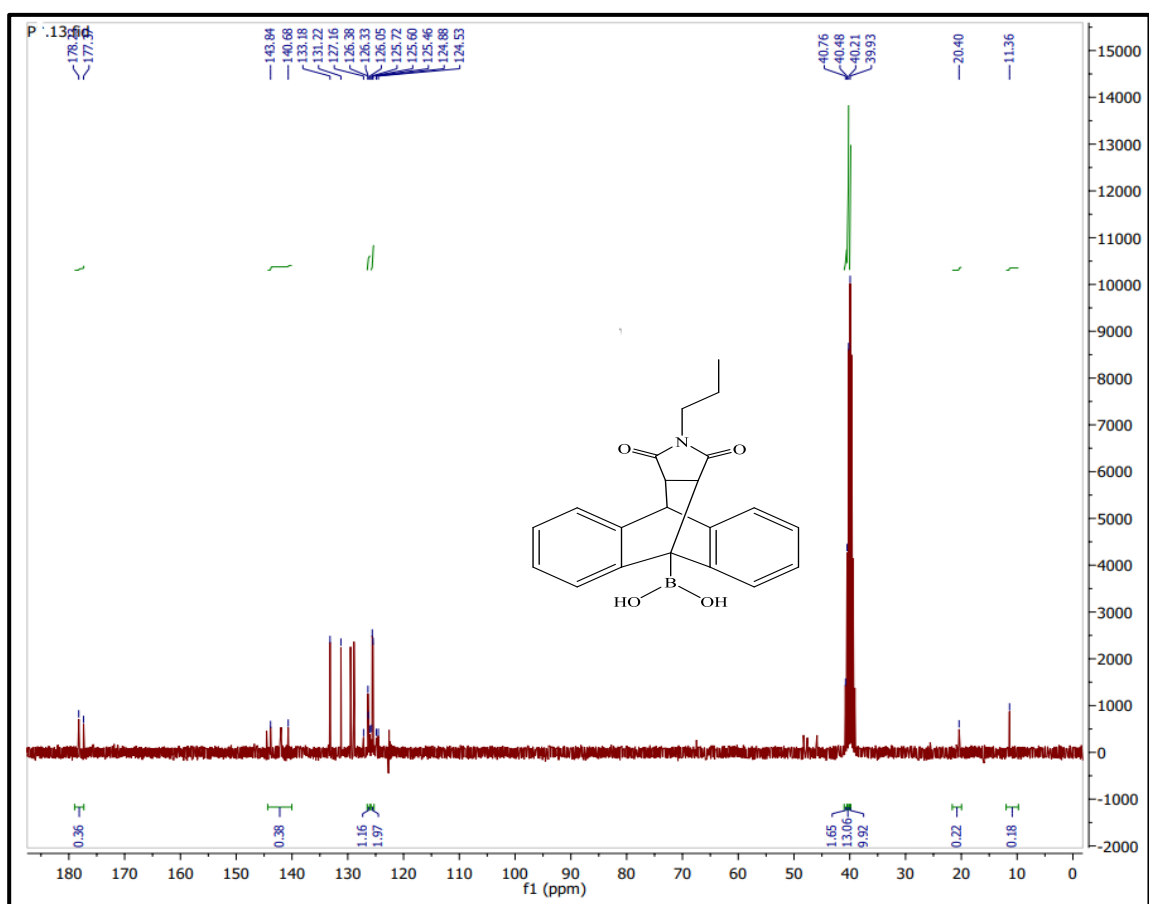


Figure (3-34): The  $^1\text{H}$  NMR spectrum for P.

The  $^{13}\text{C}$  NMR spectrum of P, in  $\text{CDCl}_3$  Figure (3-35) showed a peak at  $\delta$  (11.36) ppm attributed to the terminal  $\text{CH}_3$  of propyl that linked with pyrrole, a peak at  $\delta$  (30.40) ppm attributed to the middle  $\text{CH}_2$  of propyl, and a peak at  $\delta$  (39.93) ppm attributed to the  $\text{CH}_2$  of propyl that attached to the N of pyrrole. The peak at  $\delta$  (40.21) ppm belong to the  $\beta$ -carbon of anthracene that attached to the boric acid. The peak at  $\delta$  (40.48) ppm belong to  $\alpha$ -carbon of anthracene which closed the cycle with pyrrole. The peak at  $\delta$  (40.76) ppm attributed to the two alpha carbons of pyrrole ring. The peaks at  $\delta$  (124.03) ppm,  $\delta$  (124.88) ppm,  $\delta$  (120.46) ppm,  $\delta$  (120.60) ppm,  $\delta$  (120.72) ppm,  $\delta$  (126.00) ppm,  $\delta$  (126.33) ppm,  $\delta$  (126.38) ppm,  $\delta$  (127.16) ppm,  $\delta$  (131.22) ppm,  $\delta$  (133.18) ppm,  $\delta$  (140.63) ppm, and  $\delta$  (143.84)

attributed to the carbons of the anthracene rings. The peaks at  $\delta$  (177.37) ppm and  $\delta$  (178.23) ppm attributed to the carbons of the two carbonyl groups for the pyrrole, respectively. All peak appears in  $^{13}\text{C}$ NMR spectrum for all products seen in table (3-14).



**Figure (3-30): The  $^{13}\text{C}$  NMR spectrum for P.**

The mass spectrum of P appears at (362.1) m/z relative to the molecular ion, the value close to the calculated molecular weight (361.1) g/mole, as shown in Figure (3-36).



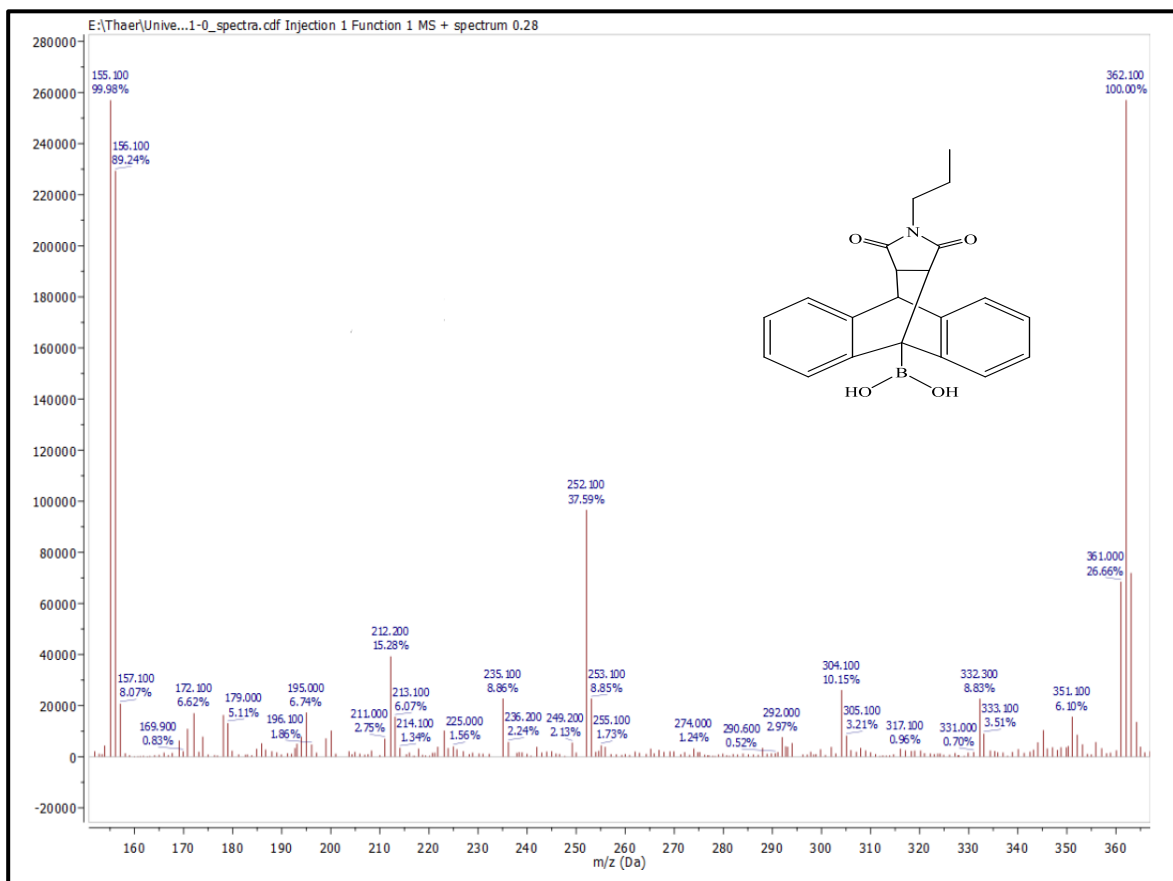
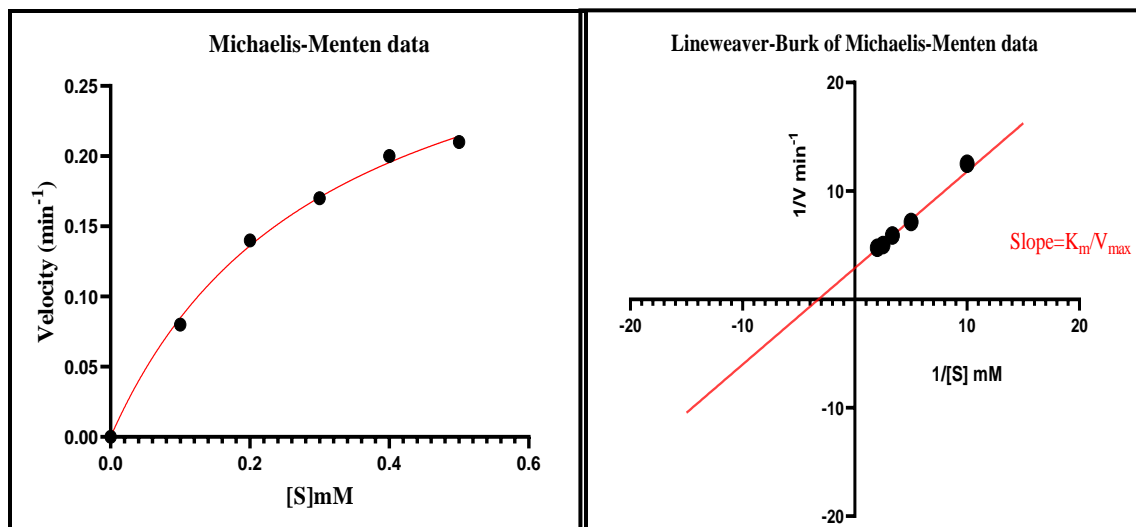


Figure (3-36): The mass spectrum for P.

3.1. Kinetic Study of Meso (1,2-dioxo-3-propyl-9,10-(epiethane[1,1,2]triazanoethane[1,2,2]triyl)anthracen-9(10H)-yl)boronic acid (P)

3.1.1. Determine the values of the reaction rate constant (Michaelis Menten constant) and the maximum velocity of the enzymatic reaction for P.

The Michaelis-Menten and Line Weaver-Burk equations were applied. the values of the maximum velocity of the enzymatic reaction and the reaction rate constant were as shown in the Figure (3-37), and in Table (3-8).



**Figure (3-37): Michaelis-Menten diagram and line weaver - Burk diagram of the D-A reaction of P.**

**Table (3-8): The Values of  $K_m$  and  $V_{max}$  for the D-A reaction of P.**

kinetic Parameters	Michaels Menten plot	line weaver Burk plot
$V_{max}$ (min <sup>-1</sup> )	0.3409	0.3409
$K_m$	0.3079	0.3079

### ۳.۱.۰.۲. Finding of Enzymatic Activity of P.

The ideal enzymatic specific activity was found by drawing the relationship between the enzyme reaction velocity and the activity, which produced a bell-like shape Figure (۳-۳۸).

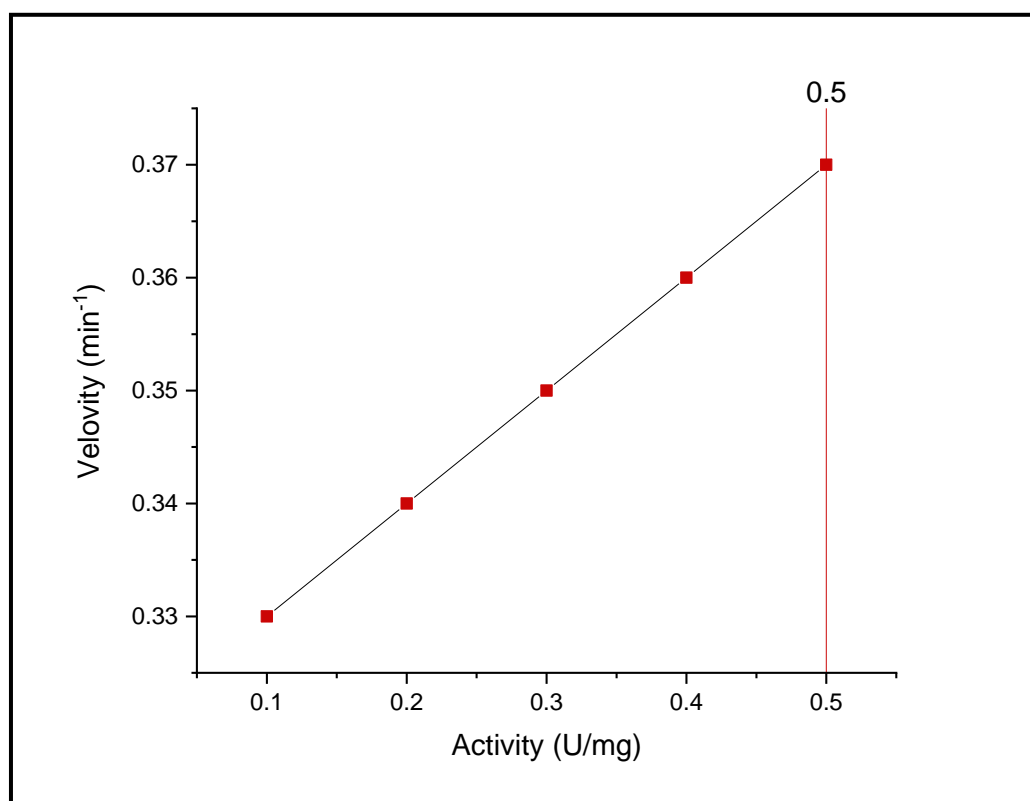


**Figure (۳-۳۸): The appropriate enzyme activity of MaDA for P.**

From the foregoing, the ideal enzymatic specific activity for this reaction is ۰.۵ (U/mg).

### 3.1.3. Finding Optimum Temperature for P.

The optimum temperature for the D-A reaction of P. was determined by plot the velocity of the reaction against the different temperatures (15, 20, 25, 30, 35, 40 C°). The 25 C° is the ideal temperature Figure, (3-39).

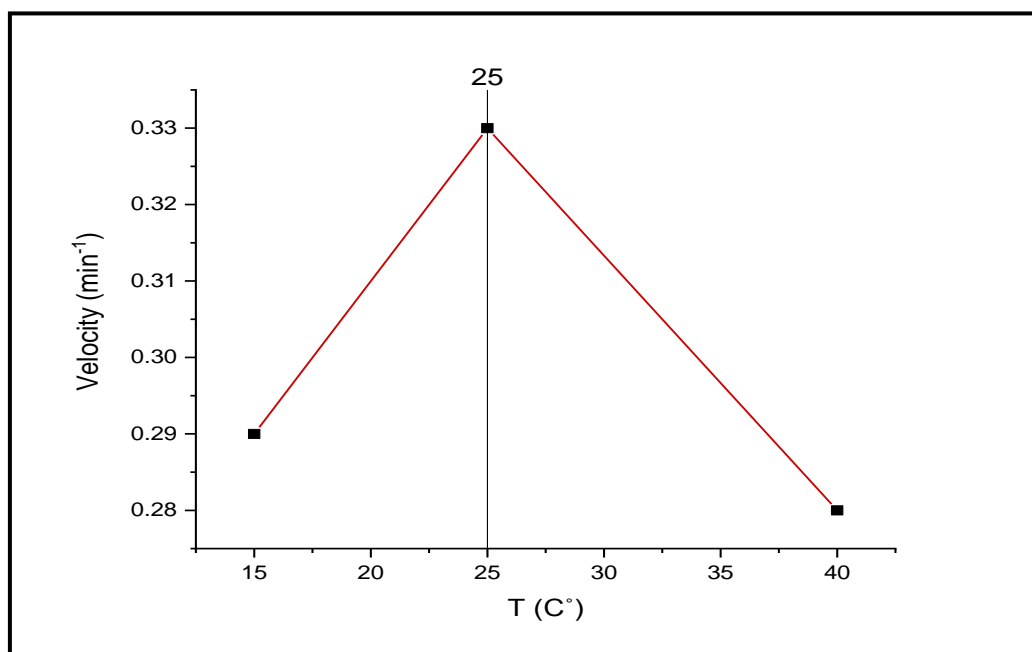
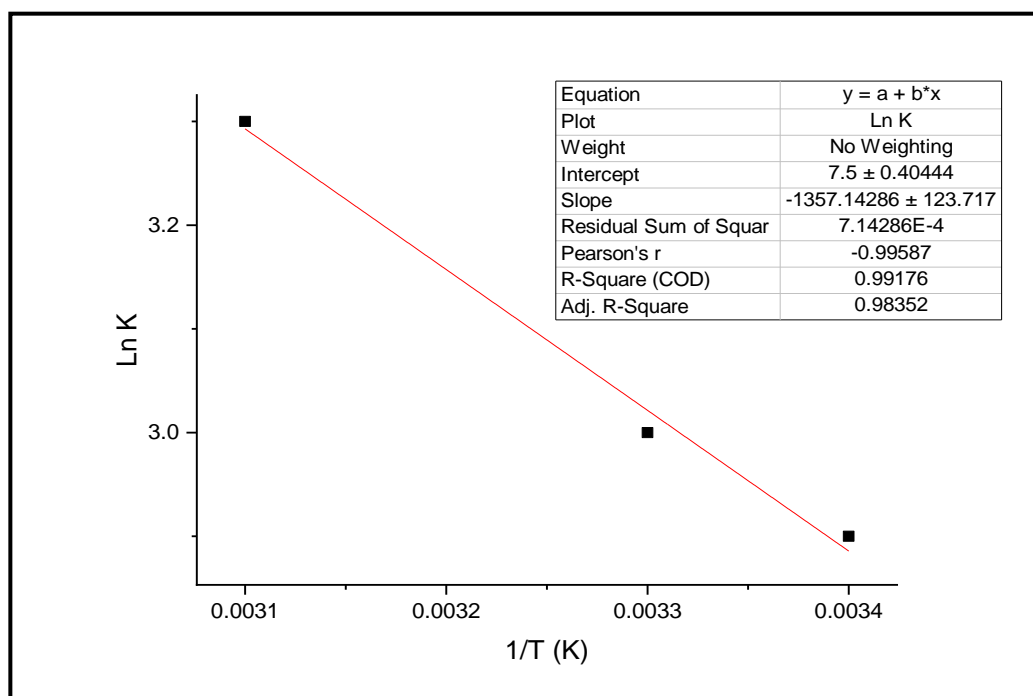


Figure (3-39): Image showing the ideal temperature for P.

### 3.1.4. Finding the Thermodynamic Parameters for P.

By creating a Van't Hoff diagram Figure (3-40), which graphs the values of (ln K) against the inverse of the temperature, and by following the previously mentioned processes, the values of the change in  $\Delta H$ ,  $\Delta S$ , and  $\Delta G$  are presented in Table (3-9).



**Figure (3-4): Van't Hoff equation for P.**

**Table (3-4): The values of ( $\Delta H$ ), ( $\Delta S$ ) and ( $\Delta G$ ) of P.**

$\Delta H$ (J.mol <sup>-1</sup> )	$\Delta S$ (J.K <sup>-1</sup> )	$\Delta G$ (J)
11283.278	62.300	-7298.64

The negative value of the Gibbs free energy indicates that the enzyme reaction is spontaneous. It also has a positive entropy value, making it random. In addition to positive enthalpy value making it endothermic.

**3.11. Characteristics of Meso (9-(dihydroxyboranyl)-12,14-dioxo-9,10-dihydro-13H-9,10-(epiethane[1,1,2]triazolanoethane[1,2,2]triazyl)anthracen-13-yl)acetic acid (P<sub>1</sub>)**

The FTIR spectrum for this product P<sub>1</sub> Figure (3-41) showed the strong a broad peak at 3329 cm<sup>-1</sup> attributed to the two OH of the boric acid that linked at 10-anthracene and the acetyl linked to the pyrrole. The weak peak at 3051 cm<sup>-1</sup> refer to the stretching C-H(SP<sup>3</sup>) for the pyrrole ring. The weak peak at 2958 cm<sup>-1</sup> attributed to C-H (SP<sup>3</sup>) of acetyl. The weak peak at 1734 cm<sup>-1</sup> and the strong peak at 1693 cm<sup>-1</sup> attributed to the stretching active carbonyl amide of pyrrole. weak peak at 1620 cm<sup>-1</sup> belong to the carbonyl of acetyl that linked to the pyrrole ring. The weak peak at 1558 cm<sup>-1</sup> belong to C=C of the anthracene rings. The medium peak at 1250 cm<sup>-1</sup> attributed to the carboxylic (C-O) bond of acetyl that attached pyrrole. While peaks at 1384, 1350 cm<sup>-1</sup> belong to B-O (123-125). All peak appears in FTIR spectrum for all products seen in table (3-12).

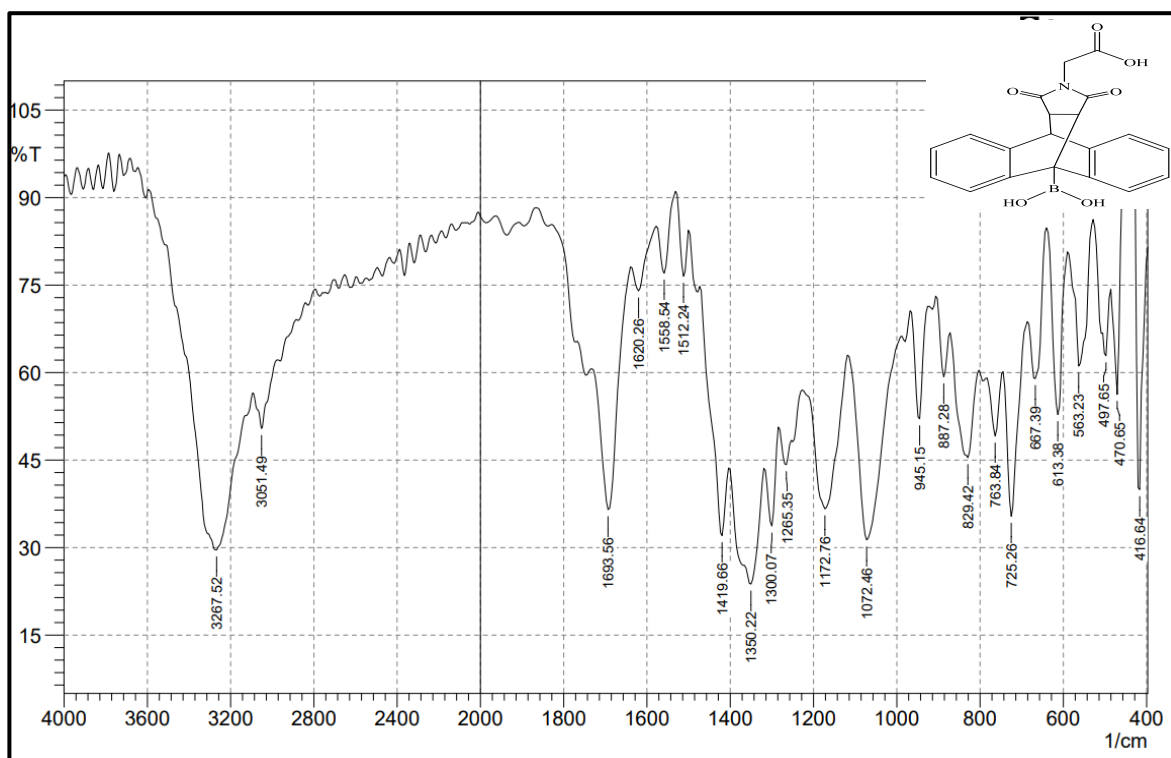


**Figure (3-41): The FTIR spectra for P<sub>1</sub>**

The <sup>1</sup>H NMR spectrum for P<sub>1</sub> in D<sub>2</sub>O (Figure 3-42) displays the singlet peak at δ (1.23) ppm attributed to the CH<sub>3</sub> of acetyl group, which is attached to the N of pyrrole. The protons of the two CH groups attached to the carbonyl of pyrrole showed multiplets at δ (2.47-2.00) ppm and at δ (3.34-2.36) ppm, respectively. The multiplet peak at δ (3.76-3.77) ppm belongs to the CH proton of the 9-H anthracene. The signal of protons of the two (OH) groups of the boronic acid-anthracene appears as a peak at δ (8.81) ppm. The multiplet peaks at δ (7.12-7.16) ppm, δ (7.47-7.02) ppm, and δ (8.04-8.08) ppm belong to the protons of aromatic rings of anthracene. The signal peak at δ (12.97) ppm is attributed to the (OH) of acetyl attached to pyrrole (126, 127). All peaks appear in the <sup>1</sup>H NMR spectrum for all products as shown in table (3-13).

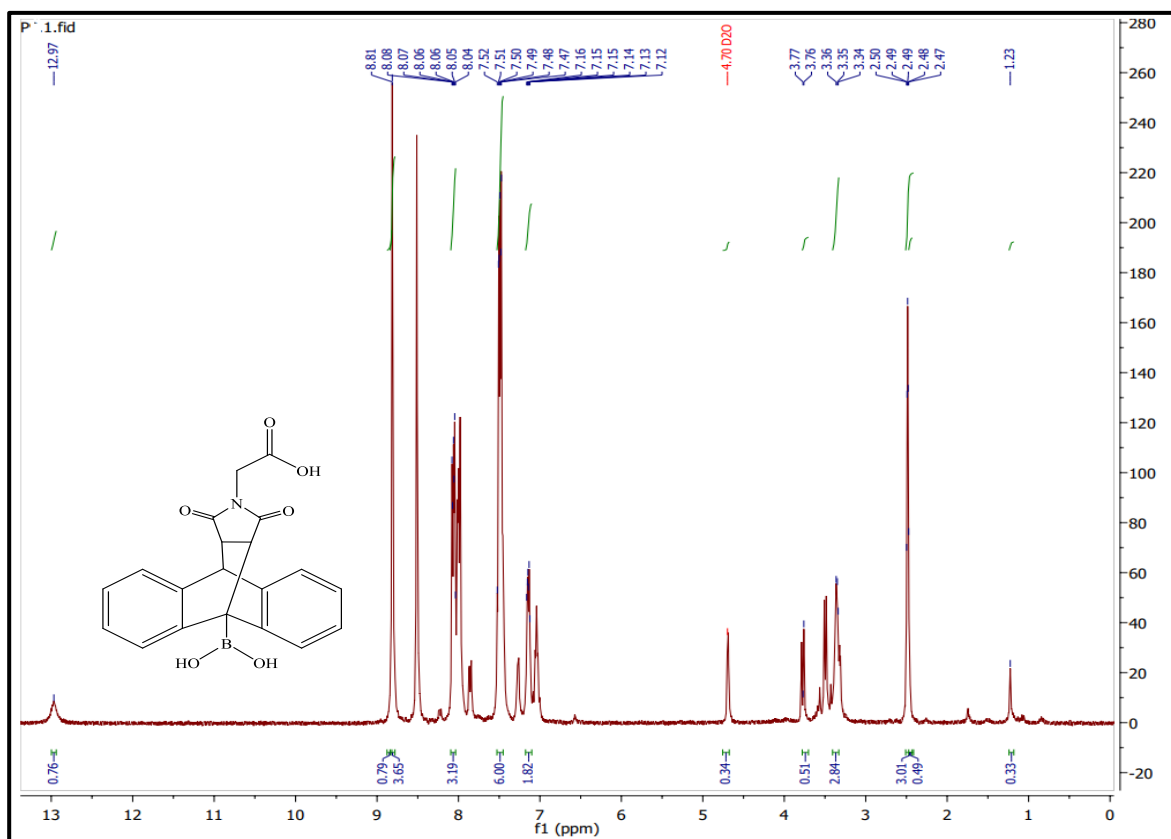


**Figure (3-42): The <sup>1</sup>H NMR spectra for P<sub>7</sub>**

The <sup>13</sup>C NMR spectrum of P<sub>7</sub> in DMSO-d<sub>6</sub> Figure (3-43) showed the peak at δ (39.19) ppm attributed to the CH<sub>3</sub> of acetyl group, which attached with the N of pyrrole. The peak at δ (11.98) ppm belong to the 10'-carbon of anthracene that attached to the boric acid. The peaks at δ (10.80) ppm and δ (17.62) ppm attributed to the two alpha carbons of pyrrole, respectively. The peak at δ (18.11) ppm belong to 9'-carbon of anthracene which closed the cycle with pyrrole. The peaks at δ (124.66) ppm, δ (124.83) ppm, δ (120.47) ppm, δ (120.61) ppm, δ (126.20) ppm, δ (126.39) ppm, δ (126.48) ppm, δ (127.10) ppm, δ (128.90) ppm, δ (131.23) ppm, δ (140.30) ppm, and δ (141.63) ppm attributed to the carbons of the anthracene rings. The peak at



$\delta$  (178.22) ppm belong to the carbon of the carbonyl for the acetyl that attached to the pyrrole. The peaks at  $\delta$  (176.55) ppm and  $\delta$  (177.31) ppm attributed to the carbons of the two carbonyl groups for the pyrrole ring, respectively. All peak appears in  $^{13}\text{C}$ NMR spectrum for all products seen in table (3-14).

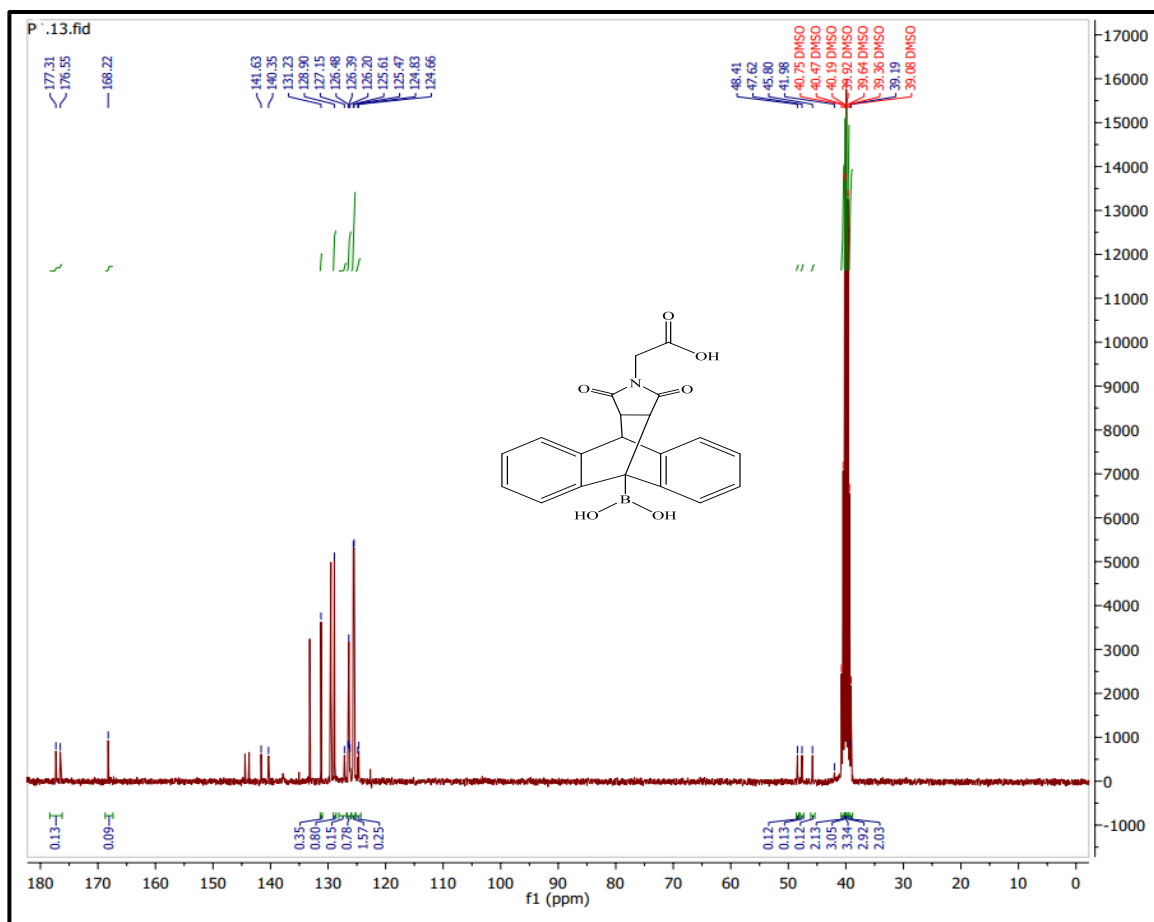


Figure (3-13): The  $^{13}\text{C}$ NMR spectra for P7

The mass spectrum of  $P_1$  appears signal at ( $m/z$ ) relative to the molecular ion, the value close to the calculated molecular weight (377.1 g/mole), as shown in Figure (3-44)

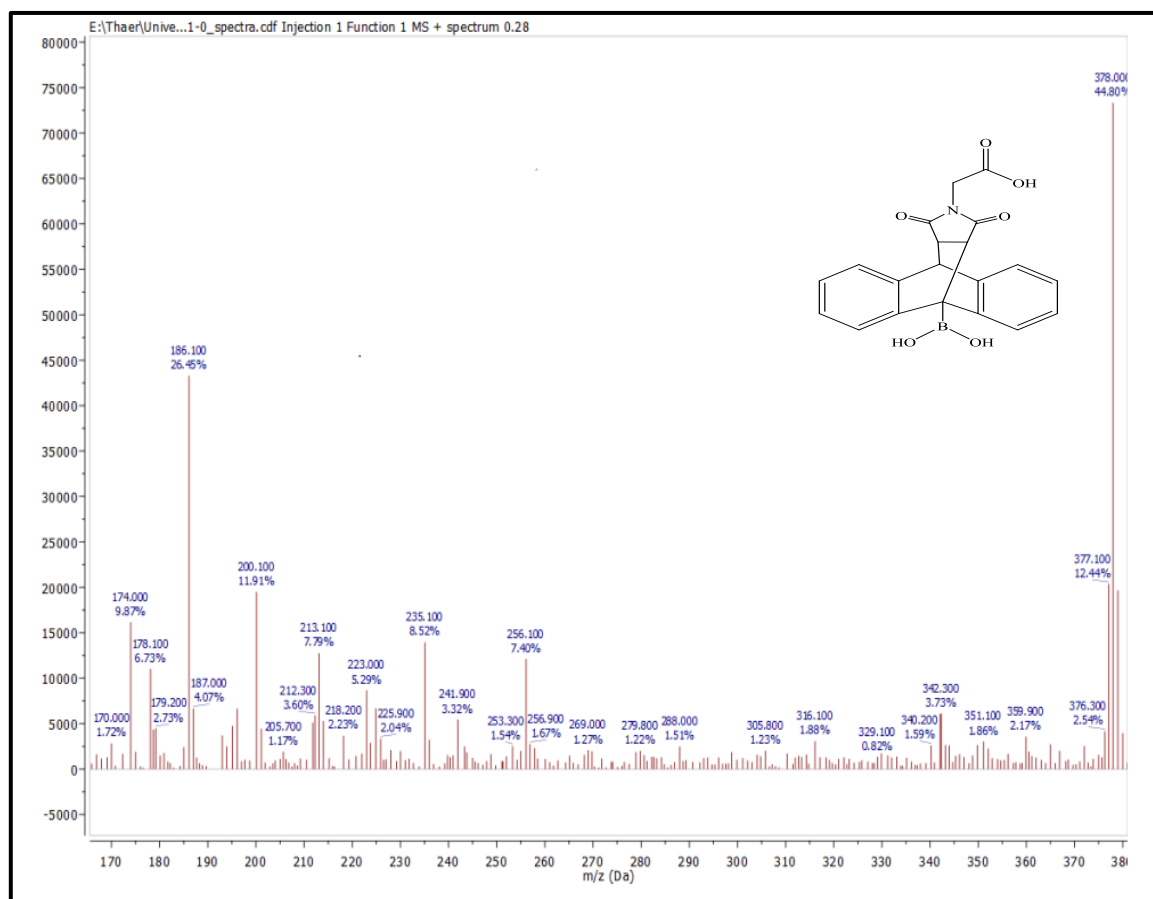
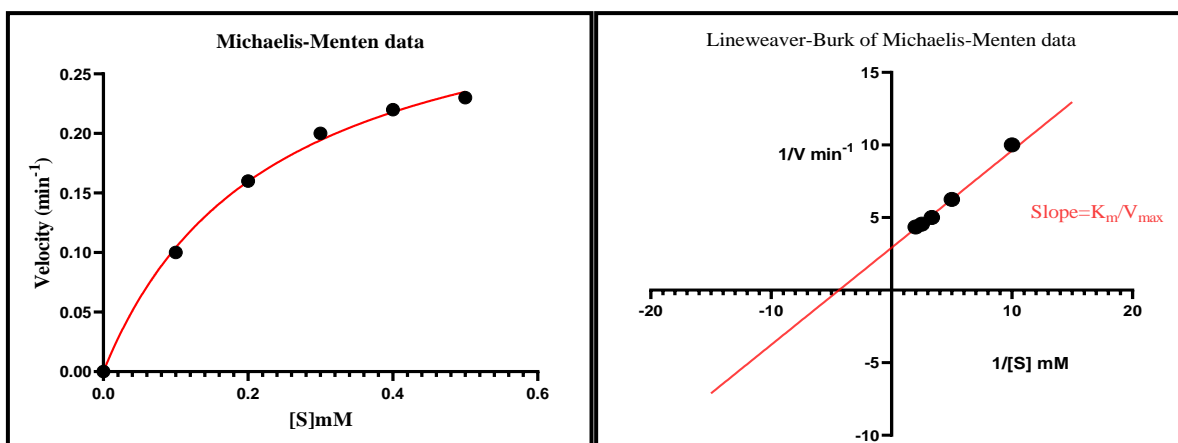


Figure (3-44): The mass spectrum of  $P_1$

**3.12. Kinetic Study of Meso (9-(dihydroxyboranyl)-1,2,3-dioxo-9,10-dihydro-13H-9,10-epiethane[1,1,2]triazanoethane[1,2,2]triazol)anthracen-13-yl)acetic acid (P<sub>1</sub>)**

**3.15.1. Determine the values of the reaction rate constant (Michaelis Menten constant) and the maximum velocity of the enzymatic reaction for P<sub>1</sub>**

The Michaelis-Menten and Line Weaver-Burk equations were applied. The values of the maximum velocity of the enzymatic reaction and the reaction rate constant were as shown in the Figure (3-40), and in Table (3-10).



**Figure (3-40): Michaelis-Menten diagram and line weaver - Burk diagram of the D-A reaction of P<sub>1</sub>.**

**Table (3-10): The Values of  $K_m$  and  $V_{max}$  for the D-A reaction of P<sub>1</sub>.**

kinetic Parameters	Michaels Menten plot	line weaver Burk plot
$V_{max}$ ( $\text{min}^{-1}$ )	0.3427	0.3427
$K_m$	0.2292	0.2292

From the above-mentioned and depending on the value of the Michaelis-Menten constant ( $K_m$ ), the affinity between the substrate (D<sub>1</sub>) and the enzyme (MaDA) in this reaction is the highest value among the other interactions mentioned.

### 3.12.2. Finding of Enzymatic Activity of P<sub>1</sub>

The ideal enzymatic activity was found by drawing the relationship between the enzyme reaction speed and the activity, which produced a bell-like shape Figure (3-16)

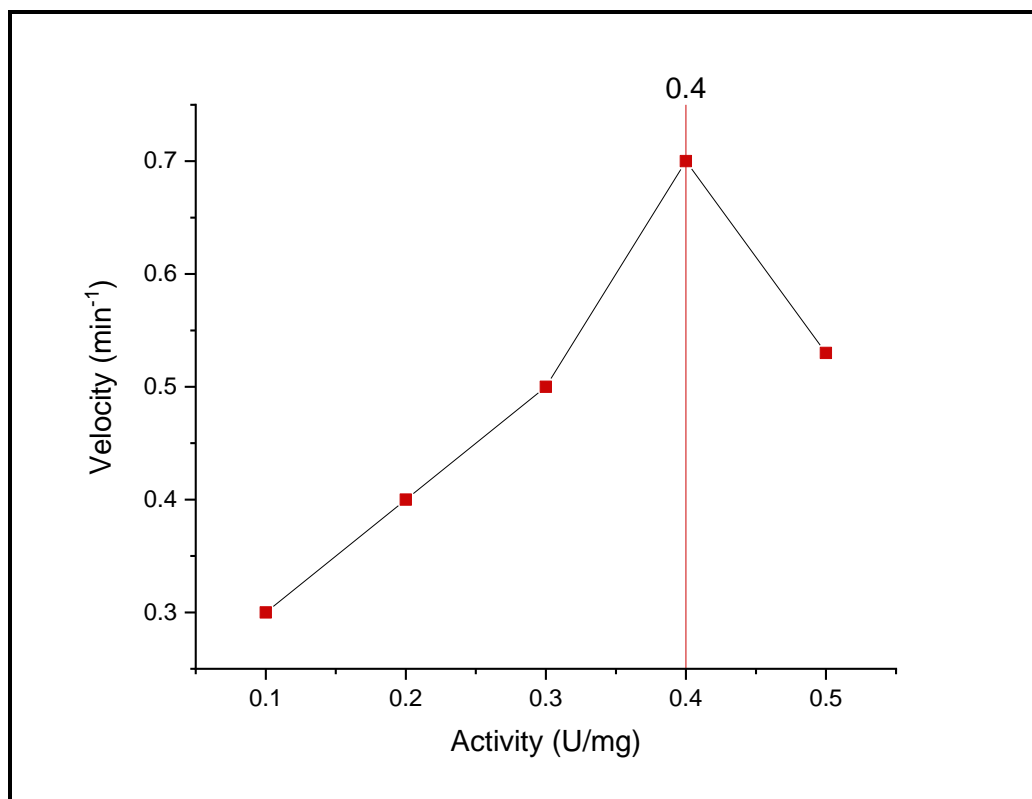


**Figure (3-46): The appropriate enzyme activity of MaDA for P<sub>1</sub>**

From the foregoing, the ideal enzymatic activity for this reaction is (0.4 U/mg).

### 3.12.3. Finding Optimum Temperature for P<sub>1</sub>

The optimum temperature for the D-A reaction of P<sub>1</sub> was determined by plot the velocity of the reaction against the different temperatures (10, 20, 30, 40 C°). The 30 C° is the ideal temperature Figure (3-47)

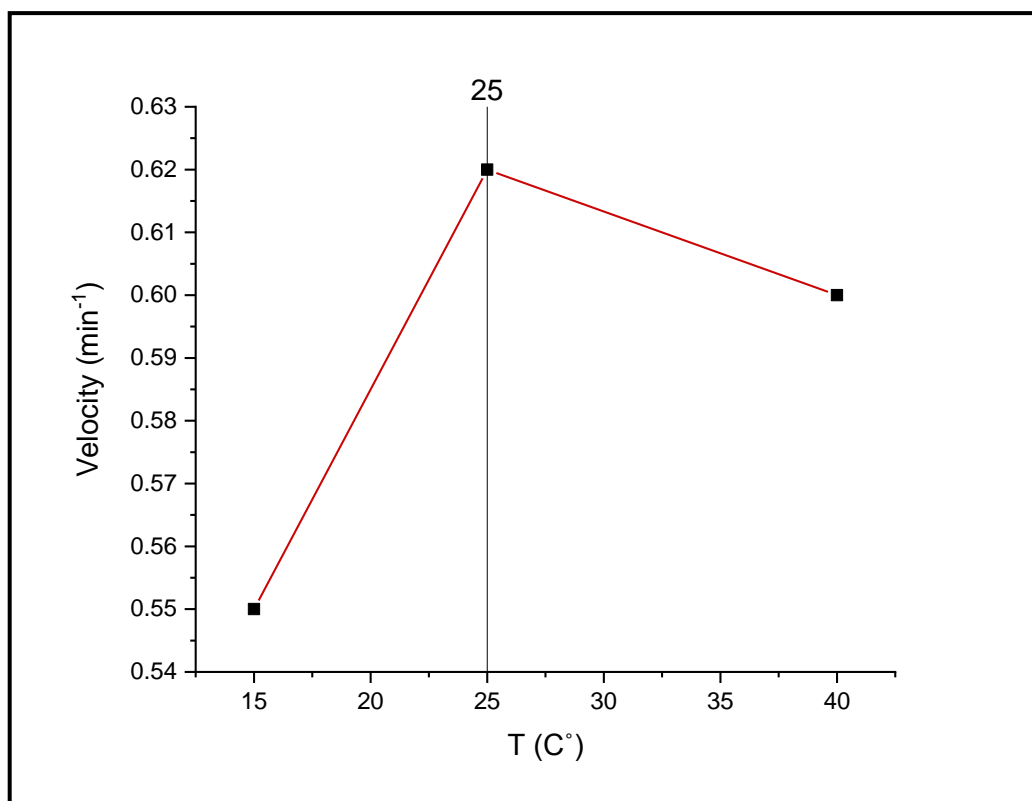


**Figure (3-4):** Image showing the ideal temperature for P<sub>1</sub>

### 3.12.4. Finding the Thermodynamic Parameters for P<sub>1</sub>

By creating a Van't Hoff diagram Figure (3-4), which graphs the values of  $\ln K$  against the inverse of the temperature, and by following the previously mentioned processes, the values of the change in  $\Delta H$ ,  $\Delta S$ , and  $\Delta G$  are presented in Table (3-1).

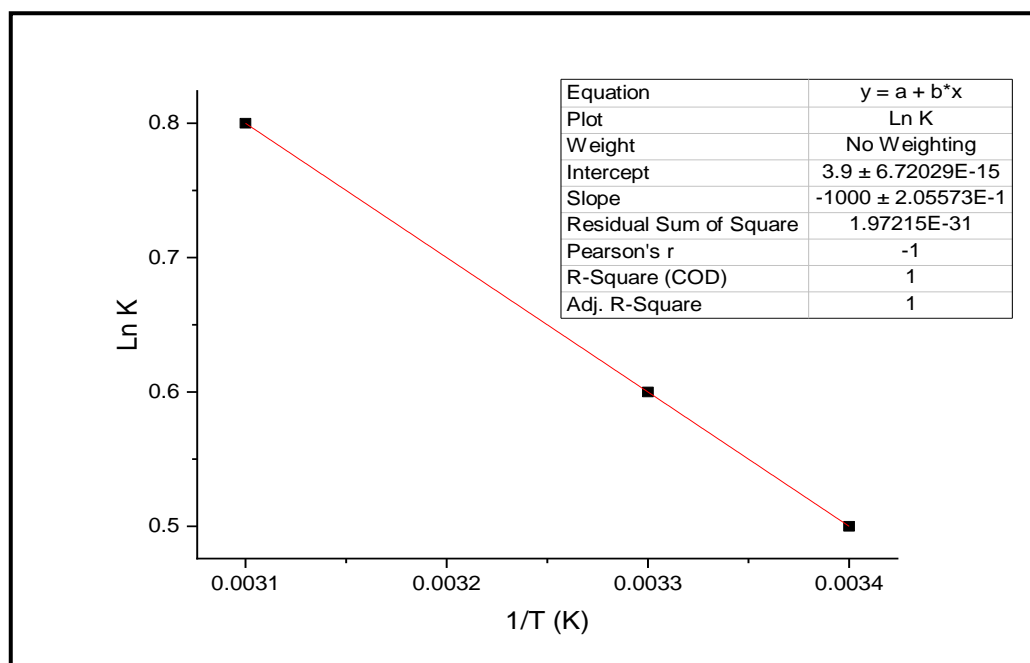


**Figure (3-18): Van't Hoff equation for P<sub>1</sub>**

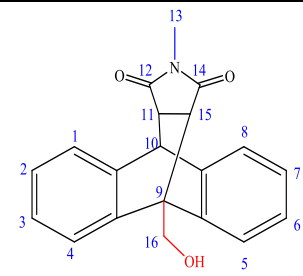
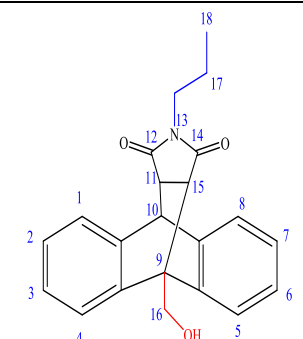
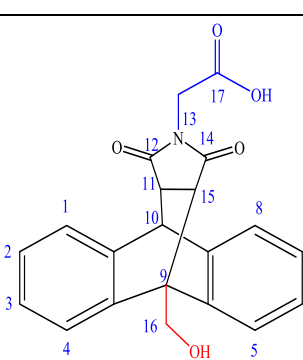
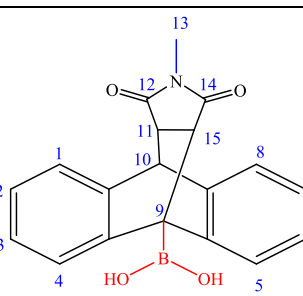
**Table (3-11): The values of ( $\Delta H$ ), ( $\Delta S$ ) and ( $\Delta G$ ) of P<sub>1</sub>.**

$\Delta H$ (J.mol <sup>-1</sup> )	$\Delta S$ (J.K <sup>-1</sup> )	$\Delta G$ (J)
8314	32.424	-1348.03

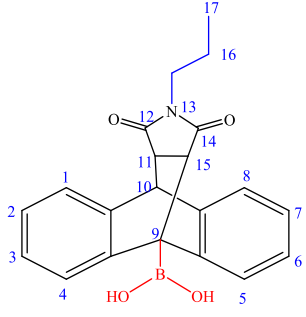
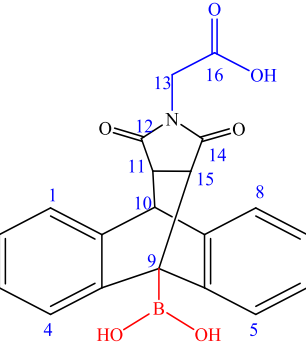
The negative value of the Gibbs free energy indicates that the enzyme reaction is spontaneous. It also has a positive entropy value, making it random. In addition to positive enthalpy value making it endothermic.

All peaks appear in FTIR, <sup>1</sup>H NMR and <sup>13</sup>C NMR spectrum for all products show in table (3-12), (3-13), (3-14) respectively.

**Table (٣-١٢): Show the FT-IR peaks for the products(P<sub>١</sub>-P<sub>٤</sub>)**

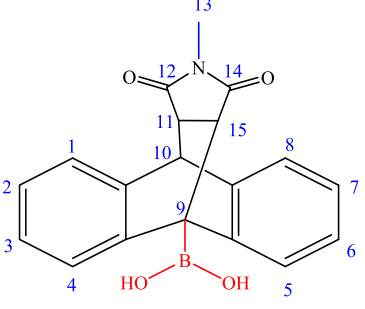
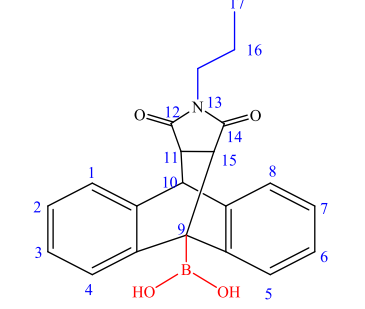
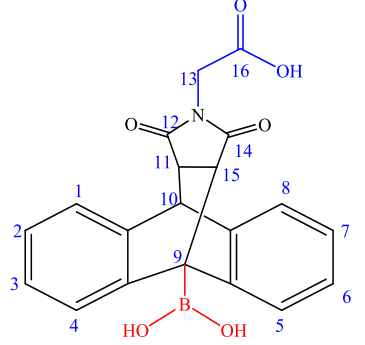
Product	Structure	OH	C-H (SP <sup>٢</sup> )	C-H (SP <sup>٣</sup> )	C=O	C=C	C-O	Other
P <sub>١</sub>		٣٥٠٢ (br,m)	٣٠٦٦ (w)	٢٩٥٨, ٢٨٧٧ (w)	١٧٦٦ (w), ١٦٩٣ (s)	١٤٦٢ (m)	١٢٠٧ (m)	
P <sub>٢</sub>		٣٤٩٥ (m)	٣٠٦٦ (w)	٢٩٤٣, ٢٨٩٧, ٢٨٣٩ (w)	١٧٦٦ (w), ١٦٨٩ (s)	١٥٤٦ (m)	١٢٩٢ (m)	
P <sub>٣</sub>		٣٤١٧ (m)	٣٠٩٣ (w)	٢٩٥١, ٢٩١٢ (w)	١٧٦٦ (w), ١٦٩٧ (s)	١٥١٦ (w)	١٢٣٤ (m)	
P <sub>٤</sub>		٣٣٣٣, ٣٢٧٩ (br,m)	٣٠٧٤ (w)	٢٩٥٥ (w)	١٧٦٦ (w), ١٦٨٥ (s)	١٥٥٠ (m)	-	(B-O) ١٣٨٤, ١٣٤٦ (m)



P <sub>0</sub>		3329 (m)	3.01 (w)	2943, 2878, 2880 (w)	1763 (w), 1681 (s)	1004 (w)	-	(B-O) 1392, 1470 (m)
P <sub>1</sub>		3329 (m)	3.01 (w)	2908 (w)	1734 (w), 1693 (s)	1008 (w)	1200 (m)	(B-O) 1384, 1300 (m)

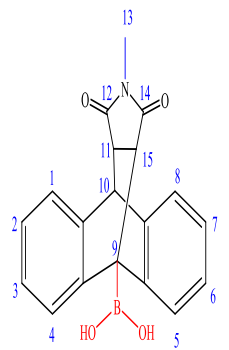
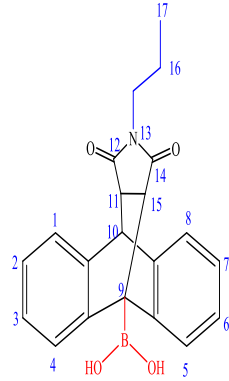
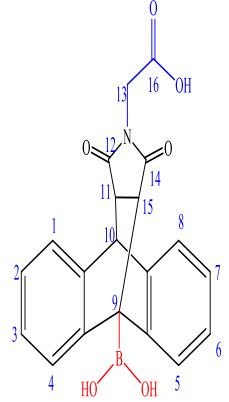
**Table (٣-١٣): Show the  $^1\text{H}$  NMR peaks for the products( $\text{P}_1$ - $\text{P}_3$ )**

product	Structure	CH (١-٨)	CH (١٠)	CH (١١,١٥)	CH (١٣)	CH (١٦)	CH (١٧)	CH (١٨)	other
$\text{P}_1$		٧.٠٩- ٧.٦٥ (m)	٣.٢٥- ٣.٢٩ (m)	٢.٣١- ٢.٥٠ (m)	١.٣٢ (s)	٥.٢٧- ٥.٣٠ (t)	-	-	٤.٦٨ (s) OH
$\text{P}_2$		٧.١١- ٨.٠٩ (m)	٣.٢٥- ٣.٢٩ (m)	٢.٤٧- ٢.٩٣ (m)	١.٢- ١.٢٢ (t)	٥.٣٠- ٥.٣٤ (t)	٠.٦٨- ٠.٧١ (t)	٠.٣٦- ٠.٤١ (m)	٤.٦٨ (s) OH
$\text{P}_3$		٧.١٤- ٨.٥٦ (m)	٣.٢٦- ٣.٤ (m)	٢.٤٨- ٢.٥٠ (m)	١.٢١ (s)	٥.٣٥- ٥.٤٣ (t)	-	-	٤.٧ (s) OH , ٨.٠٧ (s) (OH)

P <sub>ε</sub>		<p>7.00- 8.07 (m)</p>	<p>3.16- 3.34 (m)</p>	<p>2.29- 2.00 (m)</p>	<p>1.22 (s)</p>	<p>0.30- 0.43 (t)</p>	-	-	-
P <sub>σ</sub>		<p>7.12- 8.08 (m)</p>	<p>3.30- 3.62 (m)</p>	<p>1.72- 2.00 (m)</p>	<p>1.21- 1.22 (t)</p>	<p>0.67- 0.72 (t)</p>	<p>0.41- 0.43 (t)</p>	-	<p>8.47, 8.80 (s) B(OH)<sub>2</sub></p>
P <sub>γ</sub>		<p>7.12- 8.08 (m)</p>	<p>3.76- 3.77 (m)</p>	<p>2.47- 2.36 (m)</p>	<p>1.23 (s)</p>	<p>2.47- 2.36 (t)</p>	-	-	<p>8.81 (s) B(OH)<sub>2</sub> 12.97 (s) OH</p>

**Table (3-14): Show the  $^{13}\text{C}$  NMR peaks for the products( $\text{P}_1$ - $\text{P}_3$ )**

Product	Structure	C (1-8)	C (9)	C (10)	CH (11,12) o)	CH (13,14)	CH (15)	CH (16)	CH (17)	CH (18)
$\text{P}_1$		122.8 - 143.1 .	40.34	47.07	48.13 , 49.77	176.38, 177.04	24.3	58.72	-	-
$\text{P}_2$		124.0 7- 143.2 1	40.33	40.8	47.84 , 49.71	176.36, 177.07	39.06	58.7	20.46	11.22
$\text{P}_3$		120.1 4- 143.2 3	39.7	58.74	40.20 , 40.80	176.36, 177.07	39.1	50.75	178.0 4	-

<p><math>P_z</math></p> 	<p>122.8 - 143.1 .</p>	<p>40.84</p>	<p>47.8</p>	<p>48.01</p>	<p>177.42, 178.20</p>	<p>24.24</p>	<p>-</p>	<p>-</p>	<p>-</p>	<p>-</p>
<p><math>P_o</math></p> 	<p>124.0 3- 143.8 ε</p>	<p>40.21</p>	<p>40.48</p>	<p>40.76</p>	<p>177.37, 178.23</p>	<p>39.93</p>	<p>20.4</p>	<p>11.36</p>	<p>-</p>	<p>-</p>
<p><math>P_1</math></p> 	<p>124.6 6- 141.6 3</p>	<p>41.98</p>	<p>48.41</p>	<p>40.80</p>	<p>176.00, 177.31 47.62</p>	<p>39.19</p>	<p>168.2 2</p>	<p>-</p>	<p>-</p>	<p>-</p>

# Conclusions

---

## Conclusions

- 1- The variations in the substituted groups caused a small difference in the final products of these reactions.
- 2- The highest affinity between the substrate diene and the enzyme MaDA was found in  $P_1$  which have the least value of  $K_m$   $0.2292$  among other reactions that mentioned. Which is the most kinetically favored
- 3- The least affinity between substrate diene and the enzyme MaDA found in ( $P_3$ ) which have the highest  $K_m$  value  $0.3027$ .
- 4- In comparison between the products,  $P_1$  is the most thermally preferred
- 5- In comparison between the products,  $P_1$  requires a lower activation energy ( $\Delta E_a$ ).
- 6- The reaction between 9,10-diphenylanthracene with the three Dienophile in presence MaDA didn't give the expecting result due to steric effect by di phenal group

## Recommendations

---

### Recommendations

- 1- Study the effect of activator and inhibitor substances on enzyme activity.
- 2- Study the effect of other substitute groups on both diene and dienophile.
- 3- Study the effect of enzyme activity more than  $1.0$  U/mg.
- 4- Study the effect of concentration of substrate of both diene and dienophile more than  $1.0$  mM.
- 5- Study the mechanism between enzyme and the biosynthesis compound by using molecular Docking.
- 6- Study the biological activity and application of the products.
- 7- Study the effect of using other enzyme with 9,10-diphenylanthracene.

## References

---

### References:

1. Gao L, Yang J, Lei X. Enzymatic intermolecular Diels-Alder reactions in synthesis: From nature to design. *Tetrahedron Chem.* 2022 Jun 1;2:100013.
2. Fluegel LL, Hoye TR. Hexadehydro-Diels–Alder reaction: Benzyne generation via cycloisomerization of tethered triynes. *Chemical reviews.* 2021 Jan 20;121(1):2413–44.
3. Mejía L, Garay-Ruiz D, Franco I. Diels–Alder reaction in a molecular junction. *The Journal of Physical Chemistry C.* 2021 Jun 29;125(27):14099–106.
4. Tortora C, Pisano L, Vergine V, Ghirga F, Iazzetti A, Calcaterra A, Marković V, Botta B, Quaglio D. Synthesis, Biosynthesis, and Biological Activity of Diels–Alder Adducts from *Morus* Genus: An Update. *Molecules.* 2022 Nov 4;27(21):7080.
5. Quadrelli P, Moiola M. Cycloaddition reactions for antiviral compounds. In *Modern Applications of Cycloaddition Chemistry* 2019 Jan 1 (pp. 1–83). Elsevier.
6. Oliveira BL, Guo Z, Bernardes GJ. Inverse electron demand Diels–Alder reactions in chemical biology. *Chemical Society Reviews.* 2017;46(16):4890–900.
7. Opdam LV. Artificial metallo-proteins for photocatalytic water splitting: stability and activity in artificial photosynthesis.
8. Vauthier M, Jerry L, Oliveira JC, Hassouna L, Roucoules V, Bally-



## References

---

- Gall F. Interfacial thermoreversible chemistry on functional coatings: A focus on the Diels–Alder reaction. *Advanced Functional Materials*. 2019 Mar;29(10):1806766.
9. Hernández Mancera JP, Núñez- Zarur F, Gutiérrez- Oliva S, Toro- Labbé A, Vivas- Reyes R. Diels- Alder reaction mechanisms of substituted chiral anthracene: A theoretical study based on the reaction force and reaction electronic flux. *Journal of computational chemistry*. 2020 Sep 0;41(23):2022-32.
10. Oluwasanmi A, Hoskins C. Potential use of the Diels-Alder reaction in biomedical and nanomedicine applications. *International Journal of Pharmaceutics*. 2021 Jul 10;604:120727.
11. Houk KN, Liu F, Yang Z, Seeman JJ. Evolution of the Diels–Alder reaction mechanism since the 1930s: Woodward, Houk with Woodward, and the influence of computational chemistry on understanding cycloadditions. *Angewandte Chemie International Edition*. 2021 Jun 1;60(23):12660-81.
12. Gujral SS, Popli A. Introduction to diels alder reaction, its mechanism and recent advantages: a review. *Indo Am. J. Pharm. Res*. 2013;3(4):1-24.
13. Lossouarn A, Renault K, Bailly L, Frisby A, Le Nahenec-Martel P, Renard PY, Sabot C. Maleimide-based metal-free ligation with dienes: a comparative study. *Organic & Biomolecular Chemistry*. 2020;18(20):3874-87.
14. Bastin LD, Nigam M, Martinus S, Maloney JE, Benyack LL, Gainer B.

## References

---

- Synthesis of substituted N-phenylmaleimides and use in a Diels–Alder reaction: a green multi-step synthesis for an undergraduate organic chemistry laboratory. *Green Chemistry Letters and Reviews*. 2019 Apr 3;12(2):127-30.
10. Tortora C, Pisano L, Vergine V, Ghirga F, Iazzetti A, Calcaterra A, Marković V, Botta B, Quaglio D. Synthesis, Biosynthesis, and Biological Activity of Diels–Alder Adducts from *Morus* Genus: An Update. *Molecules*. 2022 Nov 4;27(21):7080.
11. Ratwani CR, Kamali AR, Abdelkader AM. Self-healing by Diels-Alder cycloaddition in advanced functional polymers: A review. *Progress in Materials Science*. 2023 Jan 1;131:101001.
12. Bruice P. Organic chemistry [Internet]. 2017 [cited 2024 Apr 19]. Available from: <https://thuvienso.hoasen.edu.vn/handle/123456789/13283>
13. Nielsen J, Keasling JD. Engineering cellular metabolism. *Cell*. 2016 Mar 10;164(6):1180-97.
14. Byrne MJ, Lees NR, Han LC, Van Der Kamp MW, Mulholland AJ, Stach JE, Willis CL, Race PR. The catalytic mechanism of a natural Diels–Alderase revealed in molecular detail. *Journal of the American Chemical Society*. 2016 May 18;138(19):6090-8.
15. Khandbahale SV, Pagar KR, Khankari RV. Introduction to Enzymes. *Asian Journal of Research in Pharmaceutical Science*. 2019;9(2):123-30.
16. Gürkök S. Microbial enzymes in detergents: a review. *Int. J. Sci. Eng.*

## References

---

- Res. 2019 Jun 19;10(9):70-81.
22. Klas K, Tsukamoto S, Sherman DH, Williams RM. Natural Diels–Alderses: elusive and irresistible. *The Journal of organic chemistry*. 2010 Dec 4;80(23):11672-80.
23. Palfey B, Switzer RL. *Kinetics of Enzyme Catalysis*. American Chemical Society; 2022 Apr 20.
24. Vesely SL. *The Chemical Reactions Involving Radiation*.
25. Ramesh A, Harani Devi P, Chattopadhyay S, Kavitha M. Commercial applications of microbial enzymes. *Microbial enzymes: roles and applications in industries*. 2020;137-84.
26. Bhardwaj D, Bharadvaja N. Phycoremediation of effluents containing dyes and its prospects for value-added products: A review of opportunities. *Journal of Water Process Engineering*. 2021 Jun 1;41:102080.
27. Bornscheuer UT. Enzymes in lipid modification. *Annual review of food science and technology*. 2018 Mar 20;9(1):80-103.
28. Ferreira P, Fernandes PA, Ramos MJ. Modern computational methods for rational enzyme engineering. *Chem Catalysis*. 2022 Oct 20;2(10):2481-98.
29. Arbige MV, Shetty JK, Chotani GK. Industrial enzymology: the next chapter. *Trends in biotechnology*. 2019 Dec 1;37(12):1300-77.
30. Christopher LP, Kumar H, Zambare VP. Enzymatic biodiesel: Challenges and opportunities. *Applied Energy*. 2014 Apr 10;119:497-

## References

---

- 52.
31. Reddy GM, Avula VK, Kopchuk DS, Kovalev IS, Zyryanov GV, Chupakhin ON, Garcia JR. Intramolecular oxazole-olefin Diels–Alder reactions: A review of the last two decades. *Synthetic Communications*. 2021 Jun 18;51(12):1782–97.
32. Fringuelli F, Taticchi A. The Diels-Alder reaction: selected practical methods. John Wiley & Sons; 2002 Jan 21.
33. Diels O, Alder K. Synthesen in der hydroaromatischen Reihe. *Justus Liebigs Annalen der Chemie*. 1928;470(1):98–122.
34. Brook K, Bennett J, Desai SP. The chemical history of morphine: an 1800-year journey, from resin to de-novo synthesis. *Journal of anesthesia history*. 2017 Apr 1;3(2):50–5.
35. Diels O. On the knowledge of the mechanism of diene synthesis, I. Comm.: On the course of the reaction between malonic esters as well as cyanoacetic esters and acetylenedicarboxylic acid esters in the presence of pyridine acetate. *Reports of the German Chemical Society (A and B Series)*. 1942 Feb 10;70(12):1402–77.
36. Alder K, Günzl W. Über den sterischen Verlauf der Additionen von  $\alpha$ - und  $\beta$ -methyl- bzw.- phenyl- substituierten Acrylsäuren an Cyclopentadien. Ein Beitrag zur Stereochemie der Dien- Synthese. *Chemische Berichte*. 1960 Apr;93(4):809–20.
37. Alder K, Stein G. Über den sterischen Verlauf von Additions- und Substitutions- reaktionen. I. Zur Stereochemie der Dien- synthese.

## References

---

- Gemeinsam mit Dr. Frhr. v. Buddenbrock, Dr. W. Eckardt, Dr. W. Frercks und Dr. St. Schneider. Justus Liebigs Annalen der Chemie. 1934; 514(1): 1-33.
38. Woodward RB, Hoffmann R. The conservation of orbital symmetry. *Angewandte Chemie International Edition in English*. 1969 Nov; 8(11): 781-803.
39. Mali G, Chauhan AN, Chavan KA, Erande RD. Development and applications of double Diels- Alder reaction in organic synthesis. *Asian Journal of Organic Chemistry*. 2021 Nov; 10(11): 2848-68.
40. Yates P, Eaton P. Acceleration of the Diels-Alder reaction by aluminum chloride. *Journal of the American Chemical Society*. 1960 Aug; 82(16): 4436-7.
41. Domingo LR, Ríos-Gutiérrez M, Pérez P. Unveiling the Lewis acid catalyzed Diels–Alder reactions through the molecular electron density theory. *Molecules*. 2020 May 29; 20(11): 2030.
42. Vermeeren P, Hamlin TA, Fernández I, Bickelhaupt FM. How Lewis Acids Catalyze Diels–Alder Reactions. *Angewandte Chemie*. 2020 Apr 7; 132(10): 6260-0.
43. Hilt G. 1, 4-Cyclohexadienes—Easy Access to a Versatile Building Block via Transition- Metal- Catalysed Diels–Alder Reactions. *The Chemical Record*. 2014 Jun; 14(3): 386-96.
44. Nicolaou KC, Snyder SA, Montagnon T, Vassilikogiannakis G. The Diels–Alder reaction in total synthesis. *Angewandte Chemie*

## References

---

- International Edition. 2002 May 17;41(10):1668-98.
45. Minami A, Oikawa H. Recent advances of Diels–Alderases involved in natural product biosynthesis. *The Journal of Antibiotics*. 2016 Jul;69(7):500-6.
46. Fleming I. *Frontier orbitals and organic chemical reactions*. (No Title). 1976.
47. Cole CJ, Fuentes L, Snyder SA. Asymmetric pyrone Diels–Alder reactions enabled by dienamine catalysis. *Chemical science*. 2020;11(8):2170-80.
48. Dorm BC, Junior JA, da Silva LH, Forato LA, de Souza Nossa T, Carvalho AJ, Resende FA, Gandini A, Trovatti E. Synthesis of a cysteine Diels–Alder-based polymer by simultaneous double-click chemistry and its cyto-genotoxicity evaluation. *Macromolecular Research*. 2024 Feb;32(2):133-44.
49. Suehiro F, Fujii S, Nishimura T. Bioorthogonal micellar nanoreactors for prodrug cancer therapy using an inverse-electron-demand Diels–Alder reaction. *Chemical Communications*. 2022;58(50):7026-9.
50. Yadav B, Ravikanth M. Anthriporphyrinoids: Design, Synthesis, and Reactivity towards Diels–Alder Reaction. *The Journal of Organic Chemistry*. 2023 Jun 20;88(13):9343-51.
51. Gregoritz M, Brandl FP. The Diels–Alder reaction: a powerful tool for the design of drug delivery systems and biomaterials. *European journal of pharmaceutics and biopharmaceutics*. 2010 Nov 1;97:438-53.

## References

---

02. Jessen BM, Taarning E, Madsen R. Synthesis, Stability, and Diels-Alder Reactions of Methyl  $\alpha$ - Oxobut-  $\beta$ - enoate. *European Journal of Organic Chemistry*. 2021 Aug 6;2021(29):4049-53.
03. Wu Q, Hu QN, Li MQ, Zhang ZW, Zhu WH. Theoretical design of new bridge-ring insensitive high energy compounds by selected normal Diels-Alder reactions between NH $\alpha$ -substituted oxazoles and NO $\alpha$ /NF $\alpha$ /NHNO $\alpha$ -substituted ethylenes/acetylenes. *Defence Technology*. 2021 Oct 1;17(5):1731-9.
04. Grimblat N, Sarotti AM. Looking at the big picture in activation strain model/energy decomposition analysis: the case of the ortho–para regioselectivity rule in Diels–Alder reactions. *Organic & Biomolecular Chemistry*. 2020;18(6):1104-11.
05. Oliveira BL, Guo Z, Bernardes GJ. Inverse electron demand Diels–Alder reactions in chemical biology. *Chemical Society Reviews*. 2017;46(16):4890-900.
06. Pagel M. Inverse electron demand Diels–Alder (IEDDA) reactions in peptide chemistry. *Journal of Peptide Science*. 2019 Jan;20(1):e3141.
07. Braun K, Wiessler M, Ehemann V, Pipkorn R, Spring H, Debus J, Didinger B, Koch M, Muller G, Waldeck W. Treatment of glioblastoma multiforme cells with temozolomide-BioShuttle ligated by the inverse Diels-Alder ligation chemistry. *Drug Design, Development and Therapy*. 2009 Feb 6;289-301.
08. Blackman ML, Royzen M, Fox JM. Tetrazine ligation: fast bioconjugation based on inverse-electron-demand Diels–Alder

## References

---

- reactivity. *Journal of the American Chemical Society*. 2008 Oct 15;130(41):13518-9.
59. Kozma E, Demeter O, Kele P. Bio-orthogonal Fluorescent Labelling of Biopolymers through Inverse-Electron-Demand Diels–Alder Reactions. *ChemBioChem*. 2017 Mar 16;18(6):486-501.
60. Wu H, Devaraj NK. Inverse electron-demand Diels–Alder bioorthogonal reactions. *Cycloadditions in Bioorthogonal Chemistry*. 2016;109-30.
61. Jiang X, Wang R. Recent developments in catalytic asymmetric inverse-electron-demand Diels–Alder reaction. *Chemical Reviews*. 2013 Jul 10;113(7):5010-46.
62. Benallou A, El Abdallaoui HE, Garmes H. C—C bond formation in the intramolecular Diels-Alder reaction of triene amides. *Heliyon*. 2018 Feb 1;4(2).
63. Bear BR, Sparks SM, Shea KJ. The type 2 intramolecular diels–alder reaction: synthesis and chemistry of bridgehead alkenes. *Angewandte Chemie International Edition*. 2001 Mar 2;40(5):820-49.
64. Hammoudan I, Chtita S, Riffi-Temsamani D. QTAIM and IRC studies for the evaluation of activation energy on the C= P, C= N and C= O Diels-Alder reaction. *Heliyon*. 2020 Aug 1;6(8).
65. Eschenbrenner-Lux V, Kumar K, Waldmann H. The Asymmetric Hetero-Diels-Alder Reaction in the Syntheses of Biologically Relevant Compounds. *Angew Chemie - Int Ed*. 2014 Oct 1;53(42):11146-57.



## References

---

66. Cao MH, Green NJ, Xu SZ. Application of the aza-Diels–Alder reaction in the synthesis of natural products. *Organic & Biomolecular Chemistry*. 2017;15(10):3100–29.
67. Hammoudan I, Chtita S, Riffi-Temsamani D. QTAIM and IRC studies for the evaluation of activation energy on the C= P, C= N and C= O Diels-Alder reaction. *Heliyon*. 2020 Aug 1;6(8).
68. Zagidullin A, Bezkishko I, Miluykov V. Review on asymmetric cycloaddition reactions at phosphorus (III) atom. *Arkivoc*. 2023 Jan 1(part iv):1-.
69. Winkler JD. Tandem Diels–Alder cycloadditions in organic synthesis. *Chemical reviews*. 1996 Feb 1;96(1):167–76.
70. Sears JE, Boger DL. Tandem intramolecular Diels–Alder/1, 3-dipolar cycloaddition cascade of 1, 3, 4-oxadiazoles: initial scope and applications. *Accounts of chemical research*. 2016 Feb 16;49(2):241–51.
71. Baiazitov RY, Denmark SE. *Methods and Applications of Cycloaddition Reactions in Organic Synthesis*.
72. Grossmann A, Enders D. N- heterocyclic carbene catalyzed domino reactions. *Angewandte Chemie International Edition*. 2012 Jan 9;51(2):314–20.
73. Oluwasanmi A, Lindsay S, Curtis A, Perrie Y, Hoskins C. Chain length impact on the retro Diels-Alder mediated release of gemcitabine from hybrid nanoparticles towards pancreatic cancer therapy. *International journal of pharmaceutics*. 2023 Sep 20;644:123304.

## References

---

٧٤. Cardoso-Gutierrez MA, Bo GD, Duwez AS, Remacle F. Steering the Mechanism of the Furan-Maleimide Retro-Diels-Alder Reaction to a Sequential Pathway with an External Mechanical Force.
٧٥. Kotha S, Banerjee S. Recent developments in the retro-Diels–Alder reaction. *Rsc Advances*. ٢٠١٣;٣(٢١):٧٦٤٢-٦٦.
٧٦. Dapsens PY, Mondelli C, Pérez-Ramírez J. Design of Lewis-acid centres in zeolitic matrices for the conversion of renewables. *Chemical Society Reviews*. ٢٠١٥;٤٤(٢٠):٧٠٢٥-٤٣.
٧٧. Vermeeren P, Hamlin TA, Fernández I, Bickelhaupt FM. How Lewis Acids Catalyze Diels–Alder Reactions. *Angewandte Chemie*. ٢٠٢٠ Apr ٦;١٣٢(١٥):٦٢٦٠-٥.
٧٨. Harada S, Nishida A. Catalytic and Enantioselective Diels- Alder Reaction of Siloxydienes. *Asian Journal of Organic Chemistry*. ٢٠١٩ Jun;٨(٦):٧٣٢-٤٥.
٧٩. Settle AE, Berstis L, Rorrer NA, Roman-Leshkóv Y, Beckham GT, Richards RM, Vardon DR. Heterogeneous Diels–Alder catalysis for biomass-derived aromatic compounds. *Green Chemistry*. ٢٠١٧;١٩(١٥):٣٤٦٨-٩٢.
٨٠. Gong W, Liu Y, Li H, Cui Y. Metal-organic frameworks as solid Brønsted acid catalysts for advanced organic transformations. *Coordination Chemistry Reviews*. ٢٠٢٠ Oct ١;٤٢٠:٢١٣٤٠٠.
٨١. Liu X, Zheng H, Xia Y, Lin L, Feng X. Asymmetric cycloaddition and cyclization reactions catalyzed by chiral N, N'-dioxide–metal

## References

---

- complexes. *Accounts of chemical research*. 2017 Oct 17;50(10):2621-31.
82. Kollmann J, Zhang Y, Schilling W, Zhang T, Riemer D, Das S. A simple ketone as an efficient metal-free catalyst for visible-light-mediated Diels–Alder and aza-Diels–Alder reactions. *Green Chemistry*. 2019;21(8):1916-20.
83. Jarrige L, Blanchard F, Masson G. Enantioselective Organocatalytic Intramolecular Aza- Diels–Alder Reaction. *Angewandte Chemie International Edition*. 2017 Aug 21;56(35):10573-6.
84. Zhang S, Zhang J, Zhu Y. ProdaMatch: a fast and accurate active site matching algorithm for de novo enzyme design. *Computers & Chemical Engineering*. 2020 Sep 2;140:106921.
85. Xu Y, Yamamoto N, Janda KD. Catalytic antibodies: hapten design strategies and screening methods. *Bioorganic & medicinal chemistry*. 2004 Oct 10;12(20):5247-68.
86. Zanghellini A. De novo computational enzyme design. *Current opinion in biotechnology*. 2014 Oct 1;29:132-8.
87. Pantazes RJ, Grisewood MJ, Maranas CD. Recent advances in computational protein design. *Current opinion in structural biology*. 2011 Aug 1;21(4):467-72.
88. Vaissier Welborn V, Head-Gordon T. Computational design of synthetic enzymes. *Chemical reviews*. 2018 Oct 2;119(11):7613-30.
89. Huang PS, Boyken SE, Baker D. The coming of age of de novo protein design. *Nature*. 2016 Sep 10;537(7620):320-7.

## References

---

90. Lassila JK, Privett HK, Allen BD, Mayo SL. Combinatorial methods for small-molecule placement in computational enzyme design. *Proceedings of the National Academy of Sciences*. 2006 Nov 7;103(45):16710-5.
91. Fazelinia H, Cirino PC, Maranas CD. OptGraft: A computational procedure for transferring a binding site onto an existing protein scaffold. *Protein Science*. 2009 Jan;18(1):180-90.
92. Zhang C, Lai L. AutoMatch: target- binding protein design and enzyme design by automatic pinpointing potential active sites in available protein scaffolds. *Proteins: Structure, Function, and Bioinformatics*. 2012 Apr;80(4):1078-94.
93. Kuhlman B. Designing protein structures and complexes with the molecular modeling program Rosetta. *Journal of Biological Chemistry*. 2019 Dec 13;294(50):19437-43.
94. Matsuo T, Miyake T, Hirota S. Recent developments on creation of artificial metalloenzymes. *Tetrahedron Letters*. 2019 Nov 7;60(45):101226.
95. Hyster TK, Ward TR. Genetic optimization of metalloenzymes: enhancing enzymes for non- natural reactions. *Angewandte Chemie International Edition*. 2016 Jun 20;55(26):7344-57.
96. Schwizer F, Okamoto Y, Heinisch T, Gu Y, Pellizzoni MM, Lebrun V, Reuter R, Kohler V, Lewis JC, Ward TR. Artificial metalloenzymes: reaction scope and optimization strategies. *Chemical reviews*. 2018 Jan 10;118(1):142-231.

## References

---

97. Oohora K, Onoda A, Hayashi T. Hemoproteins reconstituted with artificial metal complexes as biohybrid catalysts. *Accounts of Chemical Research*. 2019 Apr 1;52(4):940-49.
98. Roelfes G. LmrR: a privileged scaffold for artificial metalloenzymes. *Accounts of chemical research*. 2019 Feb 22;52(3):540-47.
99. Liang AD, Serrano-Plana J, Peterson RL, Ward TR. Artificial metalloenzymes based on the biotin–streptavidin technology: enzymatic cascades and directed evolution. *Accounts of chemical research*. 2019 Feb 8;52(3):580-89.
100. Schwizer F, Okamoto Y, Heinisch T, Gu Y, Pellizzoni MM, Lebrun V, Reuter R, Kohler V, Lewis JC, Ward TR. Artificial metalloenzymes: reaction scope and optimization strategies. *Chemical reviews*. 2018 Jan 10;118(1):142-231.
101. Chen K, Arnold FH. Engineering new catalytic activities in enzymes. *Nature Catalysis*. 2020 Mar;3(3):203-13.
102. Jeschek M, Reuter R, Heinisch T, Trindler C, Klehr J, Panke S, Ward TR. Directed evolution of artificial metalloenzymes for in vivo metathesis. *Nature*. 2016 Sep 29;537(7622):661-5.
103. Reetz MT. Directed evolution of artificial metalloenzymes: a universal means to tune the selectivity of transition metal catalysts?. *Accounts of chemical research*. 2019 Jan 28;52(2):336-44.
104. Ding Q, Guo N, Gao L, McKee M, Wu D, Yang J, Fan J, Weng JK, Lei X. The evolutionary origin of naturally occurring intermolecular Diels-

## References

---

- Alderase from *Morus alba*. *Nature Communications*. 2023 Mar 20;10(1):2492.
100. Kim HJ, Rusczycky MW, Choi SH, Liu YN, Liu HW. Enzyme-catalysed [ $\epsilon$ + $\gamma$ ] cycloaddition is a key step in the biosynthesis of spinosyn A. *Nature*. 2011 May 05;473(7340):109-12.
106. Tian Z, Sun P, Yan Y, Wu Z, Zheng Q, Zhou S, Zhang H, Yu F, Jia X, Chen D, Mándi A. An enzymatic [ $\epsilon$ + $\gamma$ ] cyclization cascade creates the pentacyclic core of pyrroindomycins. *Nature chemical biology*. 2010 Apr;11(4):209-10.
107. Liu SH, Sun JL, Hu YL, Zhang L, Zhang X, Yan ZY, Guo X, Guo ZK, Jiao RH, Zhang B, Tan RX. Biosynthesis of sordarin revealing a Diels–Alderase for the formation of the norbornene skeleton. *Angewandte Chemie*. 2022 Aug 10;134(33):e202200577.
108. Chen Q, Gao J, Jamieson C, Liu J, Ohashi M, Bai J, Yan D, Liu B, Che Y, Wang Y, Houk KN. Enzymatic intermolecular hetero-Diels–Alder reaction in the biosynthesis of tropolonic sesquiterpenes. *Journal of the American Chemical Society*. 2019 Aug 28;141(36):14052-6.
109. Ohashi M, Liu F, Hai Y, Chen M, Tang MC, Yang Z, Sato M, Watanabe K, Houk KN, Tang Y. SAM-dependent enzyme-catalysed pericyclic reactions in natural product biosynthesis. *Nature*. 2017 Sep 28;549(7673):502-6.
110. Patel A, Chen Z, Yang Z, Gutiérrez O, Liu HW, Houk KN, Singleton

## References

---

- DA. Dynamically complex  $[\gamma + \epsilon]$  and  $[\epsilon + \gamma]$  cycloadditions in the biosynthesis of spinosyn A. *Journal of the American Chemical Society*. 2016 Mar 23;138(11):3631-4.
111. Jeon BS, Ruzsyczky MW, Russell WK, Lin GM, Kim N, Choi SH, Wang SA, Liu YN, Patrick JW, Russell DH, Liu HW. Investigation of the mechanism of the SpnF-catalyzed  $[\epsilon + \gamma]$ -cycloaddition reaction in the biosynthesis of spinosyn A. *Proceedings of the National Academy of Sciences*. 2017 Sep 26;114(39):10408-13.
112. Lichman BR, O'Connor SE, Kries H. Biocatalytic strategies towards  $[\epsilon + \gamma]$  cycloadditions. *Chemistry—A European Journal*. 2019 May 17;25(28):6864-77.
113. Nomura T, Hano Y. Chemistry, biosynthesis, and biological activity of natural Diels-Alder type adducts from moraceous plants. *Plant Polyphenols 2: Chemistry, Biology, Pharmacology, Ecology*. 1999 Jan 1:279-97.
114. Su C, Tao X, Yin Z, Zhang X, Tian J, Chen R, Liu J, Li L, Ye F, Zhang PC, Zhang D. Morusalones A–D, Diels–Alder Adducts with  $\gamma/\gamma/\gamma/\gamma/\gamma/\gamma$  Hexacyclic Ring Systems as Potential PTP<sup>1</sup>B Inhibitors from Cell Cultures of *Morus alba*. *Organic letters*. 2019 Nov 20;21(23):9463-7.
115. Wang M, Gao LX, Wang J, Li JY, Yu MH, Li J, Hou AJ. Diels–Alder adducts with PTP<sup>1</sup>B inhibition from *Morus notabilis*. *Phytochemistry*. 2015 Jan 1;109:140-6.
116. Yang Y, Tan YX, Chen RY, Kang J. The latest review on the polyphenols and their bioactivities of Chinese *Morus* plants. *Journal of*

## References

---

- Asian Natural Products Research. 2014 Jun 3;16(6):690-702.
117. Wu YX, Kim YJ, Kwon TH, Tan CP, Son KH, Kim T. Anti-inflammatory effects of mulberry (*Morus alba* L.) root bark and its active compounds. *Natural product research*. 2020 Jun 17;34(12):1787-90.
118. Daniel B, Konrad B, Toplak M, Lahham M, Messenlehner J, Winkler A, Macheroux P. The family of berberine bridge enzyme-like enzymes: A treasure-trove of oxidative reactions. *Archives of Biochemistry and Biophysics*. 2017 Oct 10;632:88-103.
119. Gao L, Su C, Du X, Wang R, Chen S, Zhou Y, Liu C, Liu X, Tian R, Zhang L, Xie K. FAD-dependent enzyme-catalysed intermolecular [ $\epsilon$ + $\gamma$ ] cycloaddition in natural product biosynthesis. *Nature Chemistry*. 2020 Jul;12(7):620-8.
120. Gao L, Zou Y, Liu X, Yang J, Du X, Wang J, Yu X, Fan J, Jiang M, Li Y, Houk KN. Enzymatic control of endo-and exo-stereoselective Diels–Alder reactions with broad substrate scope. *Nature Catalysis*. 2021 Dec;4(12):1059-69.
121. Tortora C, Pisano L, Vergine V, Ghirga F, Iazzetti A, Calcaterra A, Marković V, Botta B, Quaglio D. Synthesis, Biosynthesis, and Biological Activity of Diels–Alder Adducts from *Morus* Genus: An Update. *Molecules*. 2022 Nov 4;27(21):7080.
122. Liu X, Yang J, Gao L, Zhang L, Lei X. Chemoenzymatic total syntheses of artonin I with an intermolecular Diels–Alderase. *Biotechnology Journal*. 2020 Nov;10(11):2000119.



## References

---

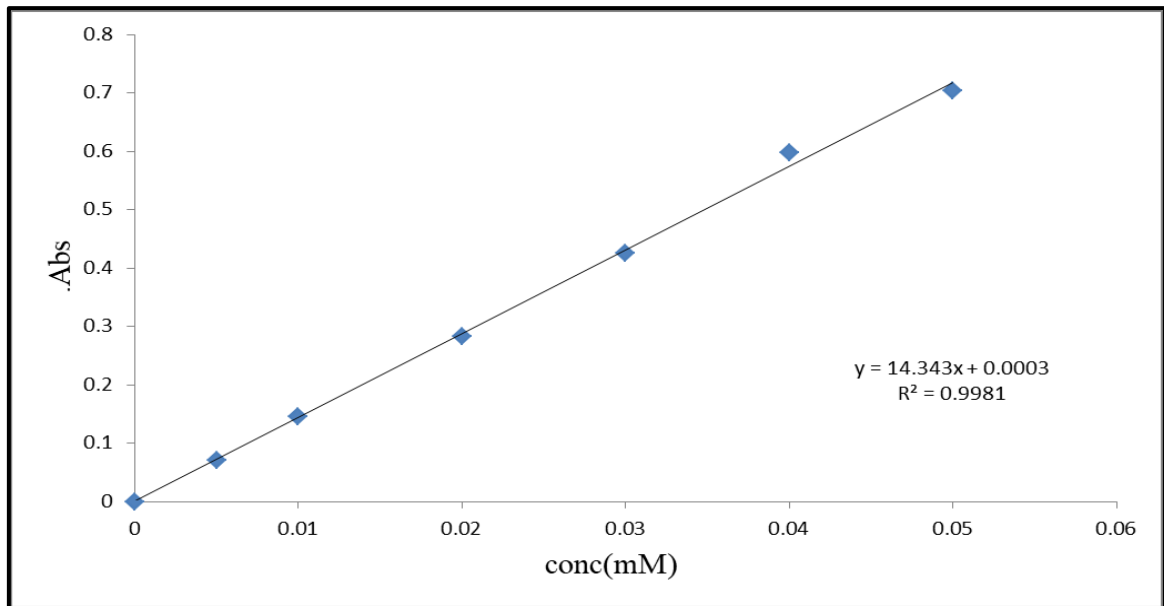
123. Liu X, Du P, Liu L, Zheng Z, Wang X, Joncheray T, Zhang Y. Kinetic study of Diels–Alder reaction involving in maleimide–furan compounds and linear polyurethane. *Polymer Bulletin*. 2013 Aug;70:2319–30.
124. Kriegel RM, Saliba KL, Jones G, Schiraldi DA, Collard DM. The rapid chain extension of anthracene- functional polyesters by the Diels- Alder reaction with bismaleimides. *Macromolecular Chemistry and Physics*. 2000 Aug 0;206(10):1479–87.
125. Girish YR, Pandit S, Pandit S, De M. AN ASIAN JOURNAL.
126. Caliskan E, Shishatskiy S, Neumann S, Abetz V, Filiz V. Investigation of the side chain effect on gas and water vapor transport properties of anthracene-maleimide based polymers of intrinsic microporosity. *Polymers*. 2021 Dec 29;14(1):119.
127. Mondal P, Jana G, Behera PK, Chattaraj PK, Singha NK. A new healable polymer material based on ultrafast Diels–Alder ‘click’chemistry using triazolinedione and fluorescent anthracyl derivatives: a mechanistic approach. *Polymer Chemistry*. 2019;10(37):5070–9.

*Appendixes*

# *Appendixes*

**Appendixes:**

## Appendixes



**Appendix (1): calibration curve of P<sub>1</sub>**

**Appendix (2): represents the values used to draw the Michaelis-Menten and Line Weaver-Burk equations for P<sub>1</sub>**

[S] mM	K=V (min <sup>-1</sup> )	1/[S] mM <sup>-1</sup>	1/V min
0	0	0	0
0.1	0.07	10	14.285
0.2	0.13	5	7.692
0.3	0.15	3.333	6.666
0.4	0.17	2.5	5.882
0.5	0.18	2	5.555

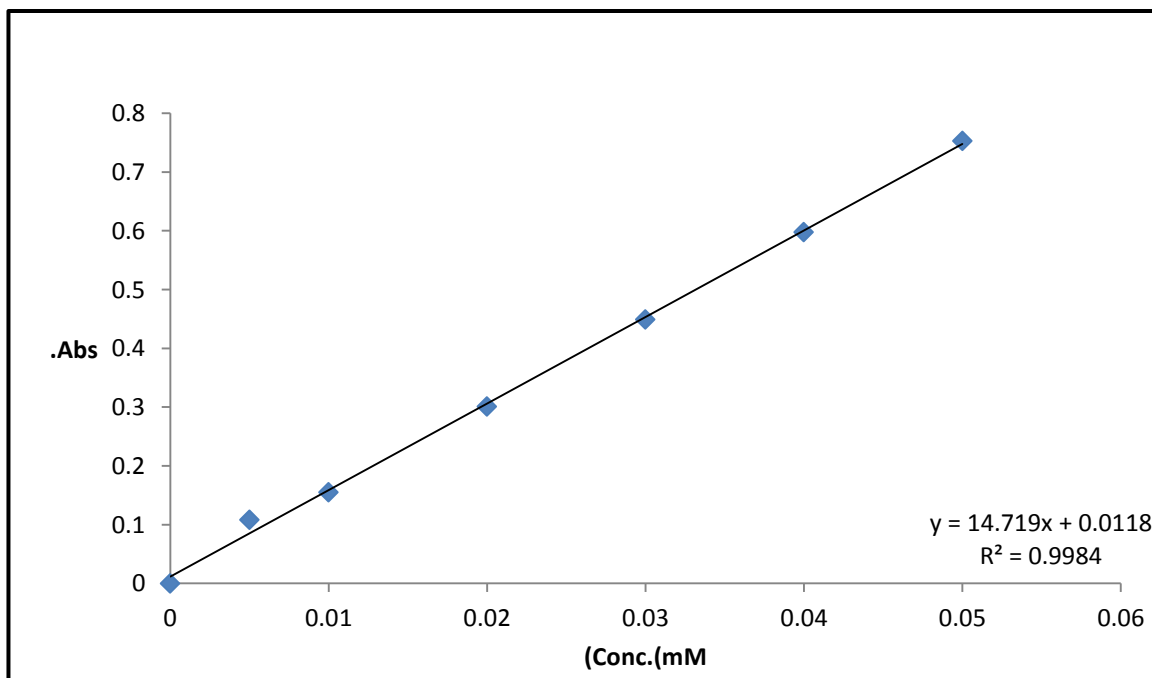
## Appendixes

**Appendix (۳): Values for P<sub>۱</sub> velocity plot against enzymatic activity.**

Velocity (min <sup>-1</sup> )	Activity (U/mg)
۰.۵	۰.۳۶۵
۰.۴	۰.۳۴۸
۰.۳	۰.۳۳۲
۰.۲	۰.۳۱۷
۰.۱	۰.۳

**Appendix (۴): Values of the velocity versus temperature plot and the Arrhenius equation, respectively for P<sub>۱</sub>**

T(C°)	Velocity (min <sup>-1</sup> )	۱/T(K <sup>-1</sup> )	ln k
۱۵	۰.۲۹	۰.۰۰۳۴	۳
۲۵	۰.۳۳	۰.۰۰۳۳	۳.۱
۴۰	۰.۲۶	۰.۰۰۳۱	۳.۳



## *Appendixes*

### Appendix (°): calibration curve of P<sub>r</sub>

**Appendix (°):** represents the values used to draw the Michaelis-Menten and Line Weaver-Burk equations for P<sub>r</sub>

[S] mM	K=V (min <sup>-1</sup> )	1/[S] mM <sup>-1</sup>	1/V min
0	0	0	0
0.1	0.09	10	11.111
0.2	0.14	5	7.142
0.3	0.18	3.333	5.555
0.4	0.2	2.5	5
0.5	0.21	2	4.761

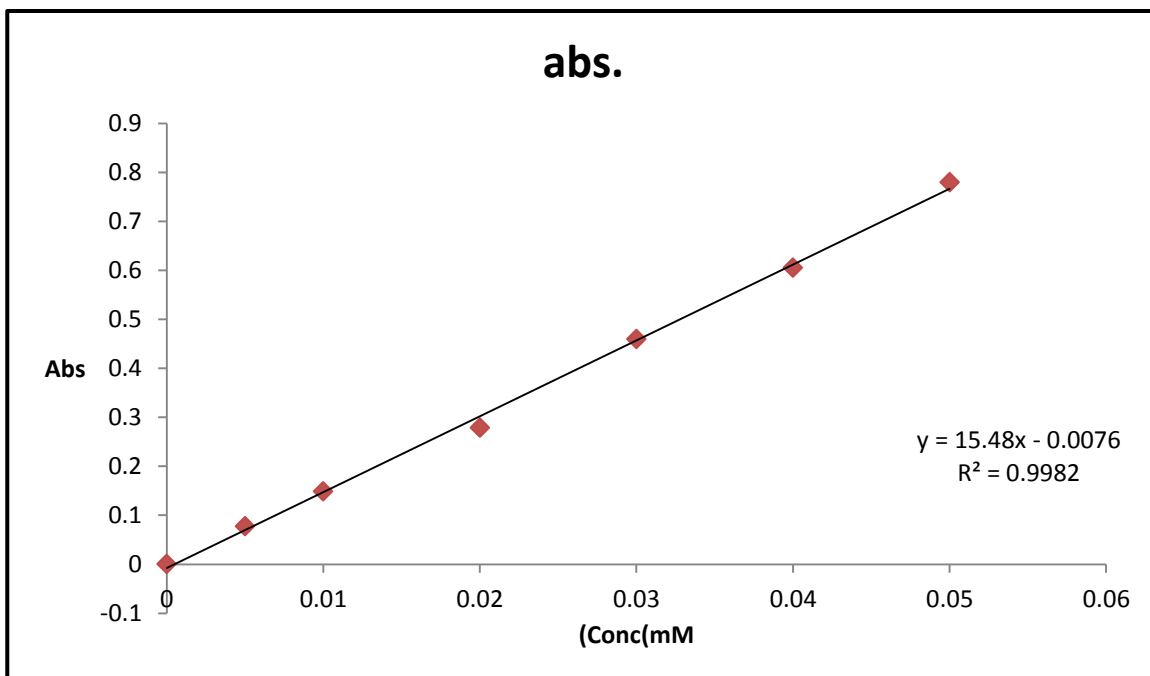
**Appendix (°):** Values for P<sub>r</sub> velocity plot against enzymatic activity.

## Appendixes

Velocity ( $\text{min}^{-1}$ )	Activity (U/mg)
0.5	0.34
0.4	0.37
0.3	0.35
0.2	0.33
0.1	0.31

**Appendix (^): Values of the velocity versus temperature plot and the Arrhenius equation, respectively for P<sub>r</sub>**

T(C°)	Velocity ( $\text{min}^{-1}$ )	1/T(K <sup>-1</sup> )	ln k
10	0.31	0.0034	3.3
20	0.36	0.0033	3.5
40	0.3	0.0031	3.8



## Appendixes

### Appendix (9): calibration curve of P<sub>r</sub>

Appendix (10): represents the values used to draw the Michaelis-Menten and Line Weaver-Burk equations for P<sub>r</sub>

[S] mM	K=V (min <sup>-1</sup> )	1/[S] mM <sup>-1</sup>	1/V min
0	0	0	0
0.1	0.08	10	12.5
0.2	0.14	5	7.142
0.3	0.17	3.333	5.882
0.4	0.2	2.5	5
0.5	0.21	2	4.761

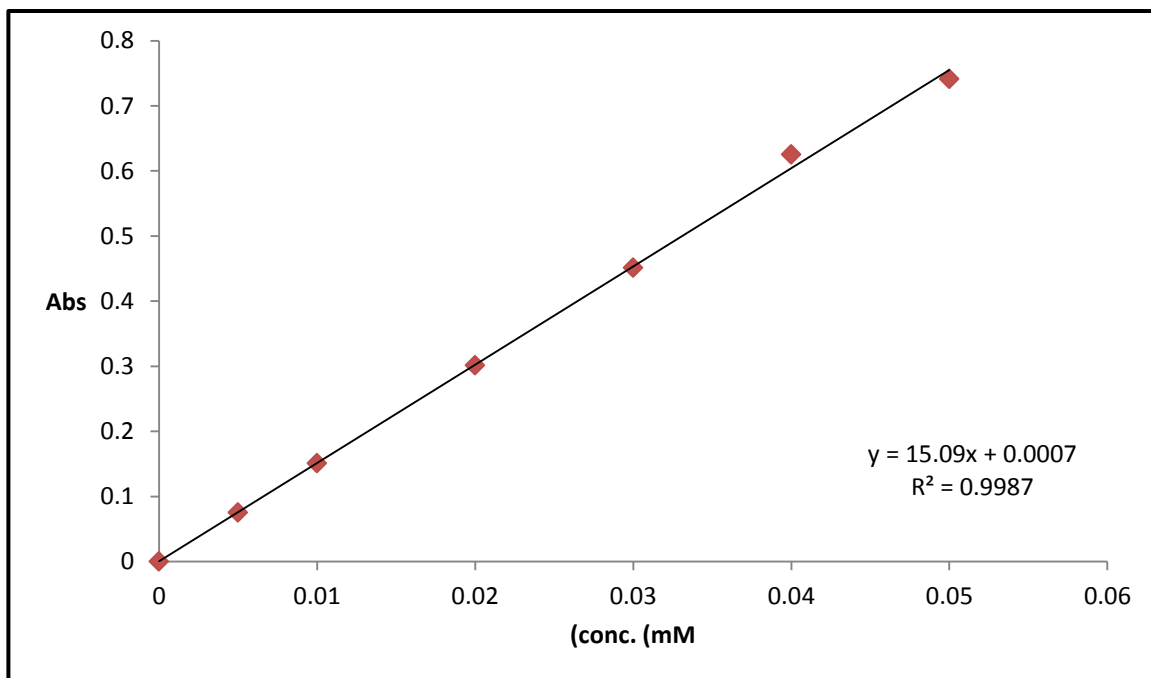
## Appendixes

**Appendix (11): Values for  $P_r$  velocity plot against enzymatic activity.**

Velocity ( $\text{min}^{-1}$ )	Activity (U/mg)
0.5	0.2
0.4	0.19
0.3	0.18
0.2	0.17
0.1	0.100

**Appendix (12): Values of the velocity versus temperature plot and the Arrhenius equation, respectively for  $P_r$**

T( $^{\circ}\text{C}$ )	Velocity ( $\text{min}^{-1}$ )	$1/T(\text{K}^{-1})$	ln k
10	0.19	0.0034	2.1
20	0.2	0.0033	2
40	0.18	0.0031	1.8





## Appendixes

### Appendix (١٣): calibration curve of P<sub>٤</sub>

Appendix (١٤): represents the values used to draw the Michaelis-Menten and Line Weaver-Burk equations for P<sub>٤</sub>

[S] mM	K=V (min <sup>-1</sup> )	١/[S] mM <sup>-1</sup>	١/V min
٠	٠	٠	٠
٠.١	٠.٠٨	١٠	١٢.٥
٠.٢	٠.١٤	٥	٧.١٤٢
٠.٣	٠.١٧	٣.٣٣٣	٥.٨٨٢
٠.٤	٠.٢	٢.٥	٥
٠.٥	٠.٢١	٢	٤.٧٦١

## *Appendixes*

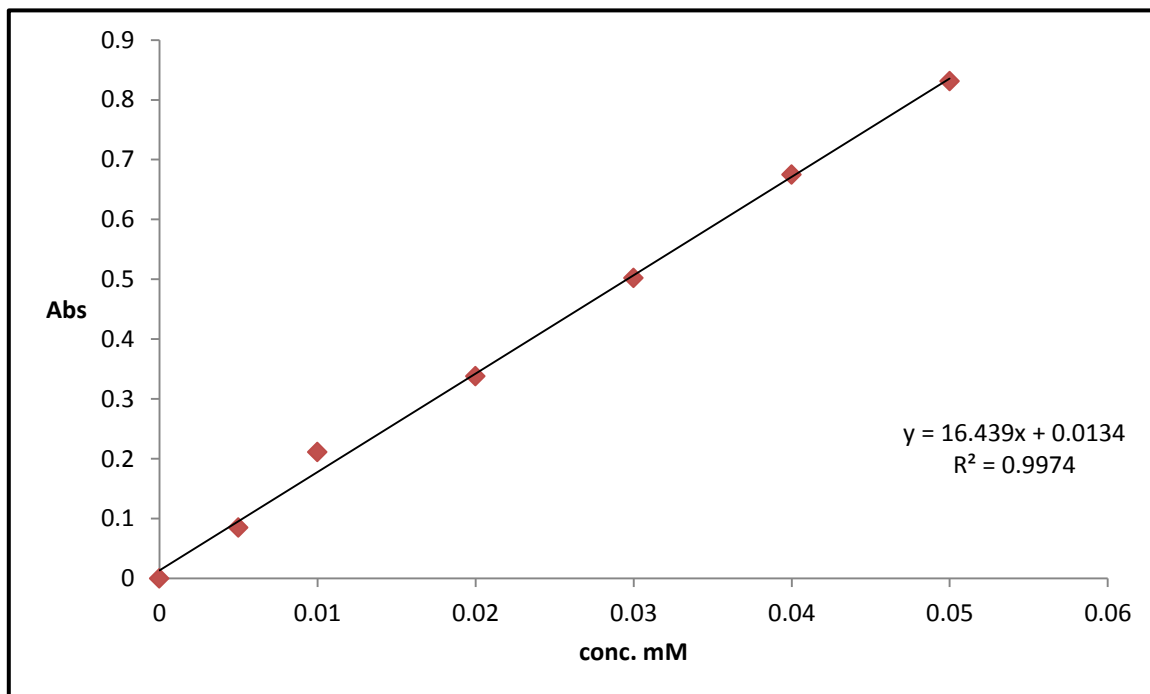
**Appendix (1<sup>o</sup>): Values for P<sub>z</sub> velocity plot against enzymatic activity.**

Velocity (min <sup>-1</sup> )	Activity (U/mg)
0.5	0.31
0.4	0.32
0.3	0.33
0.2	0.34
0.1	0.3

**Appendix (1<sup>6</sup>): Values of the velocity versus temperature plot and the Arrhenius equation, respectively for P<sub>z</sub>**

T(C°)	Velocity (min <sup>-1</sup> )	1/T(K <sup>-1</sup> )	ln k
10	0.29	0.0034	2.9
20	0.31	0.0033	3
40	0.3	0.0031	3.2

## Appendixes



**Appendix (17): calibration curve of P.**

**Appendix (18): represents the values used to draw the Michaelis-Menten and Line Weaver-Burk equations for P.**

[S] mM	K=V (min <sup>-1</sup> )	1/[S] mM <sup>-1</sup>	1/V min
0	0	0	0
0.1	0.08	10	12.5
0.2	0.14	5	7.142
0.3	0.17	3.333	5.882
0.4	0.2	2.5	5
0.5	0.21	2	4.761

## Appendixes

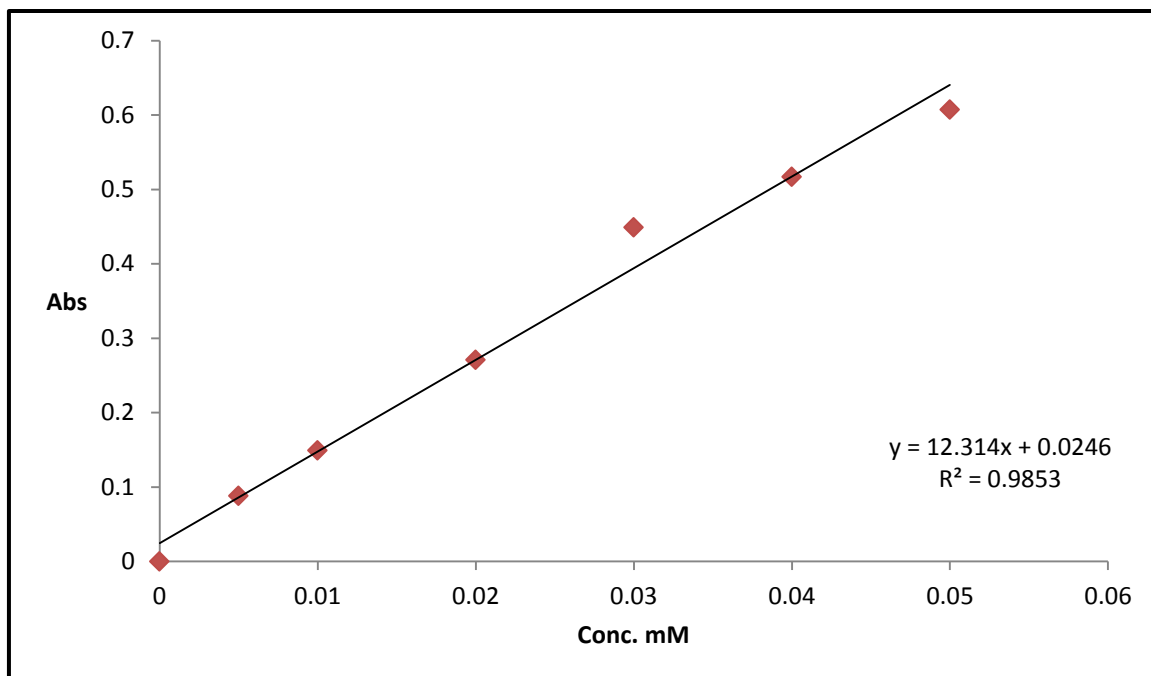
**Appendix (١٩): Values for P<sub>o</sub> velocity plot against enzymatic activity.**

Velocity (min <sup>-1</sup> )	Activity (U/mg)
٠.٥	٠.٣٧
٠.٤	٠.٣٦
٠.٣	٠.٣٥
٠.٢	٠.٣٤
٠.١	٠.٣٣

**Appendix (٢٠): Values of the velocity versus temperature plot and the Arrhenius equation, respectively for P<sub>o</sub>.**

T(C°)	Velocity (min <sup>-1</sup> )	١/T(K <sup>-1</sup> )	ln k
١٥	٠.٢٩	٠.٠٠٣٤	٢.٩
٢٥	٠.٣٣	٠.٠٠٣٣	٣
٤٠	٠.٢٨	٠.٠٠٣١	٣.٣

## Appendixes



**Appendix (٢١): calibration curve of P<sub>1</sub>**

**Appendix (٢٢):** represents the values used to draw the Michaelis-Menten and Line Weaver-Burk equations for P<sub>1</sub>

[S] mM	K=V (min <sup>-1</sup> )	1/[S] mM <sup>-1</sup>	1/V min
0	0	0	0
0.1	0.08	10	12.0
0.2	0.14	5	7.142
0.3	0.17	3.333	5.882
0.4	0.2	2.5	5
0.5	0.21	2	4.761

## *Appendixes*

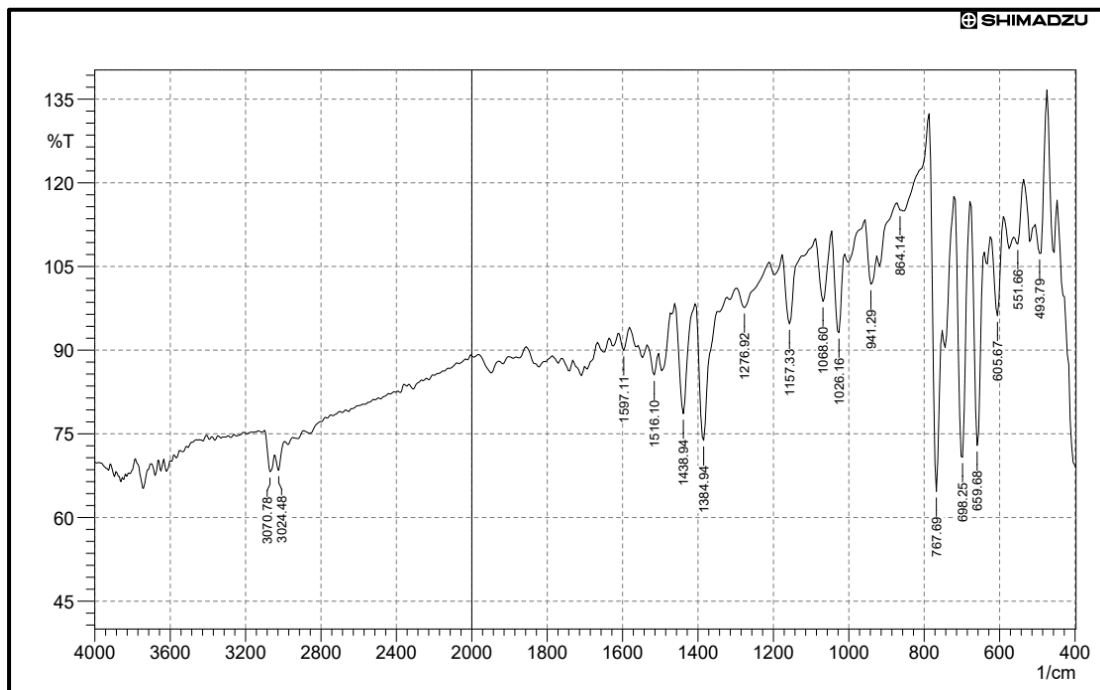
**Appendix (۲۳): Values for  $P_1$  velocity plot against enzymatic activity.**

Velocity ( $\text{min}^{-1}$ )	Activity (U/mg)
۰.۵	۰.۵۳
۰.۴	۰.۷
۰.۳	۰.۵
۰.۲	۰.۴
۰.۱	۰.۳

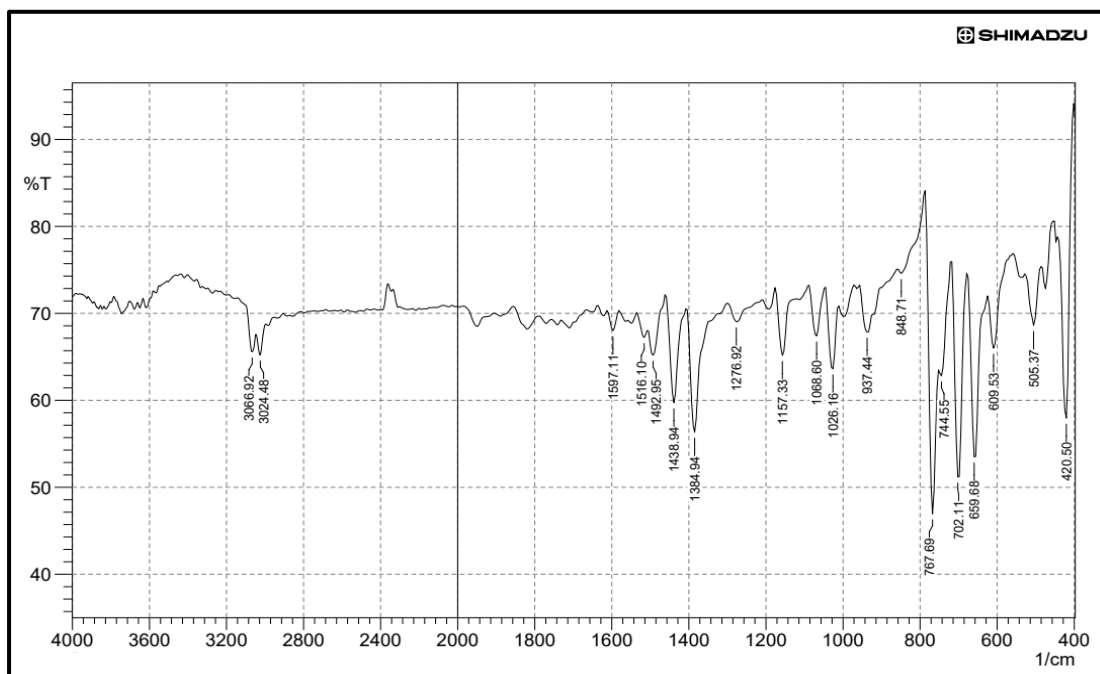
**Appendix (۲۴): Values of the velocity versus temperature plot and the Arrhenius equation, respectively for  $P_1$**

T( $^{\circ}\text{C}$ )	Velocity ( $\text{min}^{-1}$ )	$1/T(\text{K}^{-1})$	ln k
۱۵	۰.۵۵	۰.۰۰۳۴	۰.۵
۲۵	۰.۶۲	۰.۰۰۳۳	۰.۶
۴۰	۰.۶	۰.۰۰۳۱	۰.۸

## Appendixes

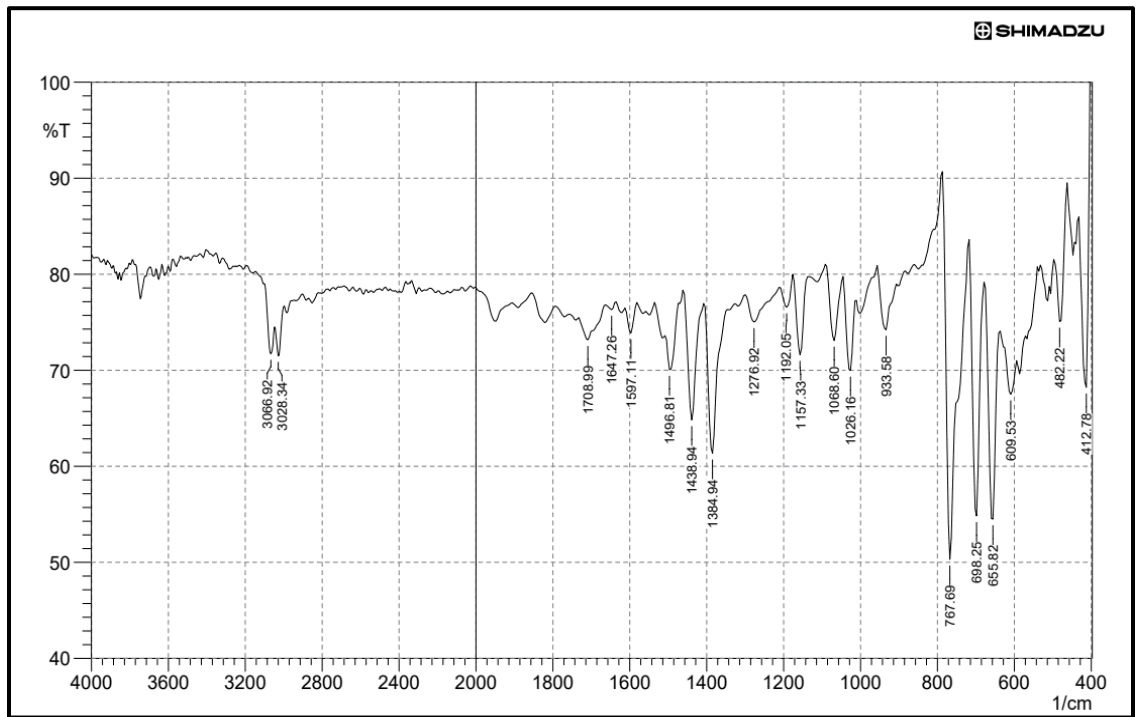


Appendix (۲۵): The FTIR spectra for P $\nu$



Appendix (۲۶): The FTIR spectra for P $\lambda$

# Appendixes



Appendix (۲۷): The FTIR spectra for P<sub>4</sub>



## الخلاصة

تفاعل ديلز-ألدز (D-A) هو أحد أهم التحولات الكيميائية بين الديين والدينوفيل في تفاعل حراري حلقي منسق لإنشاء روابط C-C مع انتقائية إقليمية ومساحة فراغية متوقعة، مما يؤدي إلى تكوين جزيئات عضوية كبيرة. وعلى الرغم من الجهود الكبيرة في هذا المجال، إلا أن التحكم في الانتقائية الفراغية لتفاعلات ديلز-ألدز لا يزال صعبًا للغاية.

الإنزيمات الحيوية، ديلز-ألدراز هي إنزيمات مميزة وظيفيًا تحفز عمليات الإضافة الحلقية [4 + 2]. يوفر تصميم تفاعلات ديلز-ألدز الأنزيمية للعلماء ميزة كبيرة في زيادة انتقائية منتجات تفاعل ديلز-ألدز.

Morus alba Diels-Alderase لديه القدرة على تحفيز تفاعلات ديلز-ألدز غير المؤكسدة والاختزالية لمختلف الدينوفيلات وأنواع مختلفة من الديينات المتعددة الفينول الطبيعية والاصطناعية. إن إنزيم Morus alba Diels-Alderase له انتقائية داخلية فقط. وعلاوة على ذلك، فقد تبين أن إنزيم Morus alba Diels-Alderase له انتقائية داخلية كبيرة عندما يتعلق الأمر بتحفيز تفاعل Diels-Alder، حيث ينتج فقط منتجات نقية داخليًا ذات انتقائية داخلية عالية.

ركز هذا العمل على تطبيق الطريقة الصديقة للبيئة والتي تتضمن تطبيق النهج الحالي في تفاعلات D-A الأنزيمية من خلال تكوين مركبات عضوية جديدة من خلال تفاعلات D-A الأنزيمية بين مشتقات الأنتراسين كداينات ومشتقات البيروول كداينوفيلات. بالإضافة إلى التحكم في الانتقائية الداخلية للمنتجات النهائية. علاوة على ذلك، مراقبة التفاعل الأنزيمي لإنزيم Morus alba Diels-Alderase.

تم إجراء جميع تفاعلات D-A في بيئة خاملة باستخدام غاز النيتروجين. تم تشخيص المركبات المحضرة باستخدام تقنيات مختلفة بما في ذلك مطيافية الكتلة والرنين المغناطيسي النووي والأشعة تحت الحمراء.

كانت المنتجات النهائية لتفاعل ديلز-ألدز هي Meso<sup>9</sup>-(hydroxymethyl)-1<sup>3</sup>-methyl-9,1<sup>0</sup>- dihydro-1<sup>2</sup>H,1<sup>4</sup>H-9,1<sup>0</sup>- (epiethane[1,1,2]triazanoethane[1,2,2]triazyl)anthracene-1<sup>2</sup>,1<sup>4</sup>-dione (P<sub>1</sub>), Meso<sup>9</sup>-(hydroxymethyl)-1<sup>3</sup>-propyl-9,1<sup>0</sup>-dihydro-1<sup>2</sup>H,1<sup>4</sup>H-9,1<sup>0</sup>- (epiethane[1,1,2]triazanoethane[1,2,2]triazyl)anthracene-1<sup>2</sup>,1<sup>4</sup>-dione (P<sub>2</sub>),

Meso(9-(hydroxymethyl)-12,14-dioxo-9,10-dihydro-13H-9,10-yl)acetic acid (epiethane[1,1,2]triazolanoethane[1,2,2]triazol)anthracen-13-yl)acetic acid (P<sub>2</sub>), Meso(13-methyl-12,14-dioxo-9,10-yl)boronic acid (epiethane[1,1,2]triazolanoethane[1,2,2]triazol)anthracen-9(10H)-yl)boronic acid (P<sub>3</sub>), Meso(12,14-dioxo-13-propyl-9,10-yl)boronic acid (epiethane[1,1,2]triazolanoethane[1,2,2]triazol)anthracen-9(10H)-yl)boronic acid (P<sub>4</sub>), Meso(9-(dihydroxyboranyl)-12,14-dioxo-9,10-dihydro-13H-9,10-yl)acetic acid (epiethane[1,1,2]triazolanoethane[1,2,2]triazol)anthracen-13-yl)acetic acid (P<sub>5</sub>)

بناءً على النتائج، تم اقتراح آليات تفاعل ديلز-ألدز الأنزيمي.

تمت دراسة حركية تحضير هذه المنتجات في وجود ديلز-ألدز موزون ألبا من خلال تطبيق معادلة ميكائيليس-مينتن. تم تحديد أقصى سرعة (Vmax) وثابت ميكائيليس-مينتن (Km) لجميع تفاعلات ديلز-ألدز الأنزيمية. تم العثور على أقل تقارب بين الدين والإنزيم في Meso(13-methyl-12,14-dioxo-9,10-yl)boronic acid (epiethane[1,1,2]triazolanoethane[1,2,2]triazol)anthracen-9(10H)-yl)boronic acid (P<sub>3</sub>) لأنه كان له أعلى قيمة Km وهي 0.3527. بينما حقق Meso(9-(dihydroxyboranyl)-12,14-dioxo-9,10-dihydro-13H-9,10-yl)acetic acid (epiethane[1,1,2]triazolanoethane[1,2,2]triazol)anthracen-13-yl)acetic acid (P<sub>5</sub>) أعلى تقارب من خلال الحصول على أقل قيمة Km وهي 0.2292.

بالإضافة إلى ذلك، تم إجراء تحسين تفاعلات ديلز ألدز الأنزيمية والتي تضمنت تركيز الركيزة والنشاط الأنزيمي ودرجة الحرارة لتحديد أفضل تركيز لكل ركيزة بالإضافة إلى أفضل نشاط إنزيمي عند درجة الحرارة المثلى. والتي وجدت في P<sub>2</sub> باستخدام anthracen-9-ylmethanol كدين وفي P<sub>6</sub> باستخدام anthracen-9-ylboronic acid كدين عند 25 درجة مئوية.

تم تحديد المعلمات الديناميكية الحرارية والتي تتضمن التغير في الانتالبي (ΔH) وتغير طاقة جيبس الحرة (ΔG) وتغير الإنتروبيا (ΔS). جميع النواتج تلقائية ومفضلة ثرموديناميكياً، في حين أن الأكثر ملاءمة هو P<sub>2</sub>. بالإضافة إلى ذلك، فإن جميع النواتج ماصة للحرارة باستثناء P<sub>3</sub> باعث للحرارة

ومع ذلك، هناك ثلاثة مركبات أخرى تم تحضيرها باستخدام 9,10-diphenylanthracene كديين لكنها لم تعطي النتيجة المتوقعة بناءً على تحليل FTIR و NMR و مطيافية الكتلة.



كلية العلوم

جامعة كربلاء

قسم الكيمياء

تخليق وتشخيص مركبات جديدة: دراسة حركية تفاعلات ديلز-الدر المحفزة انزيميا

رسالة مقدمة الى

مجلس كلية العلوم – جامعة كربلاء

من قبل

زينب عادل جاسم

بكالوريوس علوم في كيمياء (٢٠١٩) / جامعة كربلاء

بإشراف

أ.د. زيد حسن عبود

أ.م.د. ثائر مهدي مدلول

محرم/ ١٤٤٦ هـ

تموز/ ٢٠٢٤ م